

DYNAMICS AND CONTROL OF A SURFACE-CUM-UNDERWATER ROBOT

PROJECT REPORT SUBMITTED TO IIT TIRUPATI

*submitted in partial fulfillment of the requirements for the
degree of*

BACHELOR OF TECHNOLOGY

in

MECHANICAL ENGINEERING

by

**KAREKAR CHITALI UDAY
ARUNKUMAR V**

**ME20B053
ME20B004**

Supervisor

Dr. Thiagarajan R

भारतीय प्रौद्योगिकी संस्थान तिरुपति



**DEPARTMENT OF MECHANICAL ENGINEERING
INDIAN INSTITUTE OF TECHNOLOGY TIRUPATI**

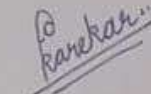
MAY 2024

DECLARATION

We declare that this written submission represents our ideas in our own words and where others' ideas or words have been included, we have adequately cited and referenced the original sources. We also declare that we have adhered to all principles of academic honesty and integrity and have not misrepresented or fabricated or falsified any idea/data/fact/source in our submission to the best of our knowledge. We understand that any violation of the above will be cause for disciplinary action by the Institute and can also evoke penal action from the sources which have thus not been properly cited or from whom proper permission has not been taken when needed.

Place: Tirupati

Date: 07-05-2024

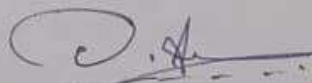


Signature

KAREKAR CHITALI UDAY
ME20B053

Place: Tirupati

Date: 07-05-2024

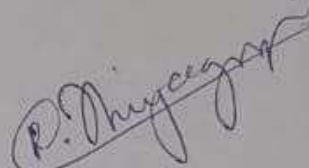


Signature

ARUNKUMAR V
ME20B004

BONAFIDE CERTIFICATE

This is to certify that the report titled : **DYNAMICS AND CONTROL OF A SURFACE-CUM-UNDERWATER ROBOT: B.TECH TERM PROJECT REPORT**, submitted by **Karekar Chaitali Uday** and **Arunkumar V**, to the Indian Institute of Technology, Tirupati, for the award of the degree of **Bachelor of Technology**, is a bonafide record of the project work done by them under my supervision. The contents of this report, in full or in parts, have not been submitted to any other Institute or University for the award of any degree or diploma.



Place: Tirupati

Date: 07-05-2024

Dr. Thiyagarajan R

Project Guide

Assistant Professor

Department of Mechanical Engineering

IIT Tirupati - 517619

III: Table of Contents

I.	Declaration	i
II.	Bonafide	ii
III.	<u>Table of Contents</u>	1
IV.	<u>Table of Figures</u>	2
V.	<u>List of Tables</u>	3
1.	<u>Introduction</u>	4
2.	<u>Literature Review</u>	6
3.	<u>Problem Definition</u>	8
4.	Results	
a.	<u>Mathematical Model</u>	10
b.	<u>Design and Development</u>	17
c.	<u>Experimental Setup</u>	23
d.	Iterations	
i.	<u>Preliminaries</u>	24
ii.	<u>Iteration 1</u>	26
iii.	<u>Iteration 2</u>	32
iv.	<u>Iteration 3</u>	36
e.	<u>Results and Discussion</u>	40
5.	<u>Conclusion</u>	43
6.	<u>Future work</u>	44
7.	<u>References</u>	45

IV: Table of figures

Fig 1	Convention used for modeling	8
Fig 2	Buoyancy Subsystem Components	17
Fig 3	Compression/Expansion Bellow for Change of Volume method	19
Fig 4	Electrical Subsystem Block	19
Fig 5	Electrical Components with 3D Printed Support Structure	20
Fig 6	Thruster, Servo motor, Double bearing arrangement and Rudder Design	21
Fig 7	Thruster block with 3D printed attachment to the acrylic cylinder	21
Fig 8	CAD Model of the Structural Subsystem (i) Navigation system Casing (ii) Buoyancy Subsystem and Electrical subsystem Casing	22
Fig 9		22
Fig 10	Figure a and b depiction for variable mass and variable volume	24
Fig 11	Representation of Rendered CAD Models for Patent Documentation	24
Fig 12	Image Renderings for Swarm of bots and Pentagonal Formation	25
Fig 13	Bounding Box and the Redesigned CAD Model	26
Fig 14	Unstructured Mesh for the Bounding Box (50 mm)	27
Fig 15	Defining Boundary Conditions (Inlet, Outlet & Wall Conditions) Static Pressure Contour obtained for Velocity along Y axis with M10 rudder angle.	27
Fig 16		30
Fig 17	Representation of Velocity contour through the model along with static pressure obtained on the surface.	30
Fig 18	Velocity and pressure effects near the head dome and tail region	31
Fig 19	Implementation of model in Simulink as stated in ‘Investigations on trajectory tracking and dynamic station keeping control of an underactuated flat fish type autonomous underwater vehicle. M. Santhakumar.	34
Fig 20	Simulation screengrab for testing out model in Simulink. The amount of water intake was varied and the system behavior was verified.	34
Fig 21	A perfect 90° dive achieved by ensuring that CoG stays near the X axis	35
Fig 22	Simplified cylinder model	35
Fig 23	Drift of 6 m for 30 s of water intake time in absence of perfect vertical dive.	36
Fig 24	Drift of 1.6 m for 10 s of water intake time in absence of perfect vertical	36

dive.

Increase in the pitch angle as distance of CoG from X axis decreases from 5 cm to 2 cm to 1 mm.	37	
Fig 25		
Fig 26	Modified model to support global variables method of updating values	38
Fig 27	CAD Model for Iteration 1 (Isometric View)	39
Fig 28	CAD Model for Iteration 1 (Side View)	39
Fig 29	Skeletal Structure of the CAD Design (Frames and Longerons Structure)	39
	Pitch angle returning to zero on release of water. This requires the pitching to be decoupled from mass change.	
Fig 30		41
Fig 31	Different scenarios of submerged volume for the cylinder.	42
	Pitch maintained at $\sim 90^\circ$ throughout the dive and resurface phase till reaching surface.	
Fig 32		42
Fig 33	Actuator Subsystem - Control of CoM of the Model	43
Fig 34	Positioning of Rudder in the front for ease of construction	44
Fig 35	CAD Model Obtained at the end of Iteration 2	44
Fig 36	CAD Model: Front and top View at the end of iteration 3	46
Fig 37	Aluminium Cap attachment along with Latches and O-Rings	46
Fig 38	CAD Model at the end of Iteration 3	46
Fig 39	Complete Design of Sealings and Gaskets for leakage prevention	49
Fig 40	Redesigned Head and Tail Dome	49
Fig 41	Integration of both the domes into the model (Twist & Lock Mechanism)	50
Fig 42	System released from 1 m - 0° naturally stabilizes at 0.057 m \sim Neutral state	52
Fig 43	System released from 1 m - 90° stabilizes at 0.057 m \sim Neutral state	52
Fig 44	Path followed by system for sequence stated in (1)	53
Fig 45	System plots for sequence stated in (1)	54
Fig 46	Velocity in global X direction	55
Fig 47	Velocity in global Y direction	55
Fig 48	Angular velocity along global theta	55
Fig 49	System plots for sequence stated in (2)	56
Fig 50	Path followed by system for sequence stated in (2)	57
Fig 51	Velocity in global X direction	57

Fig 52	Velocity in global Z direction	58
Fig 53	Angular velocity along theta direction	58
Fig 54	Path followed for different rudder angles	59
Fig 55	System plots for sequence stated in (1)	61
Fig 56	Velocity in global X direction	62
Fig 57	Velocity in global Z direction	62
Fig 58	Angular velocity along global theta direction	62
Fig 59	Path followed by system for sequence stated in (1)	63
Fig 60	System plots for sequence stated in (2)	64
Fig 61	Path followed by system for sequence stated in (2)	65
Fig 62	Velocity in global X direction	65
Fig 63	Velocity in global Z direction	66
Fig 64	Angular velocity along global theta direction	66
Fig 65	Observed path followed	66
Fig 66	Velocity in global X direction	67
Fig 67	Velocity in global Y direction	67
Fig 68	Angular velocity along global psi direction	67
Fig 69	Observed path followed	68
Fig 70	Velocity in global X direction	68
Fig 71	Velocity in global Y direction	69
Fig 72	Angular velocity along global psi direction	69
Fig 73	Observed path followed	70
Fig 74	Velocity in global X direction	70
Fig 75	Velocity in global Y direction	71
Fig 76	Angular velocity along psi direction	71
Fig 77	Observed path followed	72
Fig 78	Velocity in global X direction	72
Fig 79	Angular velocity along psi direction	73
Fig 80	System plots for diving down and surfacing up. In both cases a near 90° pitch is achieved.	73

Fig 81	Path traced when diving down and surfacing up.	74
Fig 82	Initial position of Centre of Gravity and Origin of the System (Blue Dot)	74
	Final shift of Centre of Gravity due to movement of battery pack from the	
Fig 83	origin of the System Shift along Z	75
Fig 84	Mathematical Model Framework	76

V: List of Tables

Table 1	Volume submerged	12
Table 2	X Coordinate of CoB	12
Table 3	Z Coordinate of CoB	13

Chapter 1: Introduction

Underwater robotics stands as a pivotal technology facilitating exploration in challenging underwater environments where human access is perilous or impossible. Equipped with advanced sensors and actuators, these robots are designed intricately to navigate and operate efficiently. The critical consideration of depth further complicates their development, necessitating innovative solutions for effective exploration.

Underwater systems play a vital role in diverse fields such as fisheries management, natural resource management, port safety and security, oil and mineral exploration, military operations, and scientific research, including oceanography and limnology. Autonomous Underwater Vehicles (AUVs) and Remotely Operated Vehicles (ROVs), especially AUVs, have gained prominence for inspection, surveillance, and various applications across academic research, defense, customs, delivery systems, telecommunications, repair and rescue, geological survey, oil and gas industry, marine science research, shipwreck reconnaissance, and fisheries.

Developing robust control strategies for AUVs poses challenges due to their nonlinear dynamics. The hydrodynamic parameters governing AUV dynamics are highly nonlinear, coupled, and time-varying. Unlike terrestrial or aerial vehicles, underwater vehicles cannot rely on global positioning systems (GPS) during their motion. Commonly used sonar-based sensors introduce challenges such as noise, missed detection, and poor resolution. Additionally, AUVs, being underactuated systems most of the time, present complexities in control engineering tasks with fewer control inputs than total degrees of freedom.

The project aims to design and develop a surface-cum-underwater robot with the unique capability to navigate on the water's surface and perform underwater dives. The innovative aspect lies in its ability to navigate on the surface in addition to diving, a feature not commonly found in existing underwater robots. Two diving mechanisms can be used to achieve this: a change in volume or a change in mass. The initial focus is on the change in mass concept, with future prospects for a robot incorporating the change in volume concept. The current robot is designed to navigate on the water's surface in the XY plane and execute vertical dives by adjusting the quantity of water in the system. A design for a change in volume concept robot is

also proposed here with future scope to perform a similar mathematical analysis like that done in the change in mass concept.

The design incorporates innovative solutions for controlling the change in mass during dives and ensuring stability of the entire framework during surface navigation. The project is supported by rigorous mathematical modeling and dynamic analysis of the designed prototype. The mathematical models cover the dynamic behavior of the robot for surface navigation and underwater diving. The mathematical model also captures the dynamic and rarely captured surface effect when the robot dives in and out of the surface. This is done by dynamic updation of buoyancy and center of buoyancy values. Additionally, the surface navigation model demonstrates the turning on the surface brought about by a combination of thruster and rudder.

A further development is the incorporation of CFD analysis to estimate the drag acting on the robot. The data obtained has been interpreted and fitted for incorporation into the mathematical model. On incorporation, the project also analyzes the results thus obtained and a comparative analysis with previous results.

This project thus addresses the need for a surface-cum-underwater robot, introducing a unique capability for surface navigation and underwater exploration.

Chapter 2: Literature review

Much of the literature being referred to is restricted to individual subsections as the concept involved here is fairly novel and not been dealt with previously. The mathematical modeling used references from several research papers, online resources and in due course generated new formulations to effectively capture the dynamics of the system. It was observed as a part of the literature review that a unique concept of surface and underwater navigation does not exist in currently available models. Most of them restrict themselves to pure diving. The surface navigation component adds more value to the project, but makes the designing aspect more involved.

A change in volume concept previously employed by Thiagarajan Ranganathan, Sundaravalli Aravazhi, Sambit Mishra and Asokan Thondiyath as presented in the paper, ‘Design and Analysis of a Novel Underwater Glider - RoBuoy’ shares quite a few similarities and was a good starting point to the development of this model. The paper talks about the scope of AUVs in general and how their applications span over various types of underwater missions followed by a detailed mathematical modeling of the system in Matlab and the results obtained. The system does not aim for a vertical dive in and therefore its range of operation extends over quite a few meters. This is different from what we are aiming for in this project. The paper proposes a change of volume model which uses the change in buoyancy of the system achieved by movement of a bellow controlled actuator for carrying out the diving motion. The degree of freedom of the system is similar to the one we have in mind and the challenges are noteworthy. Dealing with pressures at depths, tracking while underwater, acting against an external pressure, drag effects and drift in the path traced are topics discussed here that are valuable inputs to the model proposed in the project.

Another paper titled ‘Design of a controllable variable buoyancy module and its performance analysis as cascaded system for selective underwater deployment’ by Thiagarajan Ranganathan, Vijendra Singh, Ranjith Nair and Asokan Thondiyath focuses majorly on the actual designing and the compilation of various subsystems for the previously mentioned model. The paper goes into depth, detailing each design aspect such as the designing of the actuator, integration of the mechatronic system and the results obtained. These results shall be particularly

useful in the upcoming stages of the project that involve prototyping the model and recording and testing phases.

The thesis, ‘Investigations on trajectory tracking and dynamic station keeping control of an underactuated flat-fish type autonomous underwater vehicle’ by M. Santhakumar, forms the basis of the mathematical model in this project. The paper is an extensive thesis covering a wide range of topics including the design of mathematical models, tracking controller design, simulation of drag effects, design and behavior of thrusters, power analysis and a detailed explanation of the simulation results obtained. The main mathematical model as stated in this thesis is described further ahead in this report.

Further modeling of the drag effects (on simplification) used drag coefficients determined through available tables from ‘Fluid Mechanics : Fundamentals and Applications’ by Yunus Cengel and John Cimbala.

The ‘Handbook of Marine Craft Hydrodynamics and Motion Control’ by Thor I. Fossen is a standard reference widely referred to in many of the publications mentioned above and has been referred to and incorporated into the mathematical model at several instances throughout the mathematical modeling process, especially for discussing the stability of the robot while on the surface and surface navigating in the XY plane. The surface navigation part for the CFD based model directly uses forces in contrast to directly calculating them, however the inspiration is taken from ‘Handbook of Marine Craft Hydrodynamics and Motion Control’ by Thor I. Fossen.

Chapter 3: Problem definition

The scope of this project titled, ‘Dynamics and control of a surface-cum-underwater robot’ is the design and development of a unique underwater robot that possesses the ability to navigate on the water surface and dive to depths for maritime exploration. The particular feature of navigating on the surface is a novelty as compared to current underwater exploration robots. The motion of the robot as hypothesized in an ideal scenario can be majorly broken down into five distinct stages.

The first stage involves horizontally navigating on the water surface with the help of thrusters and rudders to reach a point in the XY plane. This is followed by a second stage which consists of diving vertically downwards in a nose down pose to a desired depth (we are currently aiming for 10 m depths). The third stage involves exploration of underwater systems or for that matter, carrying out assigned tasks at that particular depth. This stage may vary considerably depending on the application and may be eliminated as well. Design of this stage is essentially a control problem and will not be discussed as a part of this project. The fourth stage involves retracing the path back to the surface while maintaining the vertical pose. The fifth stage; though not in chronological order, involves the dynamics of the system while it performs surface transition. This includes achieving 90° pitch from an initial horizontal position while diving down and returning back to original horizontal position when it resurfaces again.

The downward motion of the underwater robot is brought about by the differential in the weight and buoyancy forces acting on the system. This differential can be either brought about by the change in mass of the system or by change in the volume. This project uses the change in mass concept to achieve diving and corresponding rising motion. The mass change is achieved by changing the amount of water taken into the system and released out of the system.

The design of this multistage model involves designing of the actual system and equally, formulating the mathematical model which will help predict the motion of the system and suggest system changes, while keeping in mind the non-idealities and design constraints.

From the standpoint of system design, the task involves strategically choosing components and arranging them while considering commercial availability, material limitations and system requirements. Several parameters come into play, with a crucial focus on accurately positioning the Center of gravity (CoG) and Center of Buoyancy (CoB) for stability and controlled pitching during dives. The prototype must handle pressure changes during dives while ensuring structural stability. Design constraints revolve around achieving a balance between compactness and water-filling capacity. Preventing water leakage is crucial to avoid damage to the electrical hardware. The information regarding position and depth are required for controlling the robot and the design aspect needs to incorporate components to track the robot, both while on surface and underwater. In essence, this design challenge is about practical considerations, ensuring the system's functionality, resilience, and precision in navigating underwater environments.

The mathematical model aims to formulate the dynamics of the system as it passes through various stages. This requires closely capturing the geometric characteristics of the model such as CoG, CoB and the various external forces and torques acting on the system dynamically. Added mass and drag effects acting on the system are also to be modeled to capture their effect on the system motion. The modeling of the system shall help in the determination of water flow rates, design parameters like diameter, length, weight etc. In particular, the mathematical model should carefully capture the shift in CoB during surface transition to model actual surface behavior.

A surface motion analysis will help in determining the surface level motion and get an idea about the turning achieved by the robot which is brought about by thruster and rudder combination. This is to be done by determining the mathematical model dictating these motions and accordingly get an estimate on the turning effect.

A CFD analysis aims at getting a close enough estimate of the drag forces acting on the system for all possible geometries brought about by change in rudder angle and corresponding velocities, and then accordingly incorporating these values into the mathematical model. This will involve fitting the obtained data, converting it into a suitable form and checking for discrepancies. The model then should be analyzed for these data values and compared with previously obtained results for validity.

Chapter 4.a: Mathematical Model

Governing equations:

Based on SNAME (1950) notation, the motion can be described with the following vectors:

$$\begin{aligned}\boldsymbol{\eta}^T &= [\boldsymbol{\eta}_1^T \quad \boldsymbol{\eta}_2^T] & \boldsymbol{\eta}_1^T &= [x \quad y \quad z] & \boldsymbol{\eta}_2^T &= [\phi \quad \theta \quad \psi] \\ \mathbf{v}^T &= [\mathbf{v}_1^T \quad \mathbf{v}_2^T] & \mathbf{v}_1^T &= [u \quad v \quad w] & \mathbf{v}_2^T &= [p \quad q \quad r] \\ \boldsymbol{\tau}^T &= [\boldsymbol{\tau}_1^T \quad \boldsymbol{\tau}_2^T] & \boldsymbol{\tau}_1^T &= [X \quad Y \quad Z] & \boldsymbol{\tau}_2^T &= [K \quad M \quad N]\end{aligned}$$

By Newton-Euler formulation for 6 DoF system, the equation simplifies to:

$$\mathbf{M}_{RB} \dot{\mathbf{v}} + \mathbf{C}_{RB}(\mathbf{v})\mathbf{v} = \boldsymbol{\tau}_{RB}$$

\mathbf{M}_{RB} is the rigid-body inertia matrix given by,

$$\mathbf{M}_{RB} = \begin{bmatrix} m & 0 & 0 & 0 & mz_g & -my_g \\ 0 & m & 0 & -mz_g & 0 & mx_g \\ 0 & 0 & m & my_g & -mx_g & 0 \\ 0 & -mz_g & my_g & I_x & -I_{xy} & -I_{xz} \\ mz_g & 0 & -mx_g & -I_{yx} & I_y & -I_{yz} \\ -my_g & mx_g & 0 & -I_{zx} & -I_{zy} & I_z \end{bmatrix}$$

\mathbf{C}_{RB} is the rigid-body Coriolis and centripetal matrix given by,

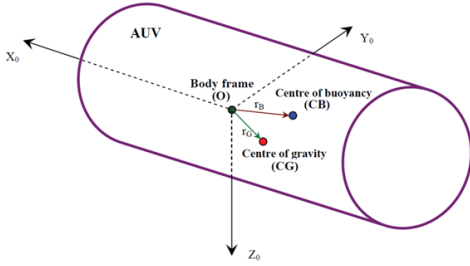
$$\mathbf{C}_{RB}(\mathbf{v}) = \begin{bmatrix} 0 & 0 & 0 \\ 0 & 0 & 0 \\ 0 & 0 & 0 \\ -m(y_g q + z_g r) & m(y_g p + w) & m(z_g p - v) \\ m(x_g q - w) & -m(z_g r + x_g p) & m(z_g q + u) \\ m(x_g r + v) & m(y_g r - u) & -m(x_g p + y_g q) \\ m(y_g q + z_g r) & -m(x_g q - w) & -m(x_g r + v) \\ -m(y_g p + w) & m(z_g r + x_g p) & -m(y_g r - u) \\ -m(z_g p - v) & -m(z_g q + u) & m(x_g p + y_g q) \\ 0 & -I_{yz}q - I_{xz}p + I_zr & I_{yz}r + I_{xy}p - I_yq \\ I_{yz}q + I_{xz}p - I_zr & 0 & -I_{xz}r - I_{xy}q + I_xp \\ -I_{yz}r - I_{xy}p + I_yq & I_{xz}r + I_{xy}q - I_xp & 0 \end{bmatrix}$$

$\boldsymbol{\tau}_{RB}$ represents external forces $\boldsymbol{\tau}_H = -\mathbf{M}_A \dot{\mathbf{v}} - \mathbf{C}_A(\mathbf{v})\mathbf{v} - \mathbf{D}(\mathbf{v})\mathbf{v} - \mathbf{g}(\boldsymbol{\eta})$

$\boldsymbol{\tau}_H$ hydrodynamic added mass, damping and restoring effects

$\boldsymbol{\tau}_E$ environmental factors including underwater currents and waves

$\boldsymbol{\tau}_C$ thrusters and control surfaces



DOF	Motion	Forces and Moments (τ)	Linear and angular velocities (v)	Positions and Euler angles (η)
1	Translation in x (surge)	X	u	x
2	Translation in y (sway)	Y	v	y
3	Translation in z (heave)	Z	w	z
4	Rotation about x-axis (roll)	K	p	ϕ
5	Rotation about y-axis (pitch)	M	q	θ
6	Rotation about z-axis (yaw)	N	r	ψ

Fig 1: Convention used for modeling

$$\mathbf{M}_A = - \begin{bmatrix} X_{\dot{u}} & X_{\dot{v}} & X_{\dot{w}} & X_{\dot{p}} & X_{\dot{q}} & X_{\dot{r}} \\ Y_{\dot{u}} & Y_{\dot{v}} & Y_{\dot{w}} & Y_{\dot{p}} & Y_{\dot{q}} & Y_{\dot{r}} \\ Z_{\dot{u}} & Z_{\dot{v}} & Z_{\dot{w}} & Z_{\dot{p}} & Z_{\dot{q}} & Z_{\dot{r}} \\ K_{\dot{u}} & K_{\dot{v}} & K_{\dot{w}} & K_{\dot{p}} & K_{\dot{q}} & K_{\dot{r}} \\ M_{\dot{u}} & M_{\dot{v}} & M_{\dot{w}} & M_{\dot{p}} & M_{\dot{q}} & M_{\dot{r}} \\ N_{\dot{u}} & N_{\dot{v}} & N_{\dot{w}} & N_{\dot{p}} & N_{\dot{q}} & N_{\dot{r}} \end{bmatrix}$$

$$\mathbf{C}_A(v) = \begin{bmatrix} 0 & 0 & 0 & 0 & -a_3 & a_2 \\ 0 & 0 & 0 & a_3 & 0 & -a_1 \\ 0 & 0 & 0 & -a_2 & a_1 & 0 \\ 0 & -a_3 & a_2 & 0 & -b_3 & b_2 \\ a_3 & 0 & -a_1 & b_3 & 0 & -b_1 \\ -a_2 & a_1 & 0 & -b_2 & b_1 & 0 \end{bmatrix}$$

$$a_1 = X_{\dot{u}}u + X_{\dot{v}}v + X_{\dot{w}}w + X_{\dot{p}}p + X_{\dot{q}}q + X_{\dot{r}}r$$

$$a_2 = Y_{\dot{u}}u + Y_{\dot{v}}v + Y_{\dot{w}}w + Y_{\dot{p}}p + Y_{\dot{q}}q + Y_{\dot{r}}r$$

$$a_3 = Z_{\dot{u}}u + Z_{\dot{v}}v + Z_{\dot{w}}w + Z_{\dot{p}}p + Z_{\dot{q}}q + Z_{\dot{r}}r$$

$$b_1 = K_{\dot{u}}u + K_{\dot{v}}v + K_{\dot{w}}w + K_{\dot{p}}p + K_{\dot{q}}q + K_{\dot{r}}r$$

$$b_2 = M_{\dot{u}}u + M_{\dot{v}}v + M_{\dot{w}}w + M_{\dot{p}}p + M_{\dot{q}}q + M_{\dot{r}}r$$

$$b_3 = N_{\dot{u}}u + N_{\dot{v}}v + N_{\dot{w}}w + N_{\dot{p}}p + N_{\dot{q}}q + N_{\dot{r}}r$$

\mathbf{M}_A and \mathbf{C}_A are the hydrodynamic added mass and Coriolis and centripetal matrix respectively.

$Z_{\dot{v}}$ represents the mass component contributing to hydrodynamic force in the Z direction due to acceleration in the y direction.

where, X_u and $X_{|u|u}$ are coefficients contributing hydrodynamic linear and quadratic damping force in x-direction due to velocity u respectively.

$$\mathbf{D}_L(\mathbf{v}) = \begin{bmatrix} X_u & X_v & X_w & X_p & X_q & X_r \\ Y_u & Y_v & Y_w & Y_p & Y_q & Y_r \\ Z_u & Z_v & Z_w & Z_p & Z_q & Z_r \\ K_u & K_v & K_w & K_p & K_q & K_r \\ M_u & M_v & M_w & M_p & M_q & M_r \\ N_u & N_v & N_w & N_p & N_q & N_r \end{bmatrix}$$

$$\mathbf{D}_Q(\mathbf{v}) = \begin{bmatrix} X_{|u|u}|u| & X_{|v|v}|v| & X_{|w|w}|w| & X_{|p|p}|p| & X_{|q|q}|q| & X_{|r|r}|r| \\ Y_{|u|u}|u| & Y_{|v|v}|v| & Y_{|w|w}|w| & Y_{|p|p}|p| & Y_{|q|q}|q| & Y_{|r|r}|r| \\ Z_{|u|u}|u| & Z_{|v|v}|v| & Z_{|w|w}|w| & Z_{|p|p}|p| & Z_{|q|q}|q| & Z_{|r|r}|r| \\ K_{|u|u}|u| & K_{|v|v}|v| & K_{|w|w}|w| & K_{|p|p}|p| & K_{|q|q}|q| & K_{|r|r}|r| \\ M_{|u|u}|u| & M_{|v|v}|v| & M_{|w|w}|w| & M_{|p|p}|p| & M_{|q|q}|q| & M_{|r|r}|r| \\ N_{|u|u}|u| & N_{|v|v}|v| & N_{|w|w}|w| & N_{|p|p}|p| & N_{|q|q}|q| & N_{|r|r}|r| \end{bmatrix}$$

$\mathbf{g}(\eta)$ is the restoring forces and moments vector

$$\mathbf{g}(\eta) = \begin{bmatrix} (W - B)\sin\theta \\ -(W - B)\cos\theta\sin\phi \\ -(W - B)\cos\theta\cos\phi \\ -(y_G W - y_B B)\cos\theta\cos\phi + (z_G W - z_B B)\cos\theta\sin\phi \\ (z_G W - z_B B)\sin\theta + (x_G W - x_B B)\cos\theta\cos\phi \\ -(x_G W - x_B B)\cos\theta\sin\phi - (y_G W - y_B B)\sin\theta \end{bmatrix}$$

This can be eventually written as,

$$\mathbf{M}\dot{\mathbf{v}} + \mathbf{C}(\mathbf{v})\mathbf{v} + \mathbf{D}(\mathbf{v})\mathbf{v} + \mathbf{g}(\eta) = \boldsymbol{\tau}$$

where,

$$\mathbf{M} = \mathbf{M}_{RB} + \mathbf{M}_A; \quad \mathbf{C}(\mathbf{v}) = \mathbf{C}_{RB}(\mathbf{v}) + \mathbf{C}_A(\mathbf{v}); \quad \mathbf{D}(\mathbf{v}) = \mathbf{D}_L(\mathbf{v}) + \mathbf{D}_Q(\mathbf{v}); \quad \boldsymbol{\tau} = \boldsymbol{\tau}_c + \boldsymbol{\tau}_E$$

Drag calculation of simplified geometry:

The drag acting on the robot is computed for three major components. These include the main cylinder body, the thruster and the rudder. The drag charts are referred to from Fluid Mechanics : Fundamentals and Applications by Yunus Cengel and John Cimbala.

ρ is the density of water, V is the velocity of flow, C_D is the drag coefficient.

Drag acting on the cylinder:

The system closely resembles that of a cylinder and the drag effects are computed keeping a cylindrical geometry in mind. The cylinder has dimensions of 0.1375 m diameter and 1.2 m length. The area used in calculations is the frontal area. The drag force is computed for the two cases of relative velocity as follows.

1. Flow along the axial direction:

The drag force is computed as:

$$F_{Dx} = 0.5 \times \rho \times V^2 \times C_{Dx} \times A_{frontal}$$

The drag coefficient for given length to diameter ratio of $(1.2/0.1375) = 8.7272$ is 1.

2. Flow along the radial direction:

The drag force is computed as:

$$F_{Dz} = 0.5 \times \rho \times V^2 \times C_{Dz} \times A_{frontal}$$

The drag coefficient for given length to diameter ratio of $(1.2/0.1375) = 8.7272$ is 0.8745.

Drag contributed by the thruster:

The thruster is modeled as a cylinder for simplification purposes to be of length 0.113 m and diameter of 0.1 m. The drag force is computed only along the axial direction as the area corresponding to the radial direction overlaps with the main body of the robot and is hence neglected. The drag force along the axial direction is computed similarly as above and the drag coefficient for length to diameter ratio of $(0.113/0.1) = 1.13$ is taken as 0.9.

$$F_{Dx} = 0.5 \times \rho \times V^2 \times C_{Dx} \times A_{frontal}$$

Drag contributed by the rudder:

The rudder in question has a NACA 0015 profile with chord length of 0.010 m, length of 0.0698 m and height of 0.040 m. There is no lift force acting while diving as the angle of attack is zero. Drag forces only along the axial direction are taken into consideration for the same reason as stated above. The drag force is computed as follows:

$$F_{Dx} = 0.5 \times \rho \times V^2 \times C_{Dx} \times A_{planform}$$

The drag coefficient is calculated as 0.01 for a chord length of 0.07 m and thickness of 0.01 m. Height of the rudder profile is 0.04 m and the area of consideration is the planform area and is calculated as a product of the chord length and the height of the rudder.

Buoyancy calculations:

The dynamics of a body especially when it is at the transition phase at the surface has not been discussed at length in academic literature. Most papers discuss the dynamics of bodies either while it is at the surface or while completely underwater. The dynamics at the transition stage is required to simulate the motion of the system in the mathematical model. Moreover, the shift in CoB and buoyancy values has an effect on the surface motion especially in this system that uses a rudder and thruster for navigating on the surface. It is also important to note that the system is likely to have a tilt that will have a significant influence on the CoB, buoyancy values and the dynamic nature of these quantities. To meet these requirements, it was decided to propose the dynamics of a body in this transition model as a new hypothesis.

The dynamics of the system is very similar to the existing model computed using the Newton Euler equations. The change is in the changing CoB and the magnitude of buoyancy. The values of these parameters are a function of the submerged volume and by extension a function of the current pose. The problem therefore is to calculate the CoB and the buoyancy magnitude as a function of the depth of the geometric center of the model and the pitch angle. This involves calculation of integrals.

The value of each integral varies on the shape of the cylinder submerged inside water. By extensive geometric analysis, the integrals were divided into two major categories: One involved when the geometric center is at a distance less than half the diameter and the other when this distance is larger. Each category is further subdivided into three categories, they being the locations at which the surface water level cuts the cylinder.

The corresponding integrals calculated after several iterations and cross verification are presented as follows:

$$0.5 \times l \times \sin(\theta_2) + 0.5 \times d \times \cos(\theta_2) - Z_0 = 0$$

$$\theta_3 = \theta_2 + 2 \times \text{atan}(d/l)$$

$$\theta_{\text{bridge}} = \text{acos}(2 \times Z_0/d) \text{ for } Z_0 < 0.5 \times d$$

$$\theta_{\text{bridge}} = 0 \text{ for } Z_0 \geq 0.5 \times d$$

$$l_t = 0.5dtan\theta + (Z_0 - 0.5dsec\theta)cosec\theta \text{ for:}$$

$$(Z_0 \geq 0.5d) \text{ or } (Z_0 < 0.5d \text{ and } \theta_{bridge} \leq \theta)$$

$$l_t = cot\theta(0.5d - Z_0sec\theta) \text{ for: } Z_0 < 0.5d \text{ and } \theta < \theta_{bridge}$$

Table 1: Volume submerged

<i>Submerged volume</i>	$Z_0 < 0.5d \text{ and } \theta < \theta_{bridge}$	$(Z_0 \geq 0.5d) \text{ or } (Z_0 < 0.5d \text{ and } \theta_{bridge} \leq \theta)$	$Z_0 \geq 0.5l$
$\theta = 0^\circ$	$\int_{-Z_0}^{0.5d} 2l\sqrt{(0.25d^2 - z^2)}dz$	$\int_{-Z_0}^{0.5d} 2l\sqrt{(0.25d^2 - z^2)}dz$	$0.25\pi d^2 l$
$\theta \leq -\theta_2 \text{ or } \theta \leq \theta_2$	$\int_{0.5ltan\theta - zsec\theta}^{0.5d} 2l\sqrt{(0.25d^2 - z^2)}dz + \int_{0.5ltan\theta - zsec\theta}^{-0.5ltan\theta - Z_0sec\theta} (2\sqrt{(0.25d^2 - z^2)} \times (l + cot\theta(z - 0.5ltan\theta + Z_0sec\theta))dz$	$0.25 \times \pi \times d^2 \times l$	$0.25\pi d^2 l$
$\theta_2 < \theta \text{ and } \theta \leq \theta_3$	$(0.25\pi d^2 l) - \int_{-0.5d}^{tan\theta(0.5l + l_t) - 0.5d} (2\sqrt{(0.25d^2 - z^2)} \times (0.5l + l_t - cot\theta(z + 0.5d))dz$	$(0.25\pi d^2 l) - \int_{-0.5d}^{tan\theta(0.5l - l_t) - 0.5d} (2\sqrt{(0.25d^2 - z^2)} \times (0.5l - l_t - cot\theta(z + 0.5d))dz$	$0.25\pi d^2 l$
$\theta > \theta_3$	$(0.25\pi d^2 (0.5l - l_t) + \int_{-0.5d}^{0.5d} (2\sqrt{(0.25d^2 - z^2)} \times cot\theta(z + 0.5d))dz$	$(0.25\pi d^2 (0.5l + l_t) + \int_{-0.5d}^{0.5d} (2\sqrt{(0.25d^2 - z^2)} \times cot\theta(z + 0.5d))dz$	$0.25\pi d^2 l$
$\theta = 90^\circ$	$0.25\pi d^2 (Z_0 + 0.5l)$	$0.25\pi d^2 (Z_0 + 0.5l)$	$0.25\pi d^2 l$

Table 2: X coordinate of CoB

<i>XoB $\times V_{submerged}$</i>	$Z_0 < 0.5d \text{ and } \theta < \theta_{bridge}$	$(Z_0 \geq 0.5d) \text{ or } (Z_0 < 0.5d \text{ and } \theta_{bridge} \leq \theta)$	$Z_0 \geq 0.5l$
$\theta = 0^\circ$	0	0	0
$\theta \leq -\theta_2 \text{ or } \theta \leq \theta_2$	$\int_{-0.5ltan\theta - Z_0sec\theta}^{0.5ltan\theta - Z_0sec\theta}$	0	0

	$(0.5l + \cot\theta(z - 0.5ltan\theta + Z_0 \sec\theta)) \int_{-0.5l}^{(0.5l + l_t)tan\theta - 0.5d} (2x \sqrt{(0.25d^2 - z^2)}) dx dz$		
$\theta_2 < \theta$ and $\theta \leq \theta_3$	$(0.5l + l_t)tan\theta - 0.5d \int_{-0.5d}^{0.5l} (2x \sqrt{(0.25d^2 - z^2)}) dx dz$ $\int_{\cot\theta(z+0.5d)-l_t}^{(0.5l + l_t)tan\theta - 0.5d} (2x \sqrt{(0.25d^2 - z^2)}) dx dz$	$(0.5l - l_t)tan\theta - 0.5d \int_{-0.5d}^{0.5l} (2x \sqrt{(0.25d^2 - z^2)}) dx dz$ $\int_{\cot\theta(z+0.5d)+l_t}^{(0.5l - l_t)tan\theta - 0.5d} (2x \sqrt{(0.25d^2 - z^2)}) dx dz$	0
$\theta > \theta_3$	$0.5 \times d \int_{-0.5 \times d}^{0.5 \times d} \int_{-l_t}^{\cot\theta \times (z+0.5 \times d) - l_t} (2x \sqrt{(0.25d^2 - z^2)}) dx dz$ $- 0.125\pi d^2 (0.25l^2 - l_t^2)$	$0.5d \int_{-0.5d}^{0.5d} \int_{l_t}^{\cot\theta(z+0.5d)+l_t} (2x \sqrt{(0.25d^2 - z^2)}) dx dz$ $+ 0.125\pi d^2 (-0.25l^2 + l_t^2)$	0
$\theta = 90^\circ$	$- 0.25l + 0.5Z_0$	$- 0.25l + 0.5Z_0$	0

Table 3: Z coordinate of CoB

ZoB \times $V_{submerged}$	$Z_0 < 0.5d$ and $\theta < \theta_{bridge}$	$(Z_0 \geq 0.5d)$ or $(Z_0 < 0.5d$ and $\theta_{bridge} \leq \theta)$	$Z_0 \geq 0.5 \times l$
$\theta = 0^\circ$	$0.5 \times d \int_{-Z_0}^{0.5 \times d} 2lz \sqrt{(0.25d^2 - z^2)} dz$	0	0
$\theta \leq -\theta_2$ or $\theta \leq \theta_2$	$0.5d \int_{0.5ltan\theta - zsec\theta}^{0.5ltan\theta - zsec\theta} 2lz \sqrt{(0.25d^2 - z^2)} dz +$ $\int_{-0.5ltan\theta - Z_0 \sec\theta}^{0.5ltan\theta - zsec\theta} (2z \sqrt{(0.25d^2 - z^2)}) \times$ $(l + \cot\theta(z - 0.5ltan\theta + Z_0 \sec\theta)) dz$	0	0
$\theta_2 < \theta$ and $\theta \leq \theta_3$	$-\int_{-0.5d}^{\tan\theta(0.5l + l_t) - 0.5d} (2z \sqrt{(0.25d^2 - z^2)}) \times$ $(0.5l + l_t - \cot\theta(z + 0.5d)) dz$	$-\int_{-0.5d}^{\tan\theta(0.5l - l_t) - 0.5d} (2z \sqrt{(0.25d^2 - z^2)}) \times$ $(0.5l - l_t - \cot\theta(z + 0.5d)) dz$	0
$\theta > \theta_3$	$0.5d \int_{-0.5d}^{0.5d} (2z \sqrt{(0.25d^2 - z^2)}) \cot\theta(z + 0.5d) dz$	$0.5d \int_{-0.5d}^{0.5d} (2z \sqrt{(0.25d^2 - z^2)}) \cot\theta(z + 0.5d) dz$	0
$\theta = 90^\circ$	0	0	0

The above equations were coded into MATLAB and their values were cross verified by values so obtained in a CAD modeling software. All the values for every case matched exactly, thus verifying the correctness of this exercise.

The buoyancy values and the CoB values for the other set of angles were calculated by making use of symmetry of the model. Limits were set as per requirement to determine border cases such as when the model becomes completely submerged and when it completely resurfaces especially during the returning sequence. The data calculated by the above mentioned exercise was incorporated into a lookup table and by carefully mapping the depth and theta angles to the rows and columns, the set of values can be easily accessed within each iteration.

Surface Model:

The surface navigation model as implemented by the analytical method, derives the mathematical modeling as stated from Thor I. Fossen's 'Handbook of marine craft hydrodynamics and motion control.' The model is defined for underwater vehicles but given the fact that the robot is almost 95% submerged, adopting this model is a reasonable hypothesis. In addition to this, there are certain constraints on which this model is based. They are as follows: The NACA 0015 is a streamlined model and hence the drag forces acting on the rudder can be neglected. It is assumed that the thruster in question produces a uniform thrust of about 20 N force which is well within the capabilities of the T200 thruster we have used in the robot design. Additionally, it is assumed that the relation between the drag coefficient and the rudder angle is linear.

The derivation as illustrated in Fossen is as follows:

The drag and lift forces are a function of the drag and lift coefficients which in turn are some function of the rudder angle. The relation is as follows:

$$F_{lift} = \frac{1}{2} \rho U_r^2 C_L(\delta_r)$$

$$F_{drag} = \frac{1}{2} \rho U_r^2 C_D(\delta_r)$$

where ρ is the density of water, U_r is the relative speed, A_r is the rudder area, δ_r is the rudder angle and C_L and C_D are the lift and drag coefficients respectively. Lift force is perpendicular to

the relative flow and drag is parallel and therefore, on resolving these forces in the body axes, we have,

$$\begin{bmatrix} X_R \\ Y_R \end{bmatrix} = \begin{bmatrix} \cos(\delta_r) & -\sin(\delta_r) \\ \sin(\delta_r) & \cos(\delta_r) \end{bmatrix} \begin{bmatrix} -F_{drag} \\ -F_{lift} \end{bmatrix}$$

Assuming linearity in the behavior of drag coefficients, we have,

$$C_L(\delta_r) = C_{L_0} + C_{L_\delta}\delta_r \quad C_D(\delta_r) = C_{D_0} + C_{D_\delta}\delta_r$$

Assuming no drag effects due to streamlined body, the drag forces can be taken as zero resulting in the following force components as expressed in the body axes,

$$X_R = -\frac{1}{2}\rho U_r^2 C_{L_\delta} \delta_r^2 \quad Y_R = -\frac{1}{2}\rho U_r^2 C_{L_\delta} \delta_r$$

This force is assumed to be acting on the point of attachment of the rudder. This is then taken as an external force acting on the system, modeled as follows for the net effect:

$$\tau = \begin{bmatrix} X_R \\ Y_R \\ 0 \\ -z_R Y_R \\ z_R X_R \\ x_R Y_R \end{bmatrix}$$

where, x_r and z_r are the distances of the rudder from the origin frame.

CFD based estimation of damping coefficients:

The drag coefficients being used in the model were estimated for a highly simplified cylindrical geometry from standard sources with little feedback w.r.t. the velocity and other surface effects. An exercise involving multiple simulations as stated above resulted in an estimation of drag values that act on the system. The first step was determining a function that would map velocities to forces. This was done using quadratic fitting of the force values. Almost 80% of the results followed a highly fitted quadratic map. The remaining cases were approximated to the nearest possible quadratic fit to avoid complicating the model. This is acceptable as deviations are obtained at higher velocities (~ 1.5 m/s) that are not normally

encountered for the current scenario. The next step was fitting these equations into the drag calculation part. The hypothesis followed for this is as follows:

The velocity of the robot can be broken down along the three body frame axes. The hypothesis states that the net force acting on the system is equal to the sum of forces acting on the system when the body moves only along each of the three directions (Principle of Superposition). The force along each direction is modeled as a vector of size 6 x 1 wherein each force component is estimated as the result of the quadratic fit previously obtained. For instance,

$$F_x = C_{LFxx} v_x + C_{QFxx} v_x |v_x| + C_{LFxy} v_y + C_{QFxy} v_y |v_y| + C_{LFxz} v_z + C_{QFxz} v_z |v_z|,$$

where C_{LFxy} and C_{QFxy} are the coefficients obtained from the quadratic fit of forces acting along the X direction due to velocity in the Y direction. Forces do not have contributions coming from rotational velocities however moments have contributions from the forces as well rotational damping forces.

$$\begin{aligned} M_{xx} = & C_{LMxx} v_x + C_{QMxx} v_x |v_x| + C_{LMxy} v_y + C_{QMxy} v_y |v_y| + C_{LMxz} v_z + C_{QMxz} v_z |v_z| \\ & + C_{LMx} p + C_{QMX} p |p|, \end{aligned}$$

where additionally C_{LMx} is the rotational damping moment about X axis and p is the angular velocity about X axis.

These rotational damping moments are the same as that obtained from the previous method of calculating damping coefficients. Empirical determination of these coefficients was not possible in this iteration. Future tasks can focus on the same. It is important to note that the forces obtained were different when the flow was reversed along the same direction. To account for the same in this highly empirical model, switching between the drag coefficients is done based on the direction of relative flow.

Chapter 4.b: Design and Development

The design of the prototype majorly consists of four interconnected subsystems, each addressing specific challenges. Those four subsystems are listed below:

a. Buoyancy Subsystem:

The main purpose of this subsystem is to control To meet the capability of staying afloat on the surface of water, resurfacing and diving into water, the two different buoyancy system are:

- Variable mass buoyancy system
- Variable volume buoyancy system

i) Variable Mass Buoyancy System:

It includes a water-filling ballast, water pump, solenoid valves, and penetrators. These penetrators were attached in the backside of the system ensuring minimal holes in the surface of the cylinder. This design aspect was considered in order to minimize leakages in the system. The ballast efficiently refills water, with its total consumption managed by the ballast. The model operates underwater, resulting in a high pressure at the inlet, with a relative pressure difference of 1 bar, given a target depth of 10 m.

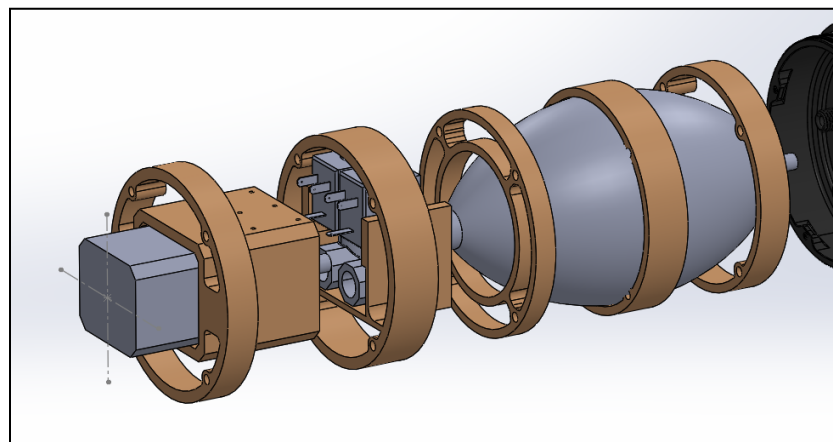


Fig 2: Buoyancy Subsystem Components

The water pump, a diaphragm pump, is specifically the KDLP600 model, featuring a maximum volume flow rate of 0.6L/min. A diaphragm pump is a type of positive displacement pump where a flexible diaphragm reciprocates, causing a change in volume to draw in and expel fluid. The bidirectional solenoid valves can handle a maximum pressure rating of 10 bar, matching the pump's 3 bar pressure rating. The system initiates with 1L of stored water, adjustable to account for miscellaneous masses in the system. Components of these subsystems are attached to the structures using fasteners.

ii) Variable Volume Buoyancy System:

In the variable volume buoyancy substem , the volume can be varied by means of a flexible member or sliding member. If a sliding member is used there is a compromise in sealing the system from water at greater depths as pressure of water increases with depth. If a flexible member is used there is no compromise in sealing rather stiffness of flexible member has to be accounted for with water pressure. Hence a flexible metallic bellow is used which has high radial stiffness and comparatively less axial stiffness. The metallic bellow behaves like a spring when compressed and let free.

If the system has to move down a ball screw mechanism coupled to a motor is used to compress the bellow. When it compresses, the net volume of the system decreases, buoyancy decreases and it goes down. By controlling the length of the bellow that can be compressed, the depth of the system from the surface can also be controlled. Ball screw mechanism has the least amount of mechanical resistance compared to lead screw mechanism, a similar mechanism that converts rotational motion of motor to linear motion. Moreover, this mechanism can produce high linear force for less rotational torque given. See figure 5 for better understanding of various parts in the variable volume system. When the system has to surface, the compressed force from the bellow helps with linear force from ball screws to push against the water pressure and expand in its volume. So, by displacing more water, more buoyancy is created and the system comes to the surface.

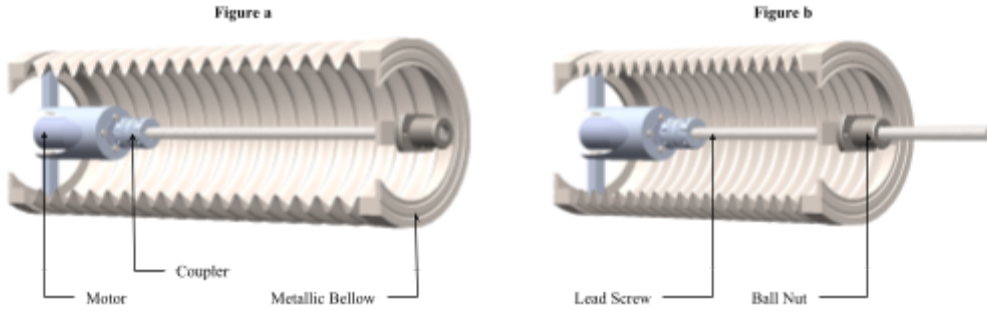


Fig. 3: Compression/Expansion Bellow for Change of Volume method

b. Electrical Subsystem:

The Electrical Subsystem functions as the central nervous system of the entire model, providing commands and overseeing the operation of the thruster and rudder. It incorporates a set of essential sensors and components, namely the pressure sensor, leak sensor, IMU sensor, GPS module, Battery Elimination Circuit (BEC), DC-DC converters, and a GoPro Camera, alongside additional penetrators. These elements are strategically positioned within a cage-like structure, securely fastened to 3D-printed components using bolts.

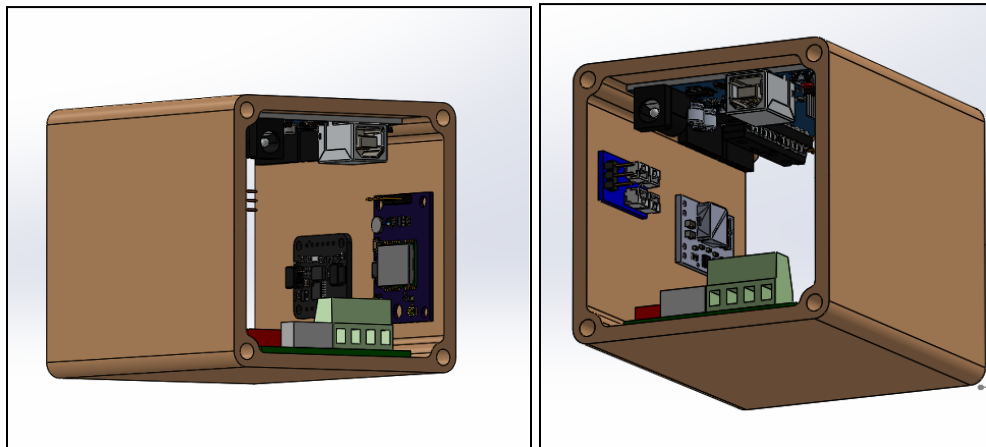


Fig 4: Electrical Subsystem Block

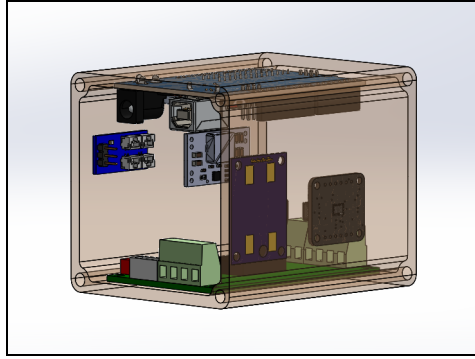


Fig 5: Electrical Components with 3D Printed Support Structure

Each sensor and component in this subsystem fulfills a critical role. The pressure sensors gauge the model's depth, facilitating the submerging and resurfacing mechanism. The leak sensor is a device designed to identify the presence of any unintended water ingress within the model, serving as a crucial safeguard against potential damage to internal components. The IMU sensor determines tilt angles, aiding in the evaluation of the mathematical model's performance and allowing for adjustments to the model's buoyancy. The GPS module, specifically the Neo GPS module, facilitates surface navigation. The Neo GPS module is a GPS technology that aids in precise navigation on the surface, providing accurate location data to the control system. The BEC regulates current flow from the battery, while DC-DC buck converters adjust the voltage levels to match the requirements of various components. The inclusion of a GoPro Camera enables capturing images from different depths, and multiple penetrators serve dual purposes of charging the battery and accommodating additional components.

c. Navigation and Control Subsystem:

The Navigation and Control Subsystem is a crucial component that comprises the rudder, thruster, ESC (Electronic Speed Control), stepper motor, motor driver, and a double-bearing arrangement. The thruster maneuvers the system on the surface, while the rudder, with its symmetrical NACA wing profile, is primarily used for thrust vectoring. To prevent water leakage, the rudder is attached through a double-bearing arrangement. The ESC is linked to the thruster to control its speed, ensuring a maximum speed of 3 m/s on the surface, with directional control managed by the rudder.

The rudder, constructed from PLA material with dimensions of 20x70 mm (Chord length x Length), is connected through a shaft within the double-bearing system. The double-bearing arrangement serves as a protective measure against water leakage by providing enhanced sealing around the attachment points of the rudder, preserving the integrity of the system.

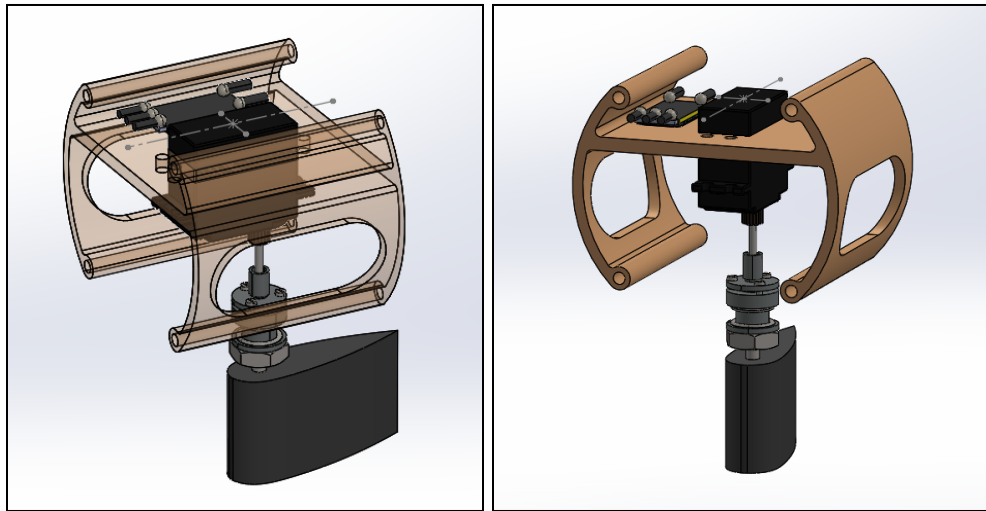


Fig 6: Thruster, Servo motor, Double bearing arrangement and Rudder Design

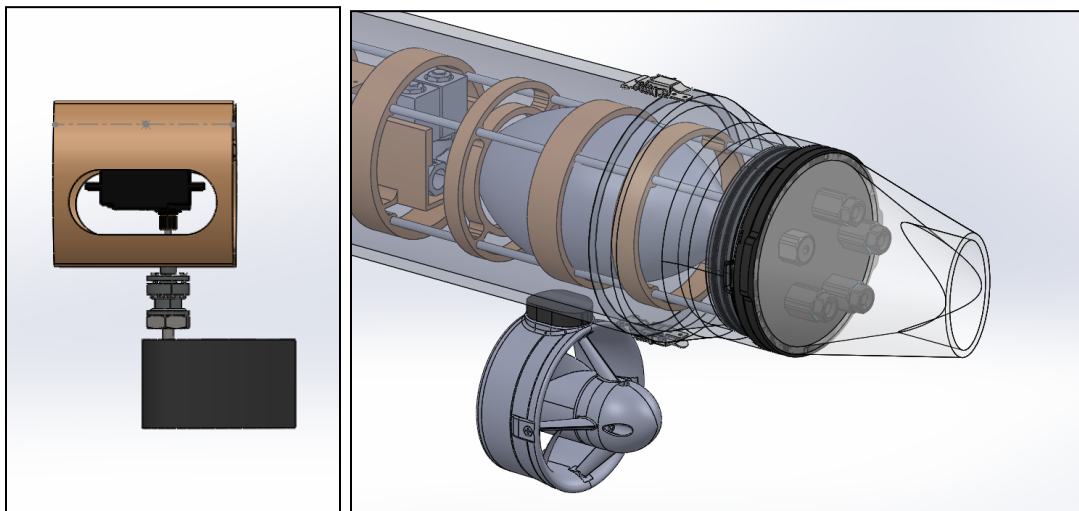


Fig 7: Thruster block with 3D printed attachment to the acrylic cylinder

The MG995 Metal Gear Servo Motor, used as the servo motor, exhibits a stall torque of 15 Kg-cm at 6.6 V, sufficient for effective thrust vectoring. Controlled by an Arduino MEGA, the TB6600 Motor Driver issues commands to the servo motor. With an operating voltage range

of 8-50V and an output current ranging from 0.3 to 4.5 A, the motor driver facilitates precise control.

d. Structural Subsystem:

The Structural Subsystem plays a pivotal role in maintaining the overall structural integrity of the model, particularly when it is in motion on the surface. Beyond its role in structural support, this subsystem provides a secure platform for the placement of various components. The primary construction material utilized is PLA, with certain components incorporating aluminum. The outer surface cylinder is constructed from acrylic, chosen for its ability to withstand pressure without leakage and its lower density compared to alternative materials.

To design the support structures, a Frames and Longerons structure design approach was employed, enhancing the overall stability. Frames and Longerons are structural elements that provide a robust framework for the model. Frames act as vertical supports, while Longerons are horizontal structural members. This combination enhances the strength and rigidity of the support structures.

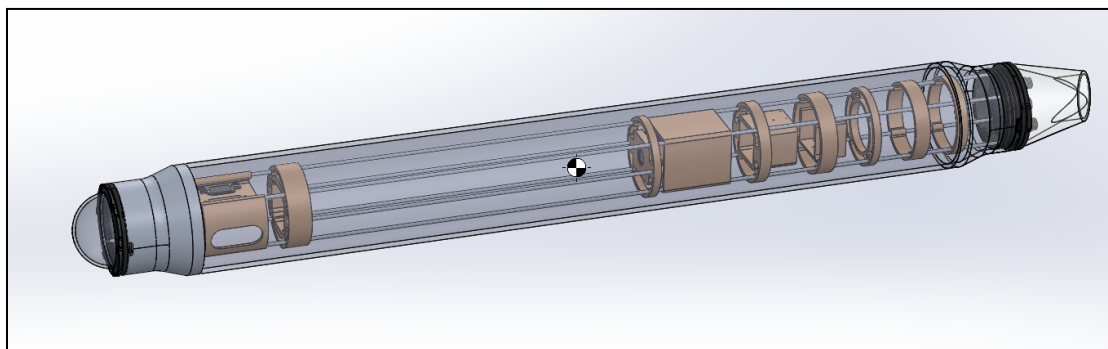


Fig 8: CAD Model of the Structural Subsystem

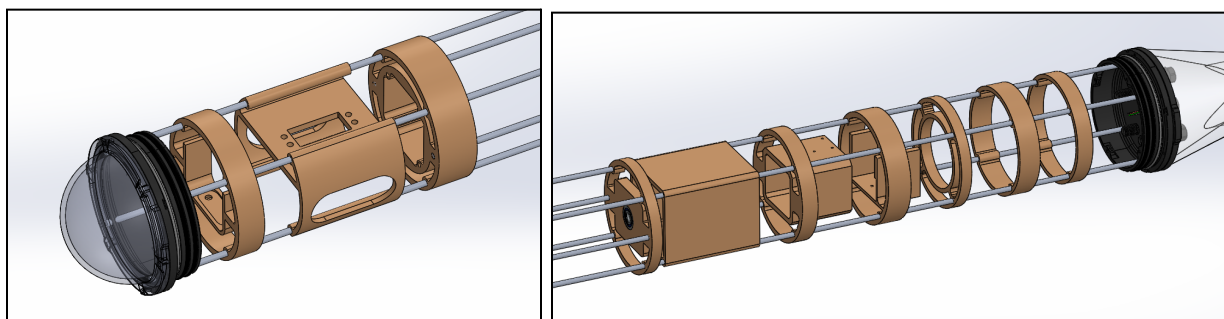


Fig 9: (i) Navigation system Casing (ii) Buoyancy Subsystem and Electrical subsystem Casing

All support structures are positioned on aluminum steel rods, strategically arranged to prevent component collapse in the face of sudden water waves. Acrylic transparent domes at the front of the cylinder enable the camera to capture essential images, and the presence of O-rings in the sealing arrangement ensures a watertight seal, preventing leakage. Similar aluminum domes at the rear house penetrators and the pressure sensor, equipped with O-ring groovings for additional sealing.

The placement of aluminum rods is meticulously planned to prevent stress accumulation at the system's corners, maintaining overall stability. A 2 mm clearance is provided for all components, with corresponding holes drilled for bolts and separate clearance for aluminum rods. This subsystem serves as a foundational support for other subsystems, preventing changes in position and orientation that could impact the model's Center of Mass. Bolts and threaded aluminum rods are utilized to secure the model in its respective positions. The 3D-printed support structures accommodate electrical components, servo motors, solenoid valves, the water pump, water ballast, and the camera.

Image Renderings:

Now that the entire design phase is concluded, our subsequent task involves creating renderings of the model. These renderings provide a realistic representation of the model's appearance in the real world. Additionally, to support the patent application process, these rendered images are crucial for inclusion. Furthermore, we've incorporated various shape configurations of the model when operating as a swarm of robots. The outcomes from the rendered images are provided below for reference. Keyshot was used to obtain all these renderings and it was coupled with Solidworks to import the material and other parameters used in the actual design,

The estimated Weight of the total model including the payloads is around 17.5 Kg and the dimensions of the total model is around 1.2 m in length and it also has a OD of 13.75 mm. Also, in the case of variable volume buoyancy systems we can have the outer cylinder made up of aluminum rather than acrylic. The reason is that aluminum have better water proofing method and it can also be clamped properly with the expansion bellow.

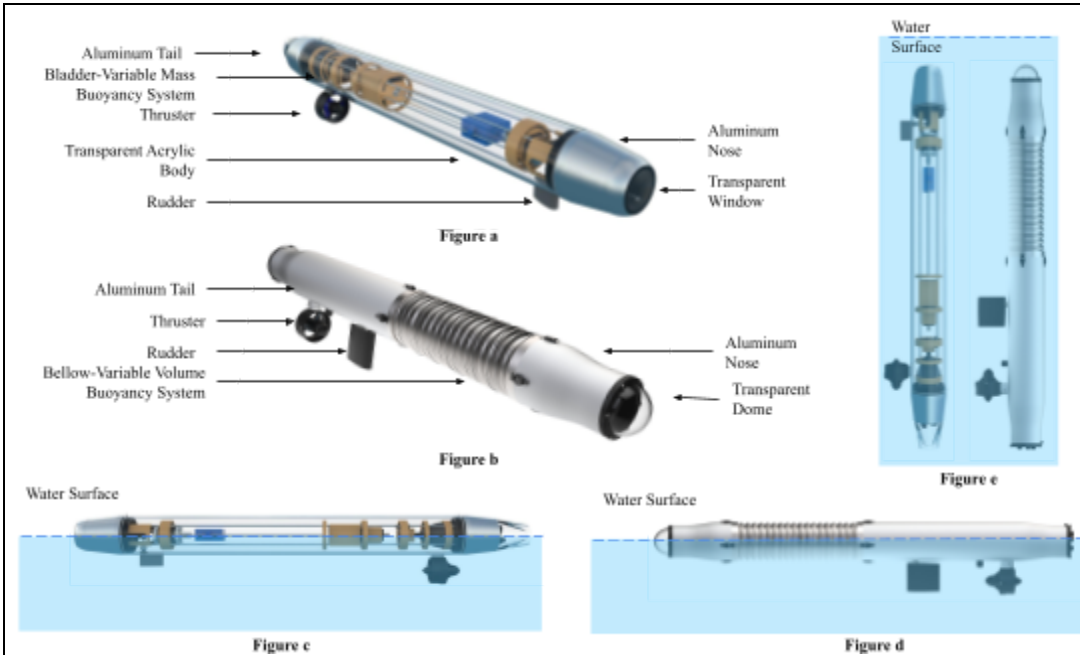


Fig 10: Figure a and b depicts the parts of variable mass and volume buoyancy prototypes. Figure c and d depicts the orientation of the system while on the surface of the water and figure e depicts the orientation of the system while underwater.

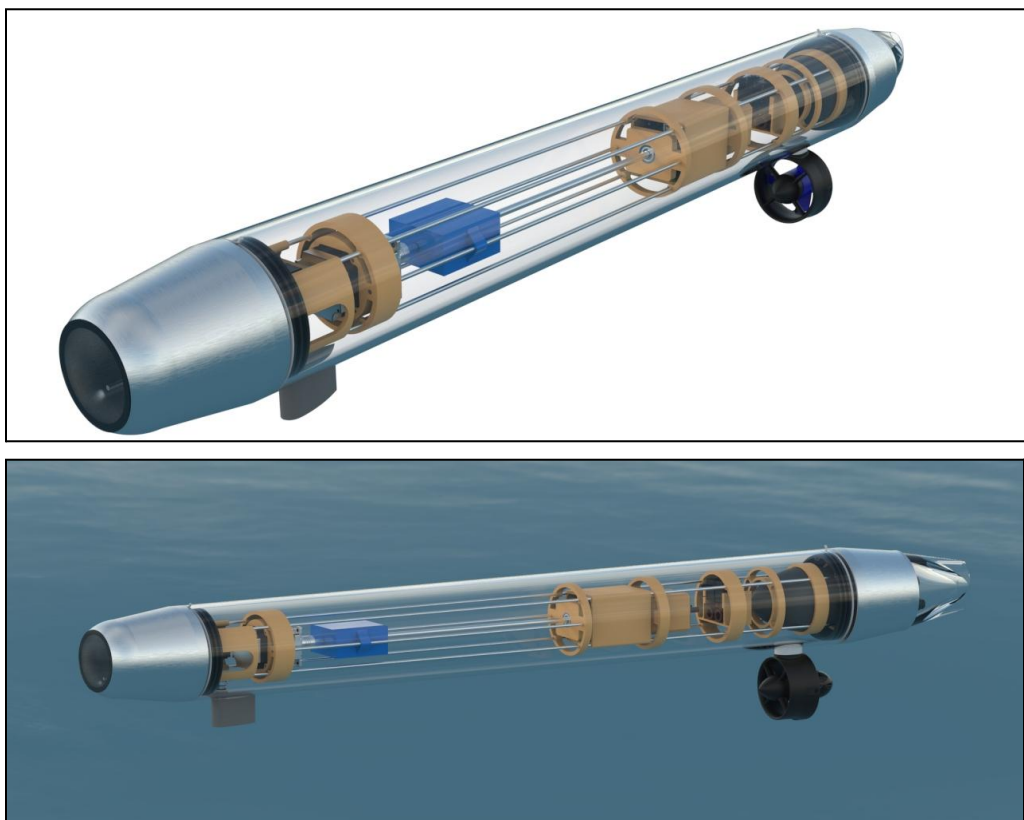


Fig11: Representation of Rendered CAD Models for Patent Documentation

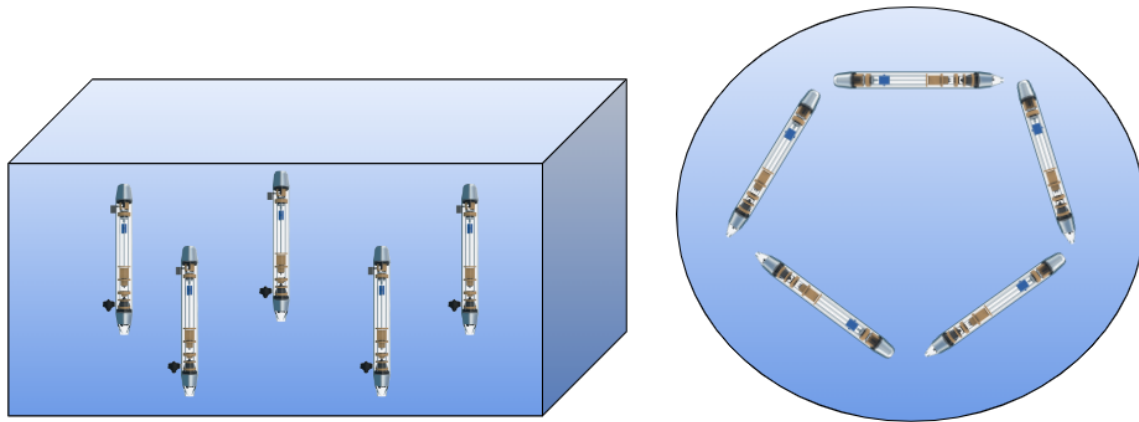


Fig 12: Image Renderings for Swarm of bots and Pentagonal Formation

Chapter 4.c: Experimental setup

The design of the entire model is done using the Solidworks assembly feature. A few of the CAD models for some on-the-shelf components are imported from online, and some of the parts were designed according to the data sheet specifications. The total structural subsystem is designed through Solidworks as a part file, and it is imported to create the final assembly. The CoM feature available in Solidworks is used to compute its position, and the mass assignment feature is used to assign the mass of those respective components.

The simulations for the mathematical model are done in Matlab and Simulink. The method of updating values is the global variables method and it is fairly clutterless. The system uses enabled systems for independently running each stage, function blocks and integrator functions available in a Simulink environment. The visual plot is done in a Matlab environment.

The Simulink model logs in data that is made available for plotting various parameters in Matlab. Currently, the sampling time being used is 0.1 seconds as the global variables method requires uniform time of computation for each function block. Initial values are sent in from the Matlab workspace. These values are particularly geometric constants.

For the buoyancy calculations, Desmos was extensively used for visualizing the various poses. Computation of integrals utilizes the symbolic toolbox available in Matlab.

CFD Simulations:

The primary aim of our Computational Fluid Dynamics (CFD) simulations is to extract the coefficients essential for the damping matrix, a critical aspect of our underwater robotics project. By thoroughly analyzing various velocities and rudder angles, we seek to understand how these factors influence hydrodynamic forces, crucial for optimizing the performance of our underwater vehicle.

Geometry Selection and Design:

In designing our simulation setup, we ensure that our model is mostly submerged, reflecting real-world conditions where the vehicle operates underwater. To define fluid flow boundaries accurately, we employ a bounding box structure, aligning it closely with the shape of our robotic model. Using tools like Solidworks, we merge the model and bounding box, creating a robust representation of our vehicle's hydrodynamic profile.

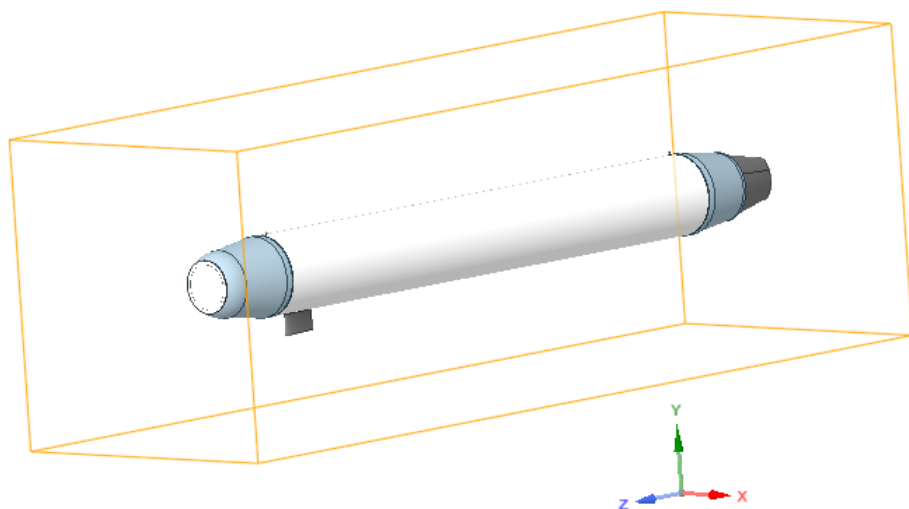


Fig 13: Bounding Box and the Redesigned CAD Model

Mesh Selection:

Meshing is a crucial step in ensuring accurate simulation results. We carefully select a bounding box size of 0.5m x 3m for the bounding box, balancing computational efficiency with accuracy. After convergence analysis, we settle on a 50mm mesh size, which effectively captures flow

dynamics. An unstructured adaptive mesh with a 40mm granularity is then generated, comprising 68,000 nodes to represent the complex fluid flow around the vehicle accurately.

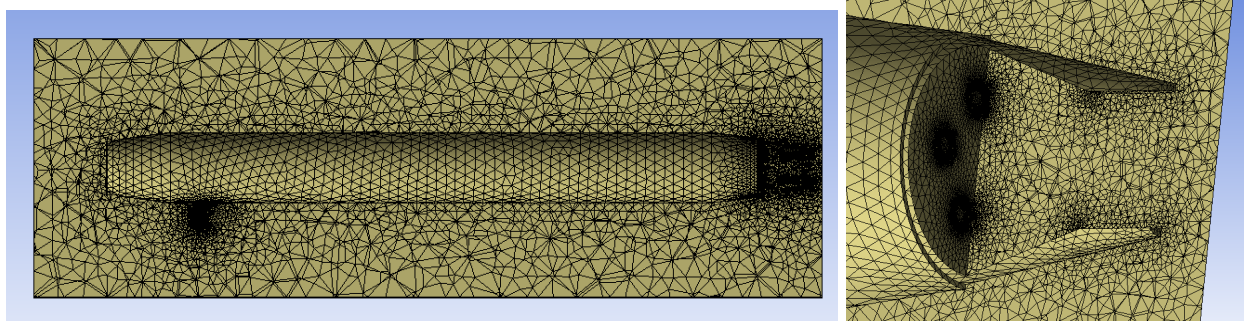


Fig 14: Unstructured Mesh for the Bounding Box (50 mm)

Boundary Conditions:

Defining precise boundary conditions is essential for reliable simulations. We meticulously set inlet and outlet boundaries, specifying fluid velocities along different axes to capture multidimensional flow patterns. Additionally, we designate model surfaces as wall boundaries to simulate surface interactions accurately. Leveraging the k-E turbulence model in ANSYS Fluent, we account for turbulent flow effects, ensuring realistic simulation outcomes. Here, for our simulations we will give an inlet velocity from 0.3 m/s to 1.5 m/s with a step of 0.3 m/s. These points help us to obtain the appropriate Force vs Velocity graph.

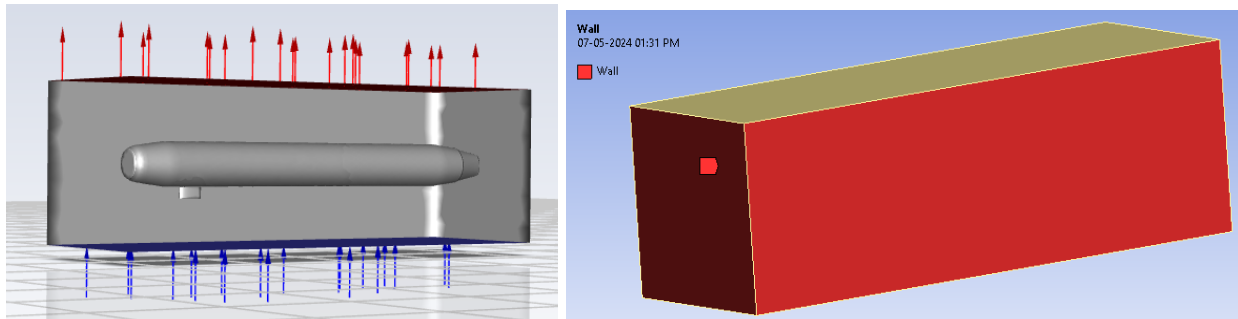


Fig 15: Defining Boundary Conditions (Inlet, Outlet & Wall Conditions)

Governing Equations:

Several governing equations are employed by ANSYS Fluent to calculate the forces exerted on the model. Additionally, we utilize fundamental equations such as the mass continuity equation

and momentum continuity equation in our analysis. The specific equations utilized in our computations are detailed below:

The **turbulent kinetic energy** equation

$$\frac{D}{Dt}(\rho k) = \nabla \cdot (\rho D_k \nabla k) + P - \rho \epsilon$$

The **turbulent kinetic energy dissipation rate** equation

$$\frac{D}{Dt}(\rho \epsilon) = \nabla \cdot (\rho D_\epsilon \nabla \epsilon) + \frac{C_1 \epsilon}{k} \left(P + C_3 \frac{2}{3} k \nabla \cdot \mathbf{u} \right) - C_2 \rho \frac{\epsilon^2}{k}$$

The **turbulent viscosity** equation

$$\mu_t = \rho C_\mu \frac{k^2}{\epsilon}$$

Continuity Equation

$$\frac{\partial \rho}{\partial t} + \frac{\partial}{\partial x_i}(\rho u_i) = 0$$

Momentum equation

$$\begin{aligned} \frac{\partial}{\partial t}(\rho u_i) + \frac{\partial}{\partial x_j}(\rho u_i u_j) &= -\frac{\partial p}{\partial x_i} + \frac{\partial}{\partial x_j} \left[\mu \left(\frac{\partial u_i}{\partial x_j} + \frac{\partial u_j}{\partial x_i} - \frac{2}{3} \delta_{ij} \frac{\partial u_l}{\partial x_l} \right) \right] + \frac{\partial}{\partial x_j}(-\rho \bar{u}_i' \bar{u}_j') \\ -\rho \bar{u}_i' \bar{u}_j' &= \mu_t \left(\frac{\partial u_i}{\partial x_j} + \frac{\partial u_j}{\partial x_i} \right) - \frac{2}{3} \left(\rho k + \mu_t \frac{\partial u_k}{\partial x_k} \right) \delta_{ij} \end{aligned}$$

Standard K-Epsilon Method:

The simplest “complete models” of turbulence are two-equation models in which the solution of two separate transport equations allows the turbulent velocity and length scales to be independently determined (7). The standard $k-\epsilon$ model in FLUENT falls within this class of turbulence model and has become the workhorse of practical engineering flow calculations in the time since it was proposed by Launder and Spalding. Robustness, economy, and reasonable accuracy for a wide range of turbulent flows explain its popularity in industrial flow and heat transfer simulations. It is a semi-empirical model, and the derivation of the model equations relies on phenomenological considerations and empiricism. As the strengths and weaknesses of the standard $k-\epsilon$ model have become known, improvements have been made to the model to improve its performance. Two of these variants are available in FLUENT: the RNG $k-\epsilon$ model

and the standard k- ϵ model. The standard k- ϵ model is a semi-empirical model based on model transport equations for the turbulence kinetic energy (k) and its dissipation rate (ϵ). The model transport equation for k is derived from the exact equation, while the model transport equation for ϵ was obtained using physical reasoning and bears little resemblance to its mathematically exact counterpart. In the derivation of the k- ϵ model, the assumption is that the flow is fully turbulent, and the effects of molecular viscosity are negligible. The standard k- ϵ model is therefore valid only for fully turbulent flows.

Thus for our fluid simulations, we considered using the k- ϵ method as the solver as it works well for fully turbulent flows.

The transport equations used for the standard k- ϵ model were given below:

$$\frac{\partial}{\partial t}(\rho k) + \frac{\partial}{\partial x_i}(\rho k u_i) = \frac{\partial}{\partial x_j} \left[\left(\mu + \frac{\mu_t}{\sigma_k} \right) \frac{\partial k}{\partial x_j} \right] + G_k + G_b - \rho \epsilon - Y_M + S_k$$

and

$$\frac{\partial}{\partial t}(\rho \epsilon) + \frac{\partial}{\partial x_i}(\rho \epsilon u_i) = \frac{\partial}{\partial x_j} \left[\left(\mu + \frac{\mu_t}{\sigma_\epsilon} \right) \frac{\partial \epsilon}{\partial x_j} \right] + C_{1\epsilon} \frac{\epsilon}{k} (G_k + C_{3\epsilon} G_b) - C_{2\epsilon} \rho \frac{\epsilon^2}{k} + S_\epsilon$$

Here, G_k represents the generation of turbulence kinetic energy due to the mean velocity gradients, G_b is the generation of turbulence kinetic energy due to buoyancy. Y_m represents the contribution of the fluctuating dilatation in compressible turbulence to the overall dissipation rate. C_1 , C_2 , and C_3 are constants. σ_k and σ_ϵ are the turbulent Prandtl numbers for k and ϵ , respectively. S_k and S_ϵ are user-defined source terms.

Solution Convergence:

Achieving convergence is paramount for obtaining reliable results. We set convergence criteria between 10^{-3} to 10^{-5} and initiate iterative computations in ANSYS Fluent. Using a hybrid initialization approach, we kickstart simulations with initial conditions conducive to convergence. Through iterative computations, we monitor convergence progress, analyzing force and moment vectors across various velocity and rudder angle configurations. These insights

drive our efforts to optimize the vehicle's hydrodynamic performance, advancing engineering innovation in underwater exploration.

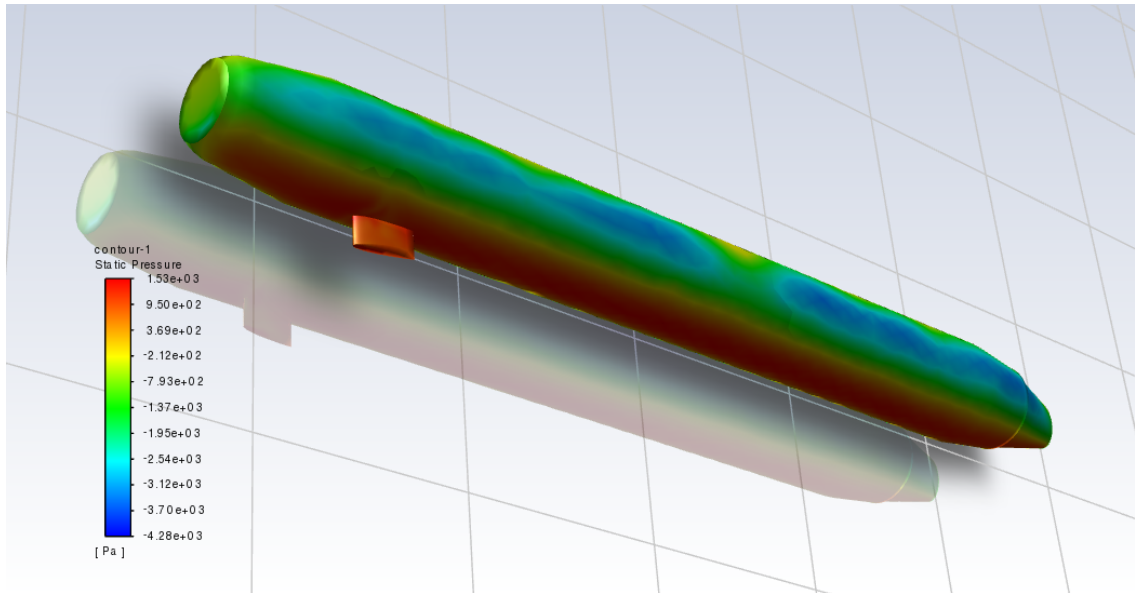


Fig 16: Static Pressure Contour obtained for Velocity along Y axis with M10 rudder angle.

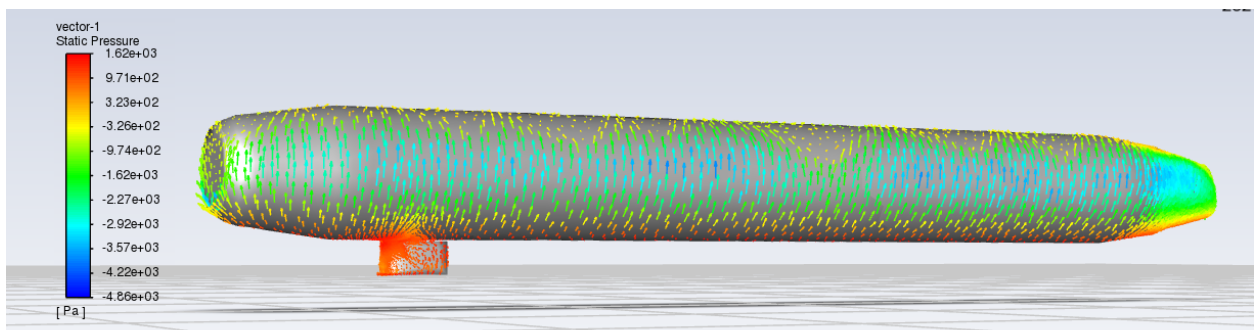


Fig 17: Representation of Velocity contour through the model along with static pressure obtained on the surface.

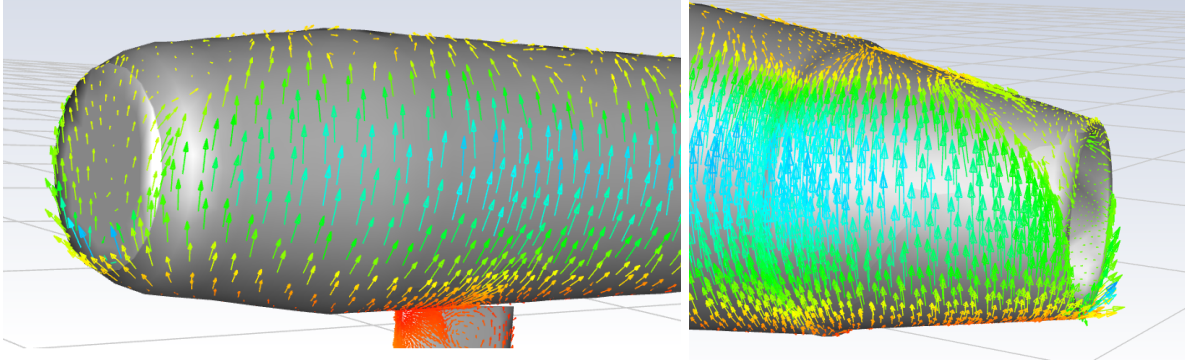


Fig 18: Velocity and pressure effects near the head dome and tail region.

Data extraction:

The mean speed of the robot while navigating on the water surface is predicted to be of the order of 1 m/s. A speed of this order is commonly found in existing applications and is a reasonable estimation given the build and design of the robot. Given the fact that on increasing the thruster force, a greater speed will be achieved, the speed won't exceed 1.5 m/s in any case. During diving and resurfacing operations the speeds do not exceed 1 m/s and linger somewhere near 0.4 m/s to 0.6m/s. To summarize, the robot speeds in any mode of operation do not exceed 1.5 m/s.

This data was used to set the limit of CFD simulations mentioned earlier. The force of damping acting on the robot is usually estimated to follow a quadratic nature. Higher order terms do exist, but their contribution is neglected. We have assumed the forces to follow a quadratic nature with linear and quadratic terms. Therefore, given a particular velocity in a certain direction, a CFD analysis for various speeds will give the forces and moments for each of these cases. This set of values for one configuration is then quadratically fitted to obtain linear and quadratic coefficients whose combination now will give forces and moments for any velocity in this range. This process is repeated for all pairs of combinations.

It is important to note that the robot in reality does not follow the level of symmetry as observed in a cylinder. It is therefore obvious that the forces and moments obtained when velocity flow is along a direction and then opposite to this direction won't be the same. Also, a

different rudder angle for surface motion will result in a different geometry and hence a different set of forces and moments. To completely cover all this cases, we performed simulations for a wide set of configurations and velocities which are stated below:

Parameters that can be varied:

Rudder angle: 0, 5 , 7.5, 10

Velocity: 0.3, 0.6, 0.9, 1.2, 1.5

Orientation of flow: Along X, Y and Z.

Direction: Positive and negative direction both.

This resulted in a total set of 120 simulations which completely covered all required combinations.

In addition to this we also performed simulations for cylinder and different orientations of rudder individually. The hope was to check if the net effect could be added up and yield the same result when both geometries were joined together. However, it was seen that this superposition was not true and this approach was discarded.

The data values obtained from 120 sets of simulation were fitted quadratically for each configuration and the results were cross verified. Nearly 21 cases showed poor fits. These poor fits were predominantly in cross diagonal entries, for example, cases like the force along Y when the velocity is along X. In these cases, outliers were removed to give reasonable fits. Moreover, the contribution of these force components is very less and has very less effect on the overall performance. A suitable assumption was made and such cases were also quadratically fitted.

The resulting coefficients were then incorporated into the mathematical model as explained previously.

Chapter 4.d: Iterations

i. Preliminaries

Mathematical Modeling:

The preliminaries of this project included a comprehensive review of research papers focused on understanding the fundamental kinematics and dynamics of surface-cum-underwater robots. The primary objective during this period was to revisit relevant literature and implement a simulation model in MATLAB Simulink based on the insights gained from these papers. Additionally, efforts were made to enhance the generality and efficiency of the model concerning input parameters and variables. The following research papers were referred to during this course:

1. *Investigations on trajectory tracking and dynamic station keeping control of an underactuated flat-fish type autonomous underwater vehicle*
 - Author: M. Santhakumar
2. *Design and Analysis of a Novel Underwater Glider – RoBuoy*
 - Authors: Thiagarajan Ranganathan, Sundaravalli Aravazhi, Sambit Mishra, and Asokan Thondiyath
3. *Design of a controllable variable buoyancy module and its performance analysis as a cascaded system for selective underwater deployment*
 - Authors: Thiagarajan Ranganathan, Vijendra Singh, Ranjith Nair, and Asokan Thondiyath

The dynamic model, as outlined in the research paper (1) by M. Santhakumar, was implemented in MATLAB Simulink. The model assumes the robot's body to be a rectangular fish with a triangular nose on one end. It accepts body characteristics and coefficients as inputs, providing a visual representation of the robot's motion. A temporal plot of various state variables and the path followed by the robot was also recorded. This initially developed dynamic model underwent generalization and improvement concerning input handling. Modifications were introduced to account for water intake into the system, responsible for controlling mass addition. The Data Storage Method was used to update values simultaneously, however it was quite tedious to keep up with the numerous values. The results obtained were similar to those suggested in the research paper that validated the correctness of the dynamic model being simulated. A preliminary literature survey was initiated to understand the surface kinematics and dynamics of a boat.

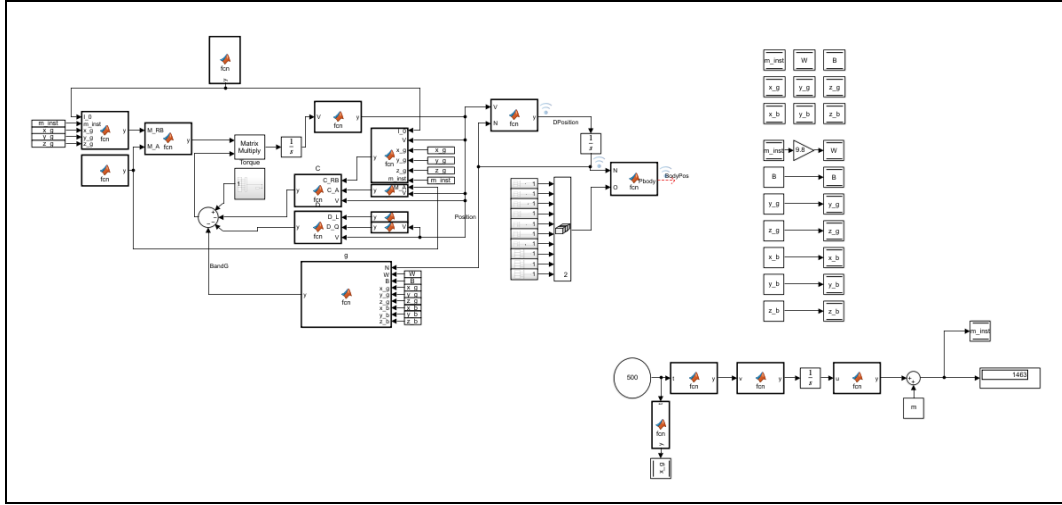


Fig 19: Implementation of model in Simulink as stated in '*Investigations on trajectory tracking and dynamic station keeping control of an underactuated flat-fish type autonomous underwater vehicle*' - M. Santhakumar. This model uses a Data Storage Method and employs a control loop.

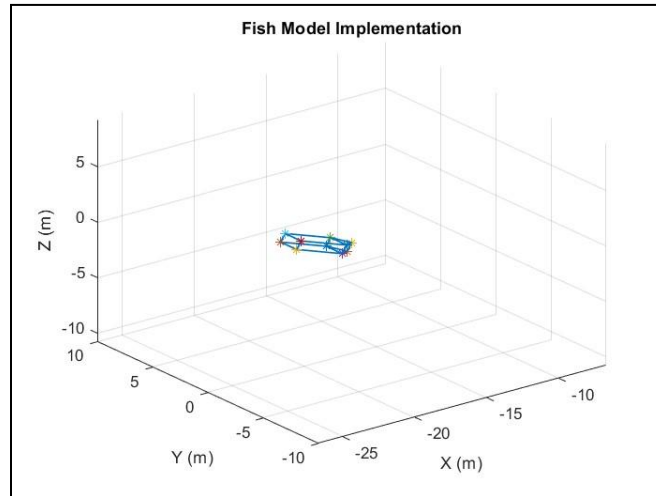


Fig 20: Simulation screengrab for testing out model in Simulink. The amount of water intake was varied and the system behavior was verified.

Design:

The initial design approach for the model involved considering a Syringe-Actuator mechanism for water intake and expulsion, with CAD design and component exploration conducted initially. However, due to limitations in space, power consumption, and pressure considerations, we decided to implement a water ballast system regulated by solenoid valves and

a water pump. The chosen water pump model, KDLP600, was carefully selected for its compatibility with the system's requirements. It can withstand a pressure rating of 3 bar, which is much anticipated for our prototype. The overall design, including the model and solenoid valves, was efficiently executed using Solidworks.

ii. Iteration 1

Mathematical Modeling:

The first iteration involved simulating the actual geometry of the system. This included incorporating the shift in the CoG with time and other parameters such as hold times, water intake speeds, water intake time etc.

The initial model consisted of a simple cylindrical geometry with the center of mass located at a distance vertically below the CoB, which was assumed to be constantly fixed at the center of the model. In this model the damping coefficients were calculated and fed into the damping matrix. Coefficients for added mass were also calculated in a similar manner and the model was simulated. The method of storing variables was updated to the global variables method that gave better control over the updation of values and was far more efficient.

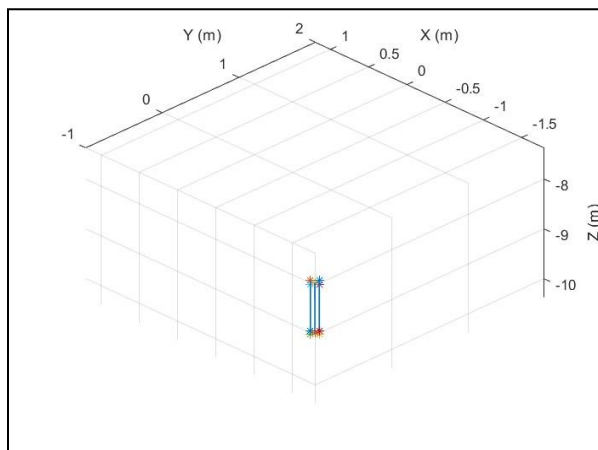


Fig 21: A perfect 90° dive achieved by ensuring that CoG stays near the X axis

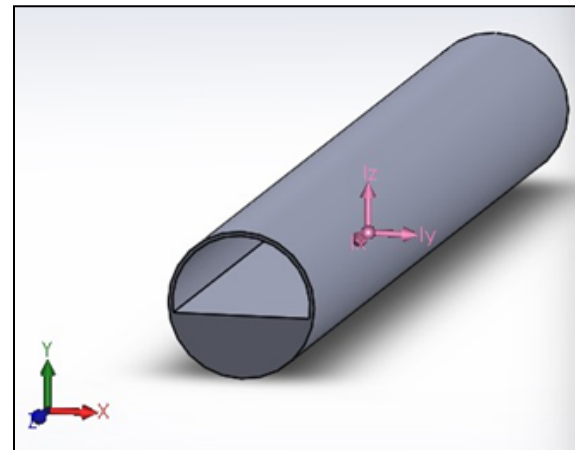
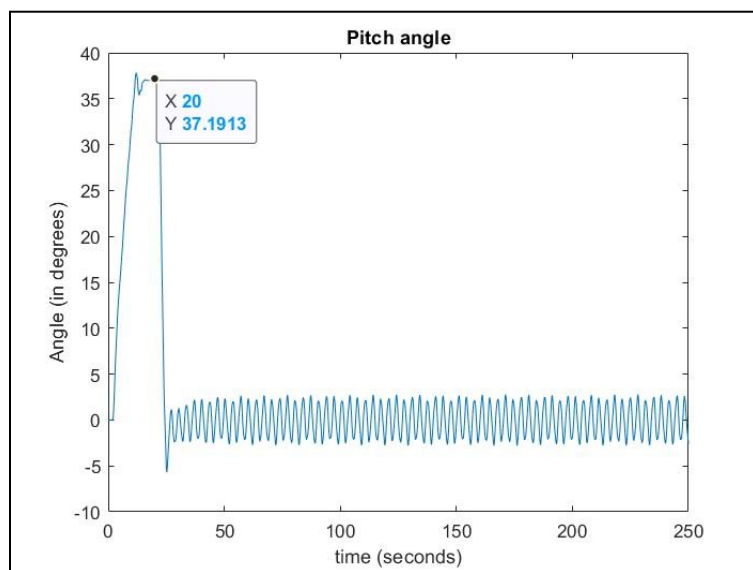
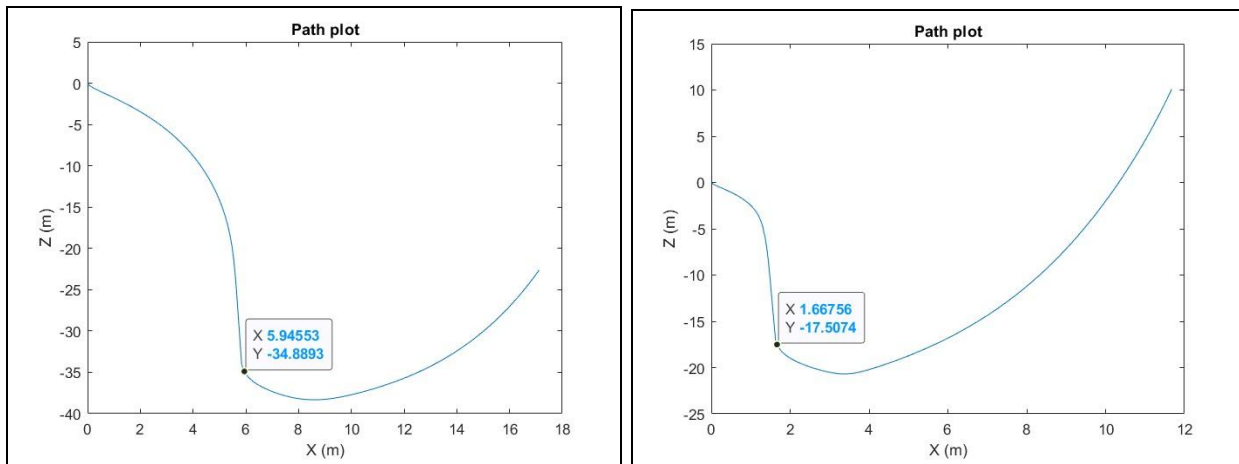
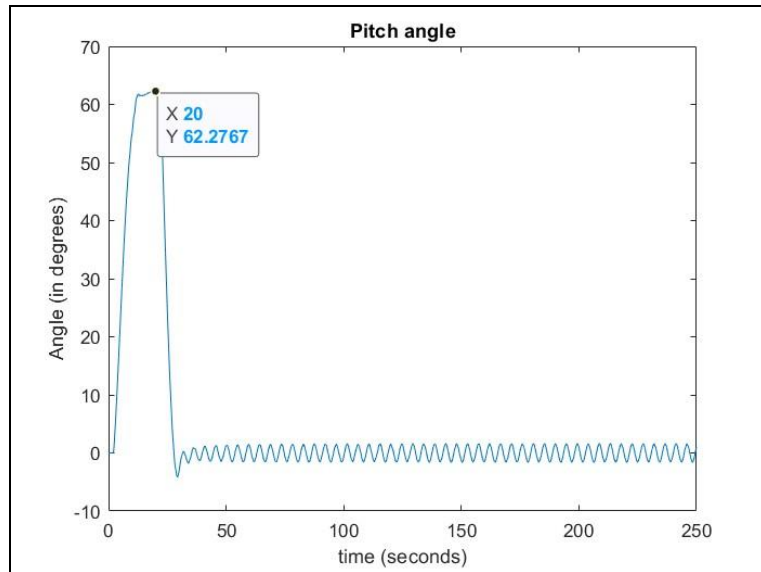
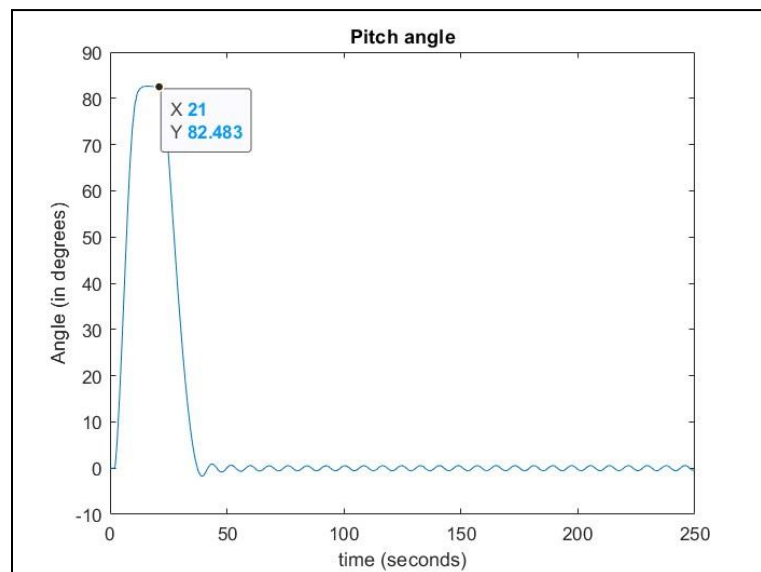


Fig 22: Simplified cylinder model.





(ii) Z coordinate 2 cm below axis



(iii) Z coordinate 1 mm below axis

Fig 25: Increase in the pitch angle as distance of CoG from X axis decreases from 5 cm to 2 cm to 1 mm.

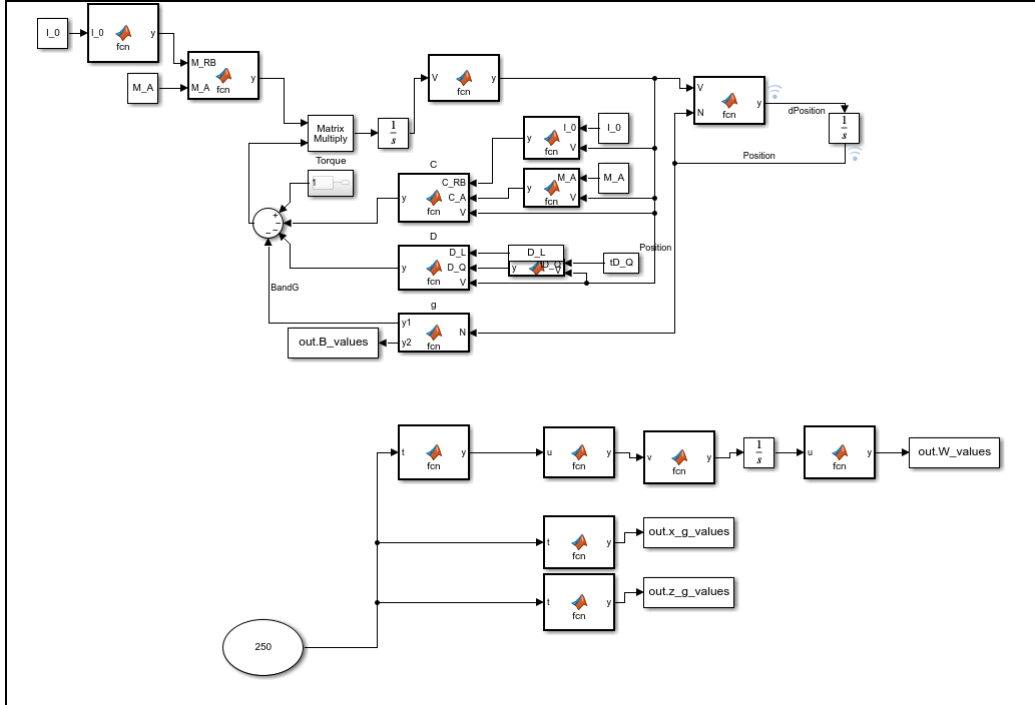


Fig 26: Modified model to support global variables method of updating values

On running simulations it was observed that the shift in CoG due to water filling was sufficient to achieve the vertical orientation however its speed was solely a function of the water filling rate. And since the downward motion and pitching motion were not decoupled, the drift increased significantly as the water filling time increased.

Another crucial observation made was that, at zero position the CoG had to vertically coincide with the CoB. Deviations would result in an increase in the initial tilt angle that was not desirable. Keeping this development in mind, it was observed that in most cases a perfect pitch was not achieved and the value saturated at around 60° , giving a large drift. This was because, though the CoG shifted horizontally, the vertical shift was negligible due to the added water. Hence an important conclusion made at this stage was that the CoG needed to shift as close to the X-axis as possible and move farther away from the geometric center to generate sufficient torque to achieve quick pitching and hence less drift. A solution to this proposed in the design model was to keep the water tank farthest away from the X axis on the other side of the CoG (which itself had limitations due to size) or to move the CoG closest to the geometric center that risked an unstable equilibrium.

Mechanical Design:

From a design standpoint, this iteration commences with the outcomes derived from the mathematical model. Calculations determined that the cylinder's diameter should be 11.3 cm and its length be 1 m. The acrylic cylinder was subsequently designed with a thickness of 9 mm. Special attention was given to the starting and ending grooves of the cylinder to ensure compatibility with commercially acquired domes from Bluerobotics. The design of frames and longerons was meticulous, aiming to accommodate all components while allowing flexible movement relative to each other.

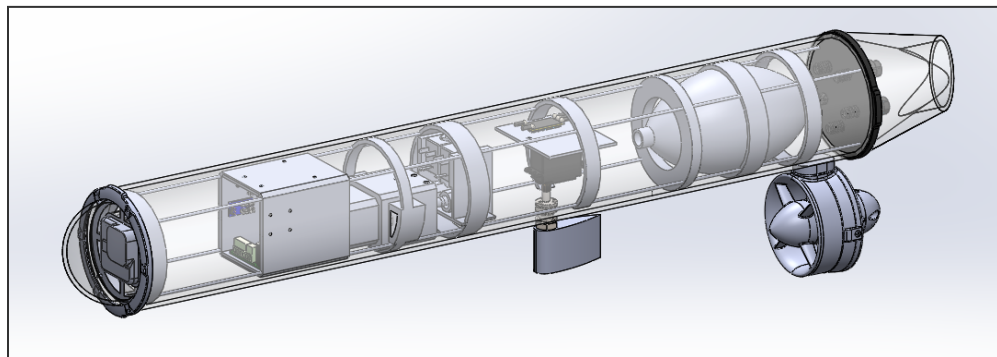


Fig 27: CAD Model for Iteration 1 (Isometric View)

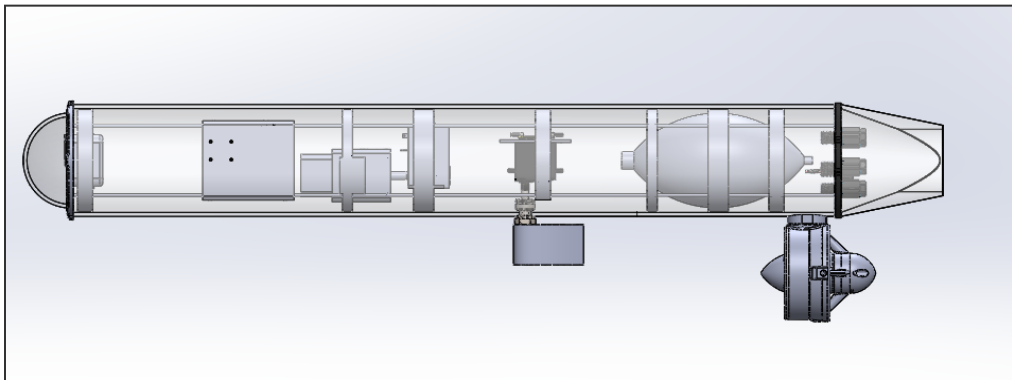


Fig 28: CAD Model for Iteration 1 (Side View)

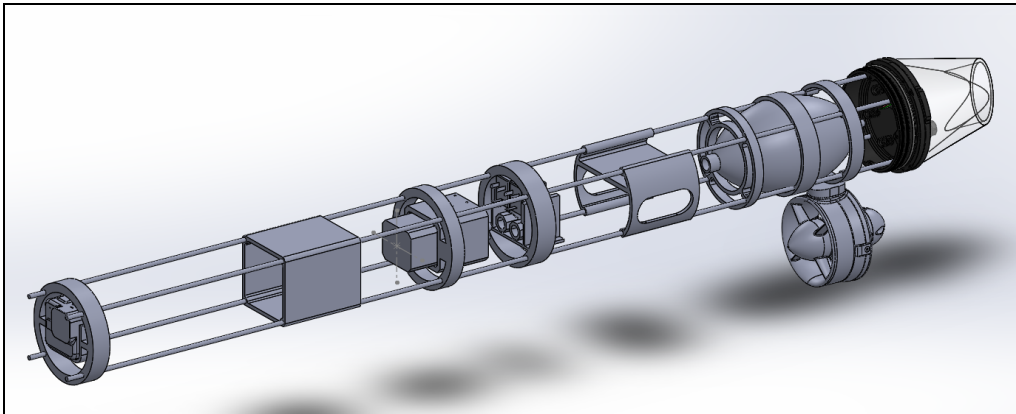


Fig 29:Skeletal Structure of the CAD Design (Frames and Longerons Structure)

The primary design objective here was to achieve a center of mass (CoM) slightly lower than the CoB (CoB) in the +z direction. Also, to factor in the shift in center of mass, the weights of each component in the system were initialized. The frames and longerons structures play a pivotal role in managing this aspect, designed to optimize the utilization of available space within the model.

In the sequencing of components, the electrical subsystem takes the lead along the aluminum rod, followed by the water pump and solenoid valves. Subsequently, the rudder part, including the servo motor, is positioned, followed by the water ballast at the end. Initially, the plan was to place the ballast at the center of the model, but a subsequent adjustment was made to position it at the end . This adjustment allows the battery, a significant weight contributor, to be accommodated in the front end. The overarching goal is to strike a balance between these components to achieve equilibrium and coincide the COB and COG vertically. The targeted mass for the system at the conclusion of this iteration is set at 10 kg. The total shift in Centre of Mass obtained for this case is around 4 cm. Increasing this shift improves the speed of tilt.

iii. Iteration 2

Mathematical Modeling:

A crucial observation made at this stage was that the change in mass needed for vertical motion had to be decoupled from the need to achieve a vertical pose. This was because, when the added mass of water is released to return back to the surface, the CoG also shifts back to the original position and the orientation returns to the horizontal position, which is contradictory to the vertical pose required. Hence, it was decided that a separate mass component inside the system should move to achieve the pitching motion. This would be independent of the intake of water taken into or released from the system and would guarantee that the pose remained vertical throughout the motion. However to achieve the fastest possible shift and a magnitude of shift sufficient enough to maintain the pose, this moving mass weight needed to be significant. Also, it was concluded that the closest one gets to a vertical pose solely depends on the distance of the CoG from the X axis. The value decreases especially on intake of water and enables the tilt to go to almost 87° , a very good figure. By way of iterations, it was decided that a moving mass of ~ 3 kg would suffice this requirement. However, this would increase the weight and demand an increase in diameter. Plus, there needed to be an additional buffer to account for the miscellaneous added weights. So, the system was revamped to now be of 13.75 cm diameter and 1.2 m long. The increase in length was adopted to increase the buoyancy as the diameter was restricted due to availability of materials.

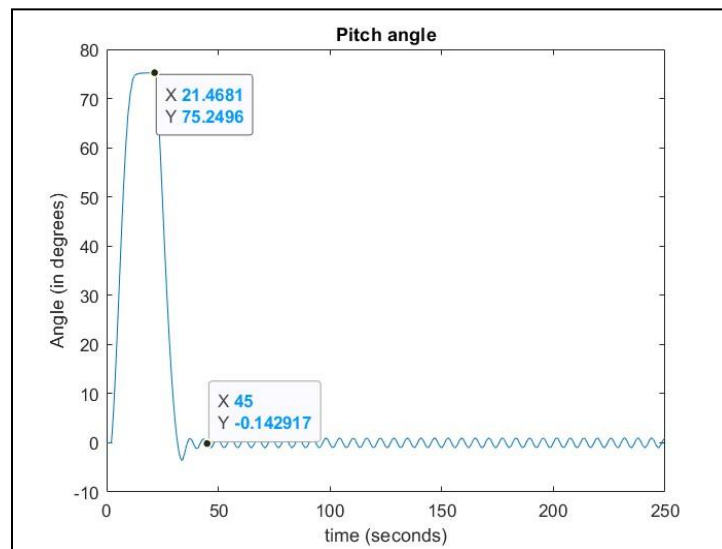


Fig 30: Pitch angle returning to zero on release of water. This requires the pitching to be decoupled from mass change.

This iteration also included computation and formulation of buoyancy related parameters. The system was visualized in Desmos to identify the various stages. The integrals were computed in Matlab and the results were cross verified by a corresponding model in CAD software for a cylinder with the same position, orientation and submerged volume. The data matched all possible cases and all results were extremely accurate.

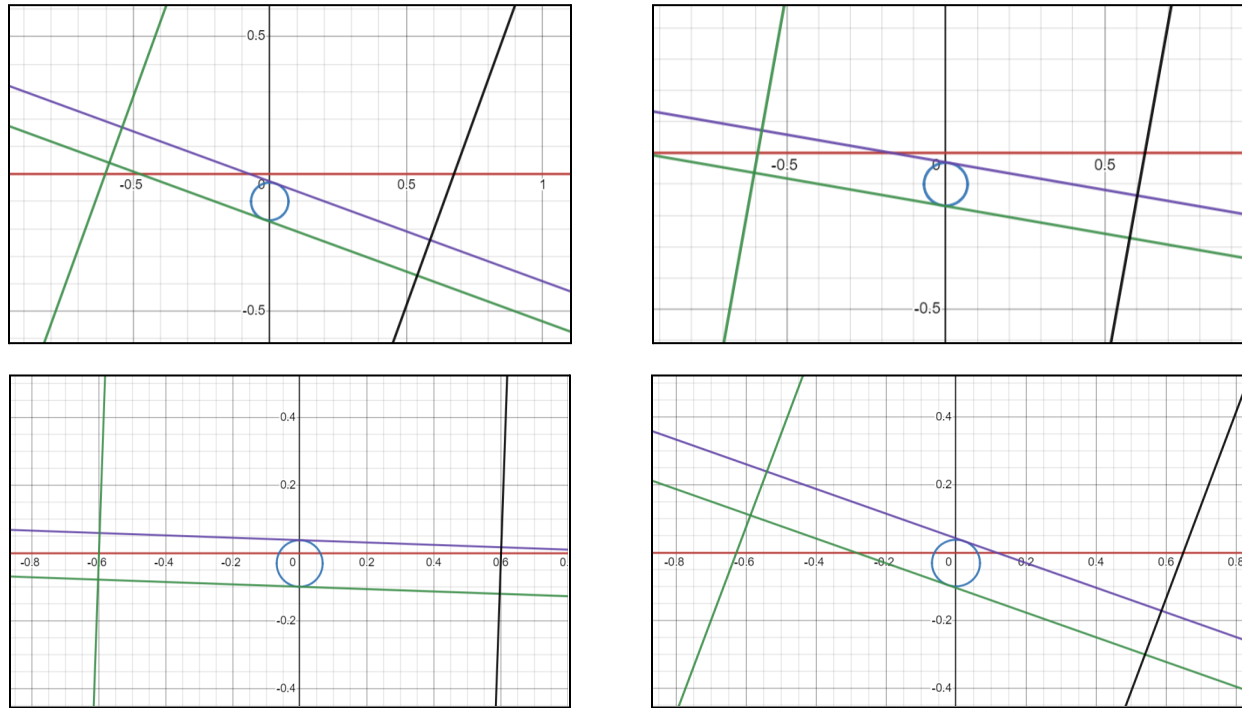


Fig 31: Different scenarios of submerged volume for the cylinder.

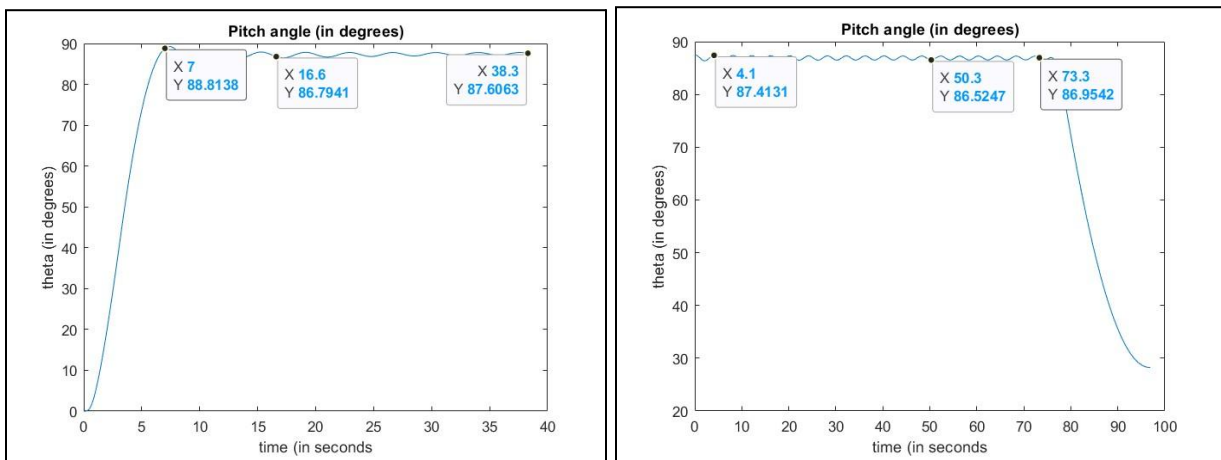


Fig 32: Pitch maintained at $\sim 90^\circ$ throughout the dive and resurface phase till reaching surface.

Design:

This iteration initiated with the insights derived from the mathematical model, leading to the calculation of the prototype's diameter and length. The targeted mass for the system in this iteration was set at an unspecified value. A new subsystem was introduced to the model, aiming to manipulate the Center of Mass (CoM) by moving the battery along the x-axis. This strategic shift assists in achieving the initial tilted position, facilitating the subsequent submersion of the model underwater through the use of the ballast.

As a part of this subsystem, initially, a lead screw mechanism was implemented for battery movement, but complications arose when accommodating the opposite end of the lead screw within the limited space allocated for the electrical subsystem. To overcome this challenge, an alternative shifting mechanism was conceived. The lead screw motor in the previous model is replaced with the NEMA 23 stepper motor, chosen for its precision. This played a critical role in controlling the battery's movement. With a remarkable maximum linear speed of 70 mm/s, when constrained to rotational motion along the x-axis. Also, the NEMA 23 stepper motor shaft end is connected to a flexible coupling. This coupling effectively linked the servo motor's shaft with an externally threaded rotating rod. The internal hole of the battery pack was threaded, facilitating smooth translational motion along the x-axis. Stability was ensured by three aluminium rods, contributing to a constrained and compact design. The rod's end positions were equipped with ball bearings securely attached to the 3D-printed structure. Additionally, a stop mechanism was incorporated to limit translational motion.

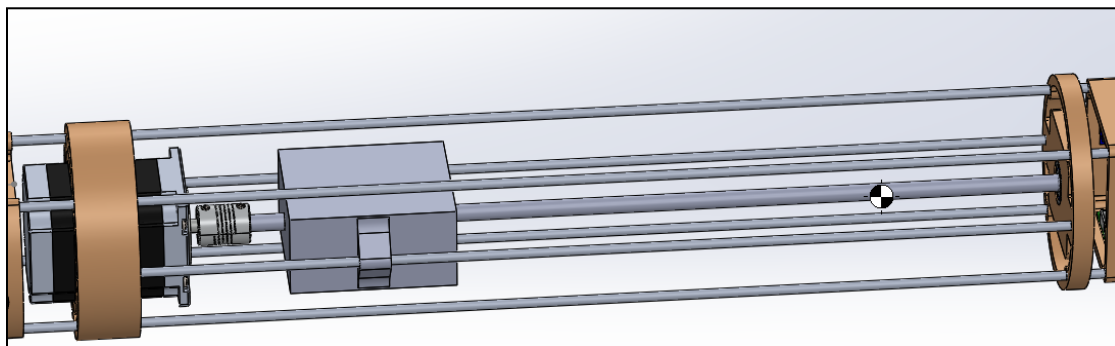


Fig 33: Actuator Subsystem - Control of CoM of the Model

The observed CoM shift in this design was a substantial 7 cm, representing a notable improvement over the previous model. To further enhance performance, buoyancy foams were strategically added in the step-down regions of the cylinder. This not only mitigated drag effects but also provided supplementary buoyancy support.

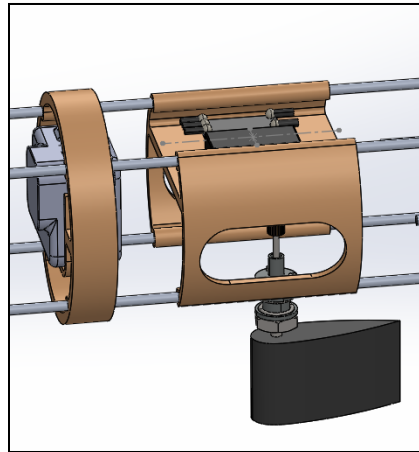


Fig 34: Positioning of Rudder in the front for ease of construction

However, challenges emerged during this iteration. The introduction of extra components and alterations to the outer diameter of the cylinder led to a significant increase in the system's mass. In response, a proposed solution involved adding an extra cylinder with an outer diameter of 11.3 cm on top of the existing one, aiming to boost the buoyancy limit. Simultaneously, the prototype's length was adjusted to approximately 1.2 m. While these modifications were anticipated to improve buoyancy, they incurred an additional mass of 3.5 kg to the system.

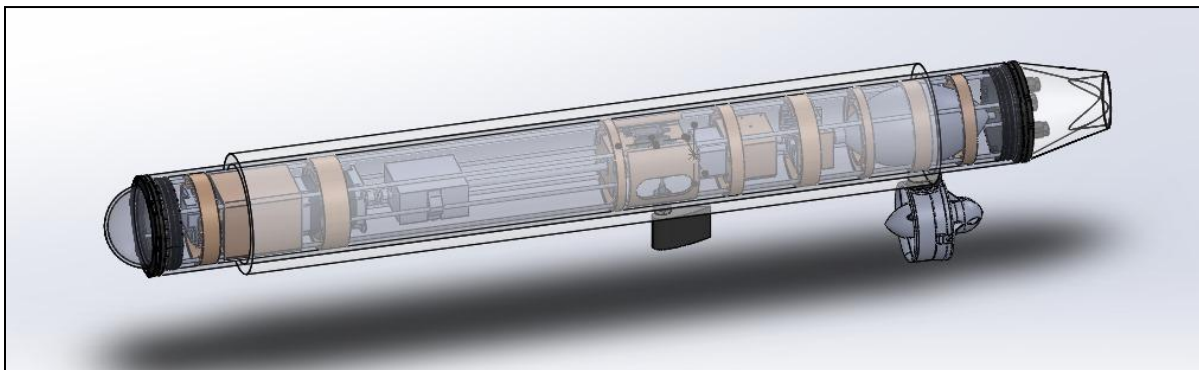


Fig 35: CAD Model Obtained at the end of Iteration 2

Another consideration was the thickness of the cylinder at the center location, initially set at 3.4 cm. Recognizing that this thickness was excessive for a system operating at a depth of 10 m, adjustments were made, resulting in a reduction of the additional payload limit. A noteworthy constraint encountered was the inability to perform internal tapering in the acrylic cylinder, posing a challenge in optimizing the model's internal geometry for enhanced performance.

iv. Iteration 3

Design:

In this iteration, a critical design challenge revolved around minimizing the mass of the entire system by addressing the excessive thickness in the CAD model, which was deemed unnecessary for the prototype. Additionally, a key consideration was ensuring the correct alignment of the front and rear domes with the cylinder, along with the incorporation of O-rings to prevent leakage into the model.

To address these concerns, a decision was made to maintain the outer diameter of the cylinder at 13.75 cm while significantly reducing the thickness to 6 mm. The cylinder's length was set at 1 m, with an additional 20 cm length accommodated by employing two aluminum cap structures—one at the front end and the other at the rear end—connecting to the main cylinder. External latches and O-rings were utilized to secure these aluminum structures to the acrylic cylinder, ensuring a watertight seal. External latches are mechanical fasteners that secure the aluminum cap structures to the acrylic cylinder, providing a streamlined solution for connecting and disconnecting components. Bolts were employed to attach the latches to the model, enhancing structural integrity and preventing water leakages.

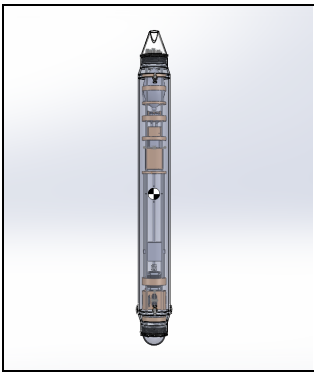
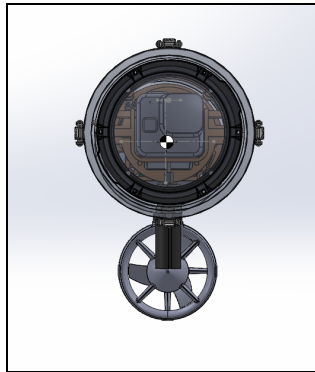


Fig 36: CAD Model: Front and top View at the end of iteration 3

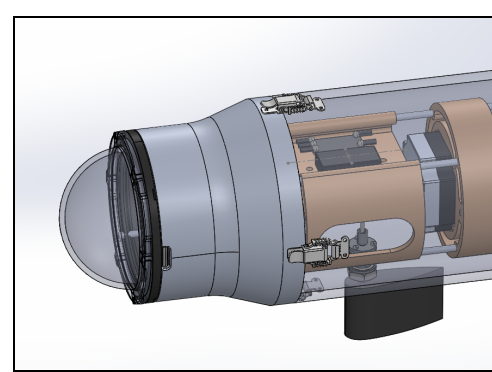


Fig 37: Aluminium Cap attachment along with Latches and O-Rings

With these design changes, the current model achieved a reduced mass of 12.6 kg, accounting for an additional 2.5 kg for bolts and other payload considerations. An increased positive buoyant consideration of 2.65 kg was factored in, resulting in a total mass of 17.75 kg for the entire system. Importantly, these alterations did not affect the total length of the model, and there was no variation in the outer diameter of the model.

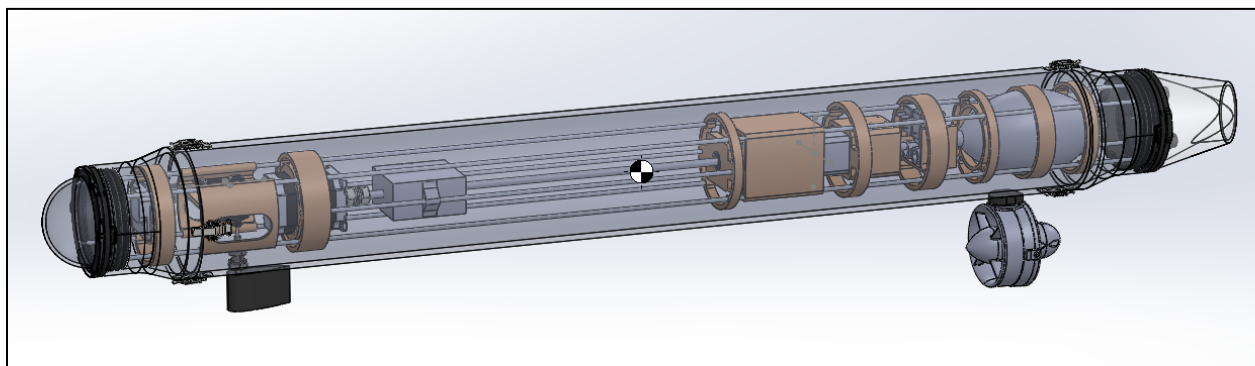


Fig 38: CAD Model at the end of Iteration 3

Mathematical Modeling:

At this stage, the actual values of the system were computed from the updated CAD model and fed into the current model. These updated values included geometric parameters like center of mass of crucial components, initial and final position of actuator, dynamic parameters such as actuator speeds, water intake speeds, location of water ballast etc. Another development was to model the drag coefficients for the thruster and rudder as illustrated in the math model section. The Simulink system was modified to separate the various stages so as to run them independently. In order to execute precise maneuvers, a specific sequence of motions was devised for the surface-cum-underwater robot. This strategic sequence involves a step-by-step process to achieve desired actions, ensuring effective control and stability throughout the operation.

Shifting Mass for Turn:

- The initial motion entails controlling the actuator which in turn moves the battery pack to induce a shift in mass, facilitating the desired vertical pitch.

Drawing in Water for Differential and Downward Motion:

- The subsequent step involves drawing in water to create a differential effect, leading to the desired downward motion. It is essential to note that, at this point, the system encounters a predefined floor at 10 meters depth and comes to a halt.

Releasing Water Contents for Surface Alignment:

- Once the system reaches the designated depth, the entire water contents are released from the ballast. This action is orchestrated to realign the system with its surface position. The system remains in a vertical orientation during this phase due to the actuator being locked in position.

Ascending Motion after Water Release:

- Following the release of water, the system initiates an upward movement. Approximately a meter above the floor, the actuator is retracted, allowing the system to return to its original horizontal pose.

Retracting Actuator for Horizontal Pose:

- At the appropriate height, the actuator is retracted, guiding the system back to its initial horizontal pose. This marks the completion of the defined sequence of motions.

This meticulously planned sequence ensures that the surface-cum-underwater robot executes controlled and purposeful movements, showcasing adaptability to different depths and orientations. The actuator's strategic deployment and retraction play a crucial role in achieving the desired maneuvers throughout the operation. Important updates include that the thruster and rudder help in the achievement of vertical pitch. Even though the increase in pitch is not much, it does help in reducing the drift.

v. Iteration 4:

While Iteration 3 provided sufficient conceptual understanding and functionality of the model, there were concerns about potential water leakage over prolonged use, particularly due to the clamps. To address this issue, a new twist and lock mechanism have been implemented.

Twist-locking mechanism is a type of sealing mechanism commonly used in underwater robotics to prevent water leakage into sensitive components. Here's how it generally works:

Design: The mechanism typically consists of two parts - a male and a female connector. These connectors are designed to fit together securely, forming a watertight seal when locked.

Threads: Both the male and female connectors have threaded components. When the male connector is inserted into the female connector, these threads interlock, creating a tight seal.

Twist Locking: The final step in the process involves twisting the connectors together. This twisting action engages the threads, pulling the connectors closer and compressing the O-ring, thereby forming a secure seal.

Release: To disengage the connectors, they are twisted in the opposite direction, which loosens the threads and releases the seal, allowing for separation.

O-ring Seal: To further ensure waterproofing, an O-ring seal is often integrated into the design. This O-ring is placed within a groove on one of the connectors (usually the female connector) and is compressed when the connectors are twisted together. This compression creates a watertight seal between the two connectors. We have used one O-ring and three gaskets to provide sufficient leakage proof.



Fig 39: Complete Design of Sealings and Gaskets for leakage prevention

This twist-locking mechanism is favored in underwater robotics for its reliability, ease of use, and effectiveness in preventing water leakage, thus protecting sensitive electronics and ensuring the safe operation of the underwater vehicle.

Correspondingly, adjustments have been made to the front and rear dome of the model to accommodate this new mechanism. Opting for an aluminum construction offers notable advantages, including exceptional strength and the ability to be precisely shaped to our specifications with minimal tolerance deviations. Notably, we've carefully adjusted the frontal dome's geometry to ensure optimal hydrodynamic performance, mitigating turbulence as our model maneuvers underwater.

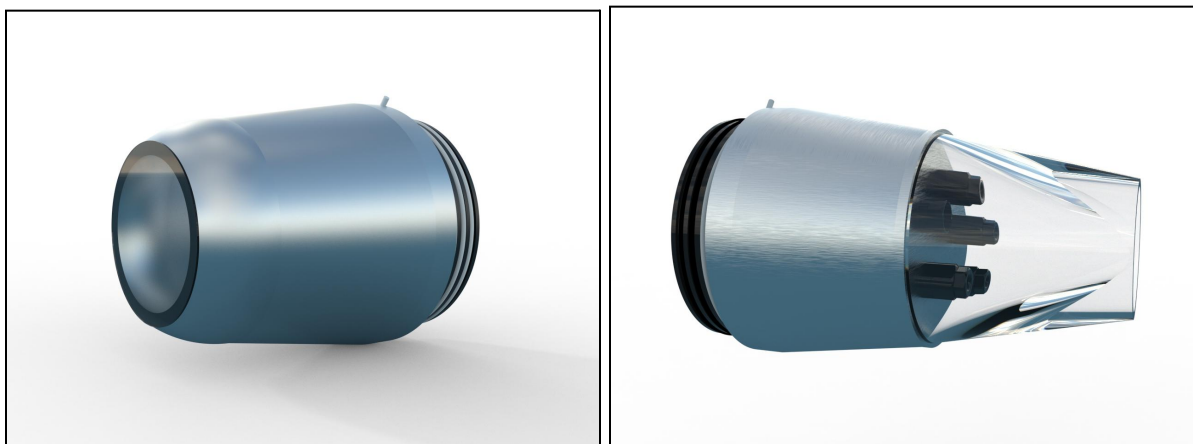


Fig 40: Redesigned Head and Tail Dome

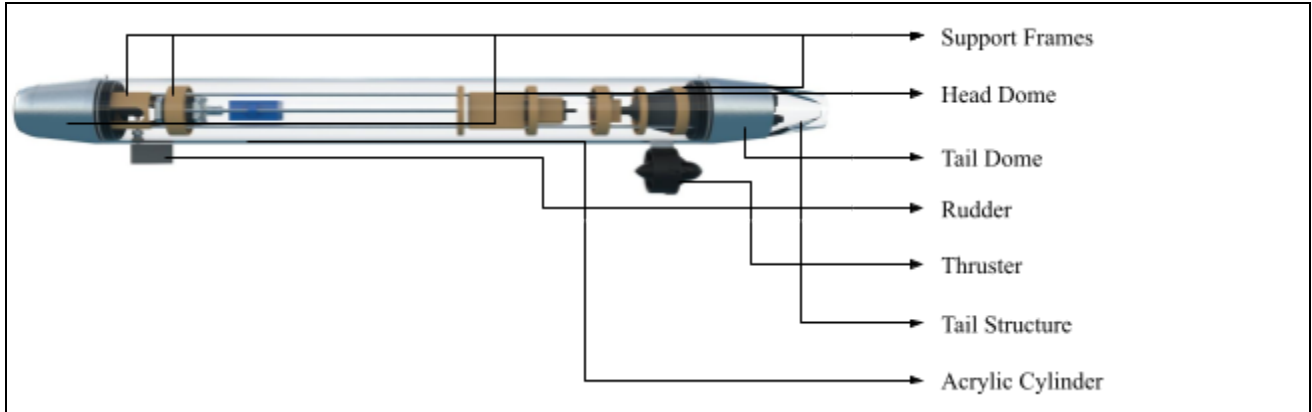


Fig 41: Integration of both the domes into the model (Twist & Lock Mechanism)

Internally, meticulous attention has been dedicated to frame design, facilitating secure fastening of aluminum rods to bolster structural integrity. A critical consideration in the front dome's redesign was the allocation of sufficient space to seamlessly integrate our camera sensor for essential obstacle detection and data retrieval. Additionally, the incorporation of an acrylic transparent layer at the dome's leading edge serves a dual purpose: ensuring optical clarity while effectively preventing leaks.

Similarly, the redesign of the rear dome underwent thorough consideration of various operational elements, including penetrator placement, thruster attachment points, and tail structure compatibility. Given our reliance on a twist-and-lock mechanism, precise carvings and O-ring arrangements on the aluminum component have been implemented to guarantee reliable sealing. Notably, a three-tiered sealing system has been employed, with the initial Buta-N material O-ring strategically positioned between the cylinder radii to withstand underwater pressures up to 10 meters without compromising containment integrity.

Mathematical model:

The focus in this iteration was to model the behavior of the system near the surface of the water, especially during the transition phases when the robot resurfaces and dives down. There is no available analytical literature dictating the behavior of the system during this phase. As a result, a hypothesis was made as follows: The mathematical model of the system is exactly the same as that used previously but the only difference is brought about by the rapidly changing center of

buoyancy and buoyancy values. The previous iteration provided a detailed data set consisting of the CoB and buoyancy magnitude values for depths from 0 to 6 m with an accuracy of 1 mm and angle changes from 0 to 90° with steps of 1° each. This dataset was then incorporated into the mathematical model by means of a lookup table with linear interpolation between the known data points. The buoyancy values were updated at every iteration using this lookup table. An important point to note is that, suitable additions were made to the function to calculate values for positions which were symmetric and set limits for border cases like when the system becomes completely submerged and completely resurfaces to reduce computational load.

An observation on implementing this methodology was that the system showcased dynamics that are seen in real life, validating the accuracy of the system. In fact the system actually stabilized to positions where the buoyancy and the weight nullified each other to accuracy of the order of millimeters.

To achieve this result, three major situations were overcome. It was observed that stabilization was observed only for a simulation step size of less than 0.01. So, the simulations were now run for step sizes lesser than this threshold value. The second situation was that absence of linear damping caused oscillations about the stabilization position which did not damp. This was overcome by including non-zero linear damping coefficients. As a result, the system smoothly damped to the stabilization point. The value of this linear damping coefficient is however not derived and approximated. The third discrepancy observed was that increasing the number of datapoints in the buoyancy data set improved accuracy of the stabilization point which was why the dataset was made accurate to 1 mm from an initial dataset with 1 cm accuracy.

The cumulative results achieved are shown below:

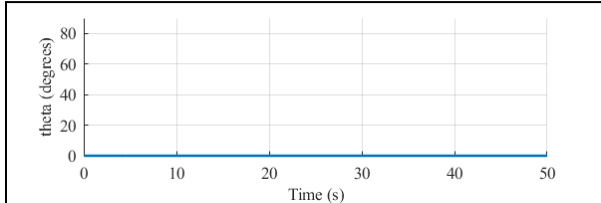
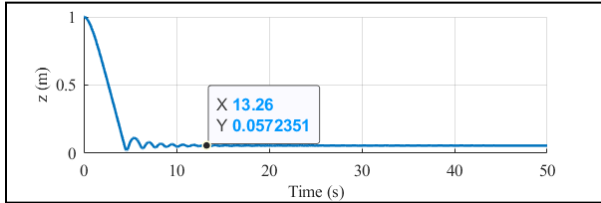


Fig. 42: System released from 1 m - 0° naturally stabilizes at 0.057 m ~ Neutral state

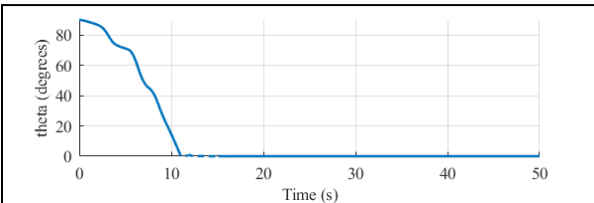
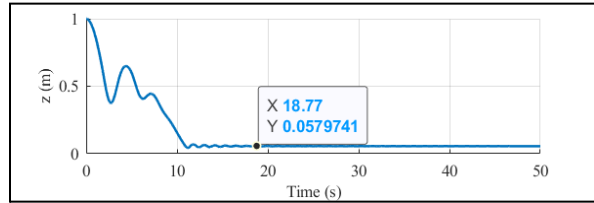


Fig. 43: System released from 1 m - 90° stabilizes at 0.057 m ~ Neutral state

vi. Iteration 5

The system designed up until this iteration was successfully able to individually describe the motion of the system either when it was completely submerged and when it was just near the surface. In this iteration, the surface effects and the diving sequences were combined together to provide a comprehensive model of the robot for the entire process in succession. The modifications thus worked about enable the user now to input the starting conditions of the model - initial water in the ballast and initial actuator position; the sequence of events as per their choice - actuator in, actuator out, water input and water output; and the corresponding timings for each operation. Two sequences of operations are stated below, these include a case of holding the actuator and the other of releasing the actuator immediately after release of water.

1. Initial state: System is positively buoyant and horizontal on surface.
Sequences: Extending actuator \rightarrow Intake of water to make system negatively buoyant \rightarrow Release of water to make system positively buoyant \rightarrow Retracting actuator

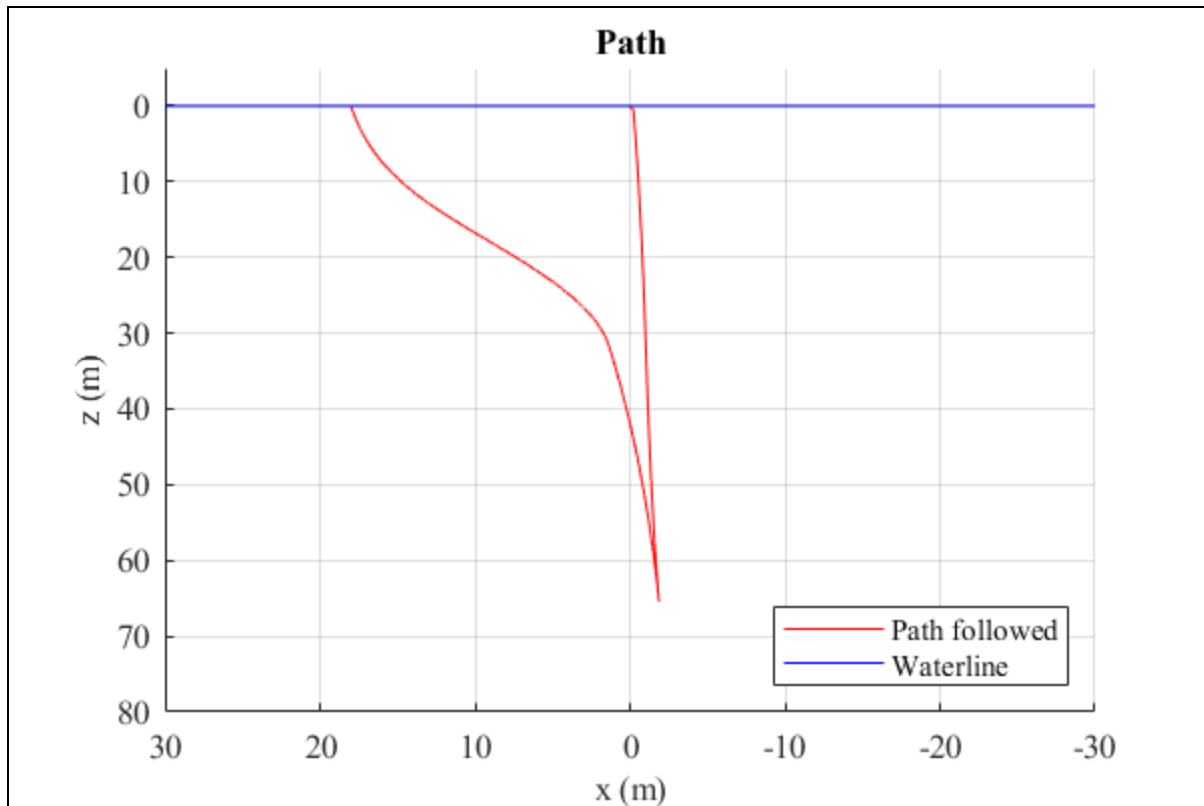


Fig 44 : Path followed by system for sequence stated in (1)

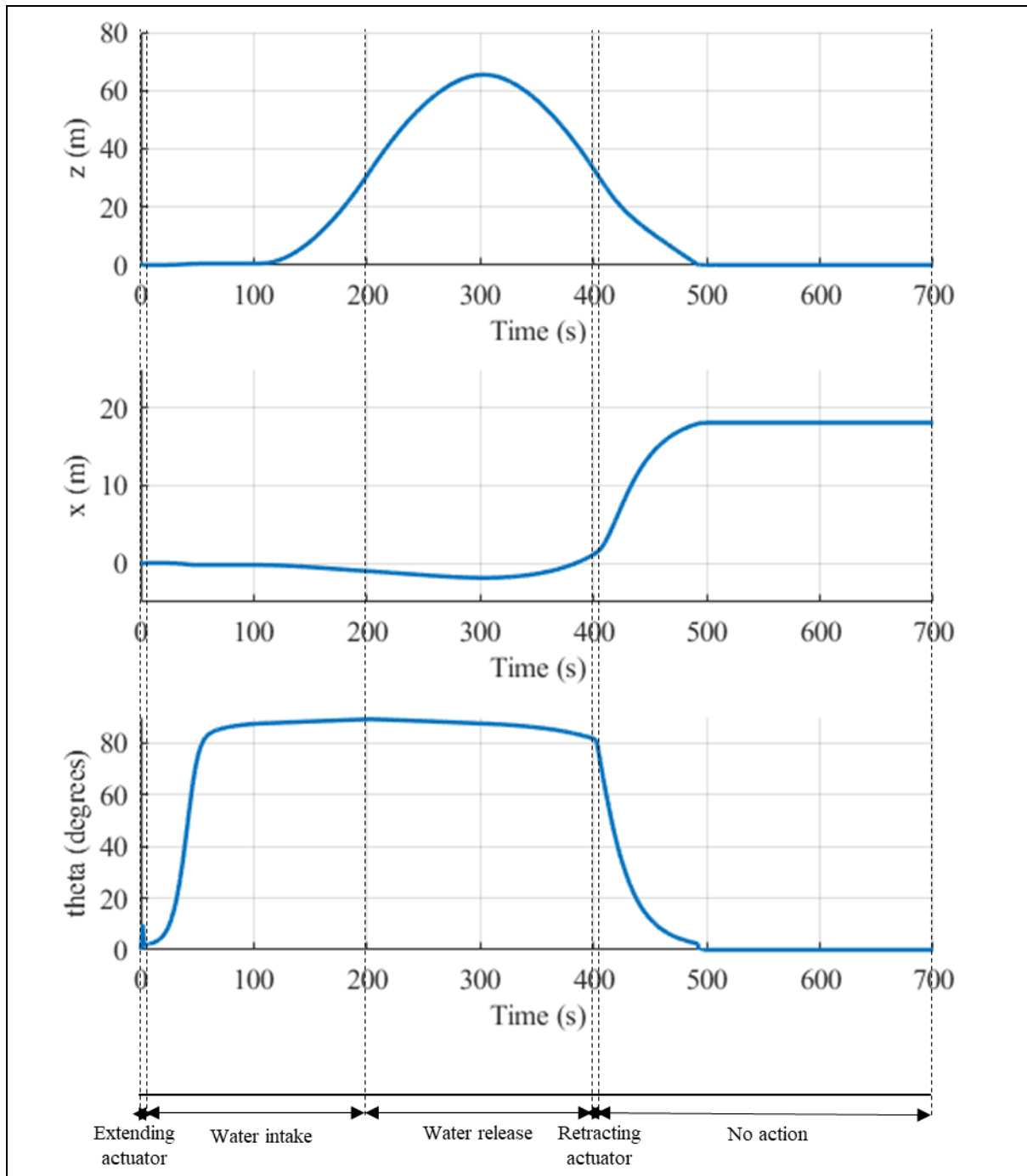


Fig 45 : System plots for sequence stated in (1)

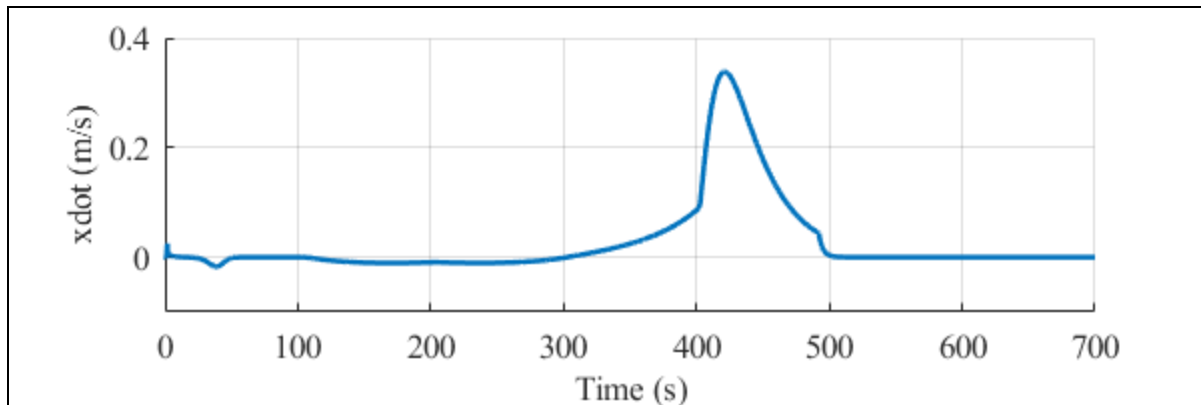


Fig 46: Velocity in global X direction

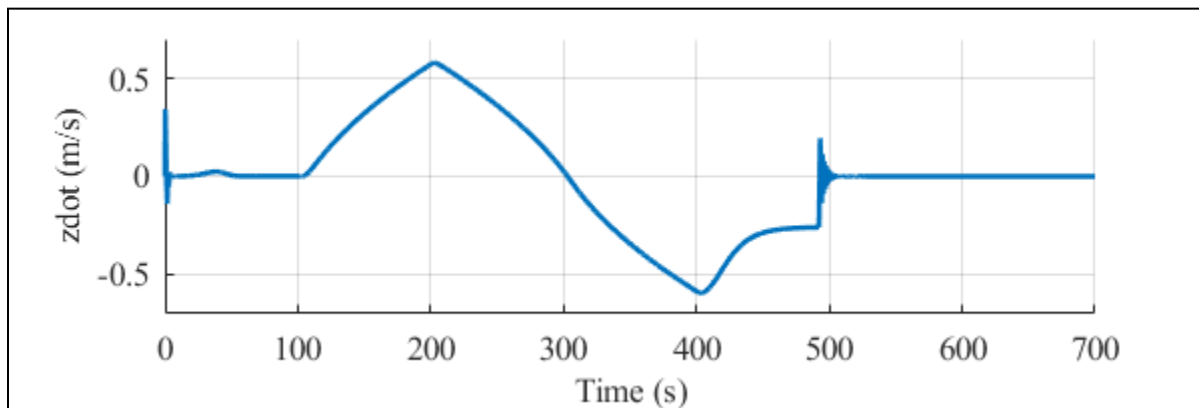


Fig 47: Velocity in global Y direction

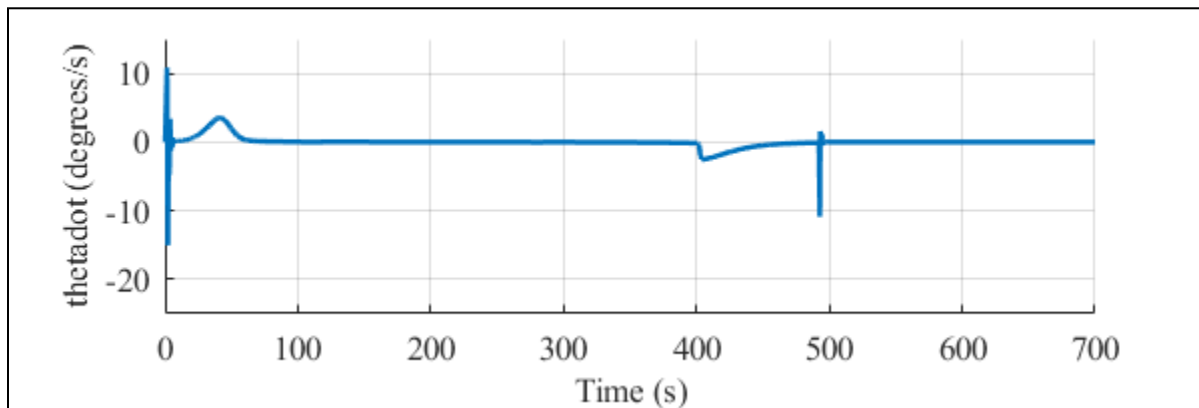


Fig 48: Angular velocity along global theta

2. Initial state: System is positively buoyant and horizontal on surface.

Sequences: Extending actuator → Intake of water to make system negatively buoyant → Release of water to make system positively buoyant → No action → Retracting actuator

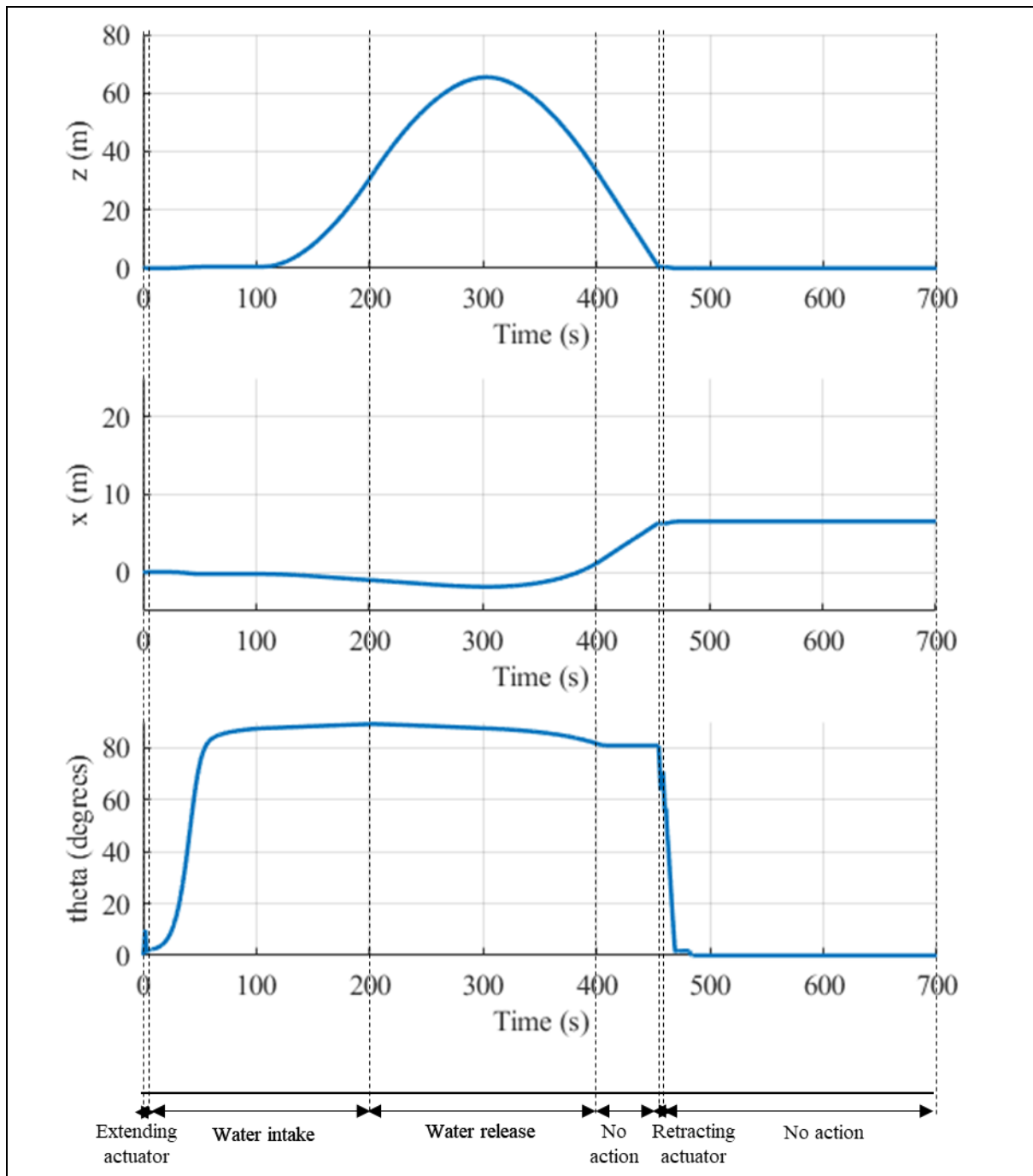


Fig 49 : System plots for sequence stated in (2)

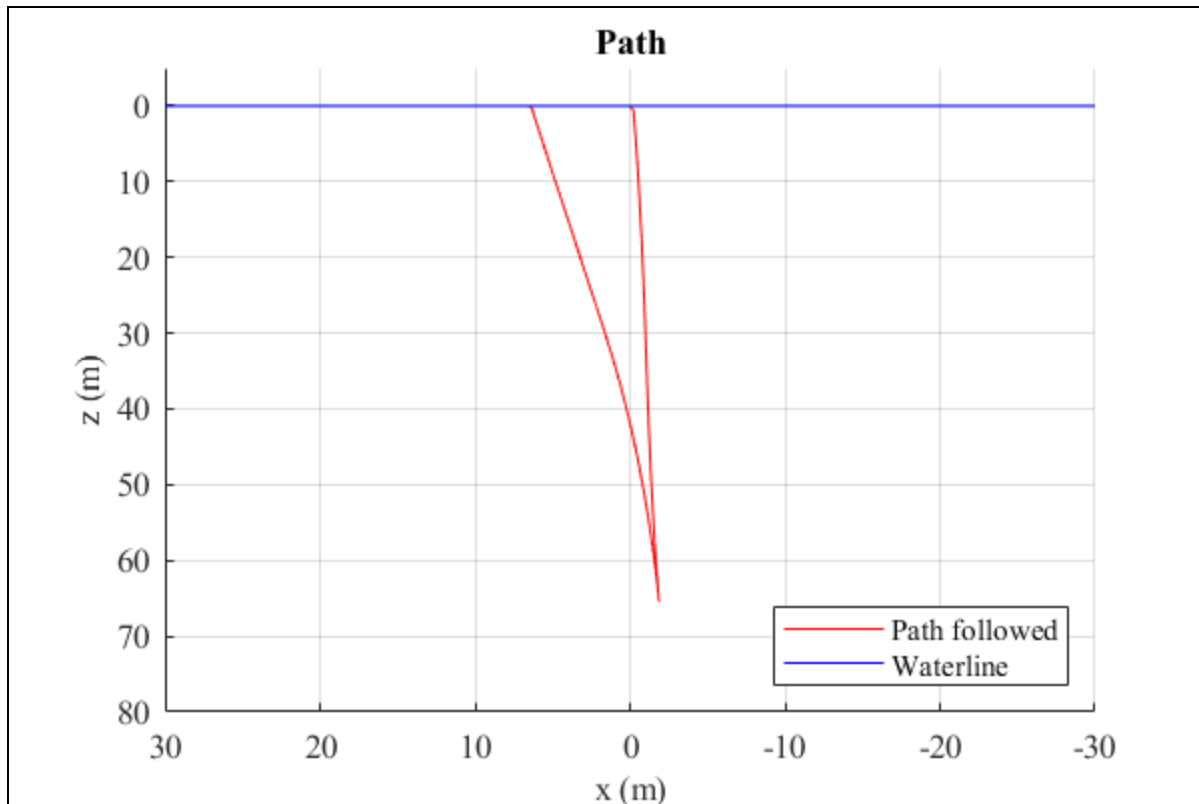


Fig 50 : Path followed by system for sequence stated in (2)

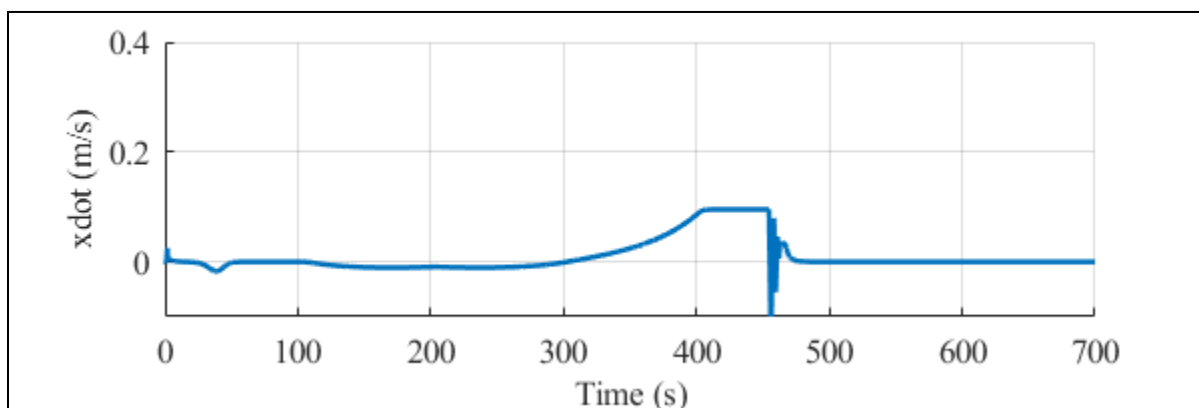


Fig 51: Velocity in global X direction

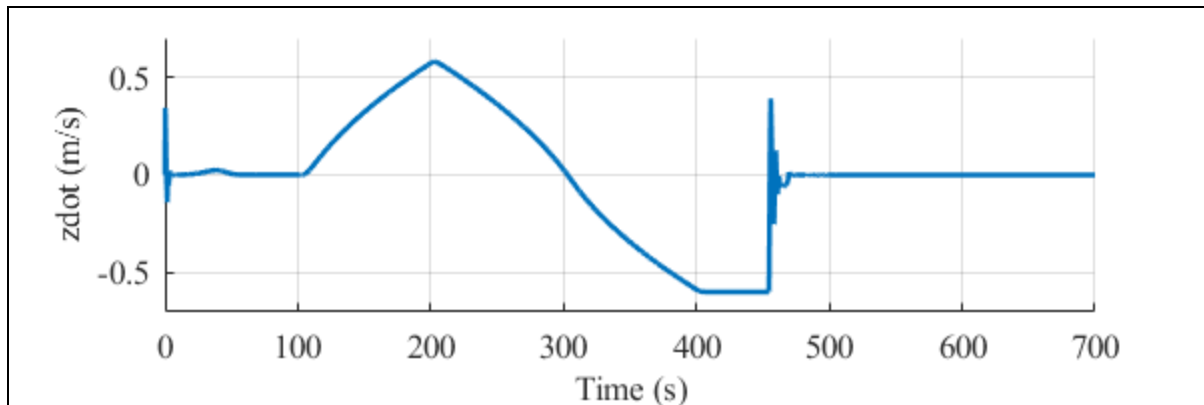


Fig 52: Velocity in global Z direction

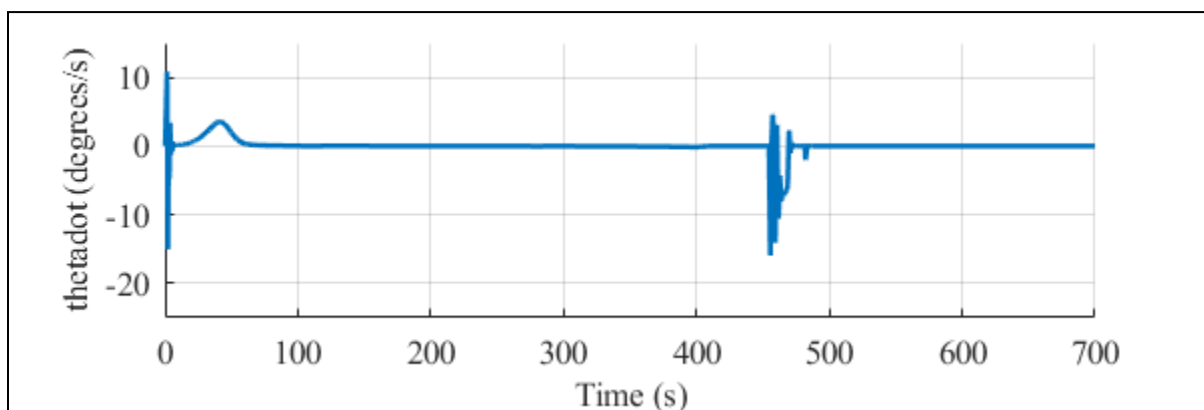


Fig 53: Angular velocity along theta direction

vii. Iteration 6:

In this iteration, the surface navigation model was worked upon. The mathematical model as stated previously was incorporated into the mathematical model. The behavior of the system was observed for different rudder angles. It was also observed that as there is no feedback in the model the system performs continuous loops for simulations that run for a long time. For brevity, results for small time durations are stated to indicate that turning is achieved. The results are stated as follows:

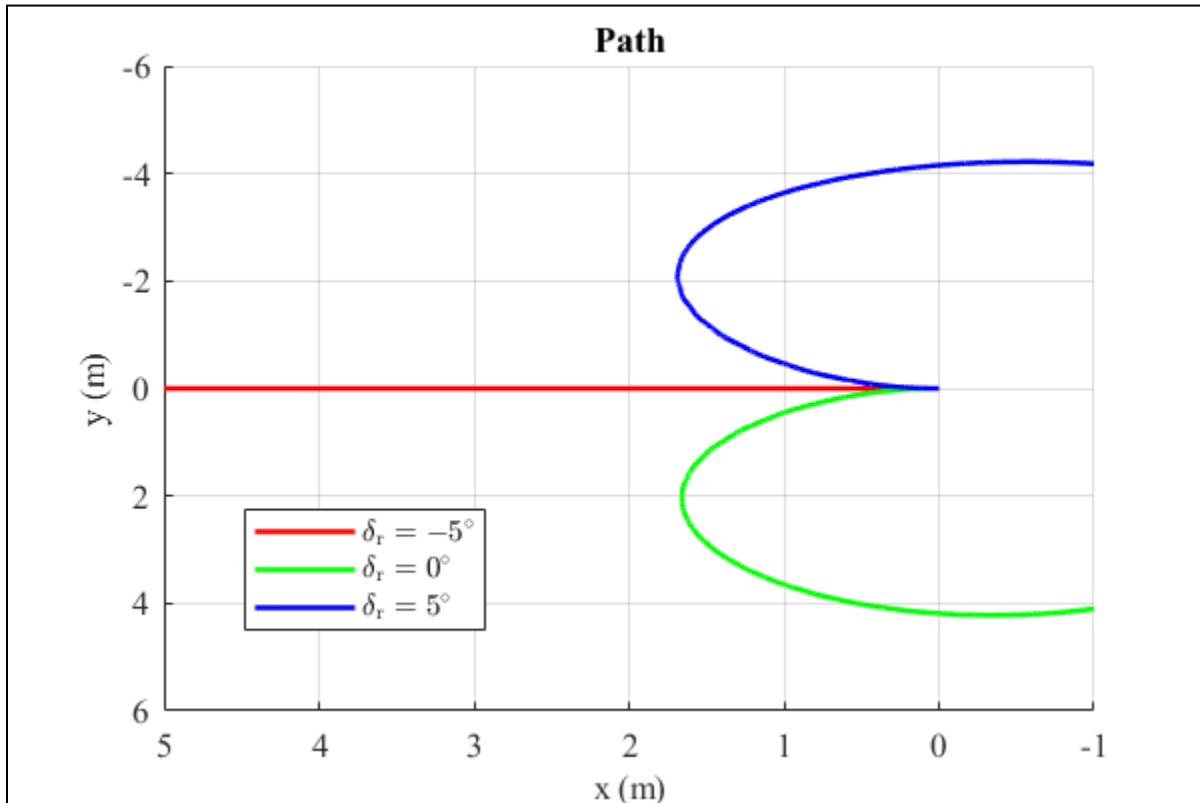


Fig 54: Path followed for different rudder angles

viii. Iteration 7:

All previous iterations derived the damping coefficients from standard textbooks and were approximated for a simplified geometry. The linear damping coefficients were assumed and had no prior available literature that would suit the design of the robot we had developed. To get an estimate on how valid our results are we carried out CFD based simulations as described in detail above. The results from the simulations were carefully fitted and mapped to produce equivalent damping forces as explained in the mathematical modeling part. On incorporating these into the mathematical model, the following results were obtained which illustrate the similarities or differences in both ways of approximating damping coefficients.

The nature of the graphs is identical to the ones which use analytically derived damping values. Here the damping coefficients are of smaller magnitude and hence enable greater depths as compared to the previous ones.

1. Initial state: System is positively buoyant and horizontal on surface. Sequences:
Extending actuator → Intake of water to make system negatively buoyant → Release of water to make system positively buoyant → Retracting actuator

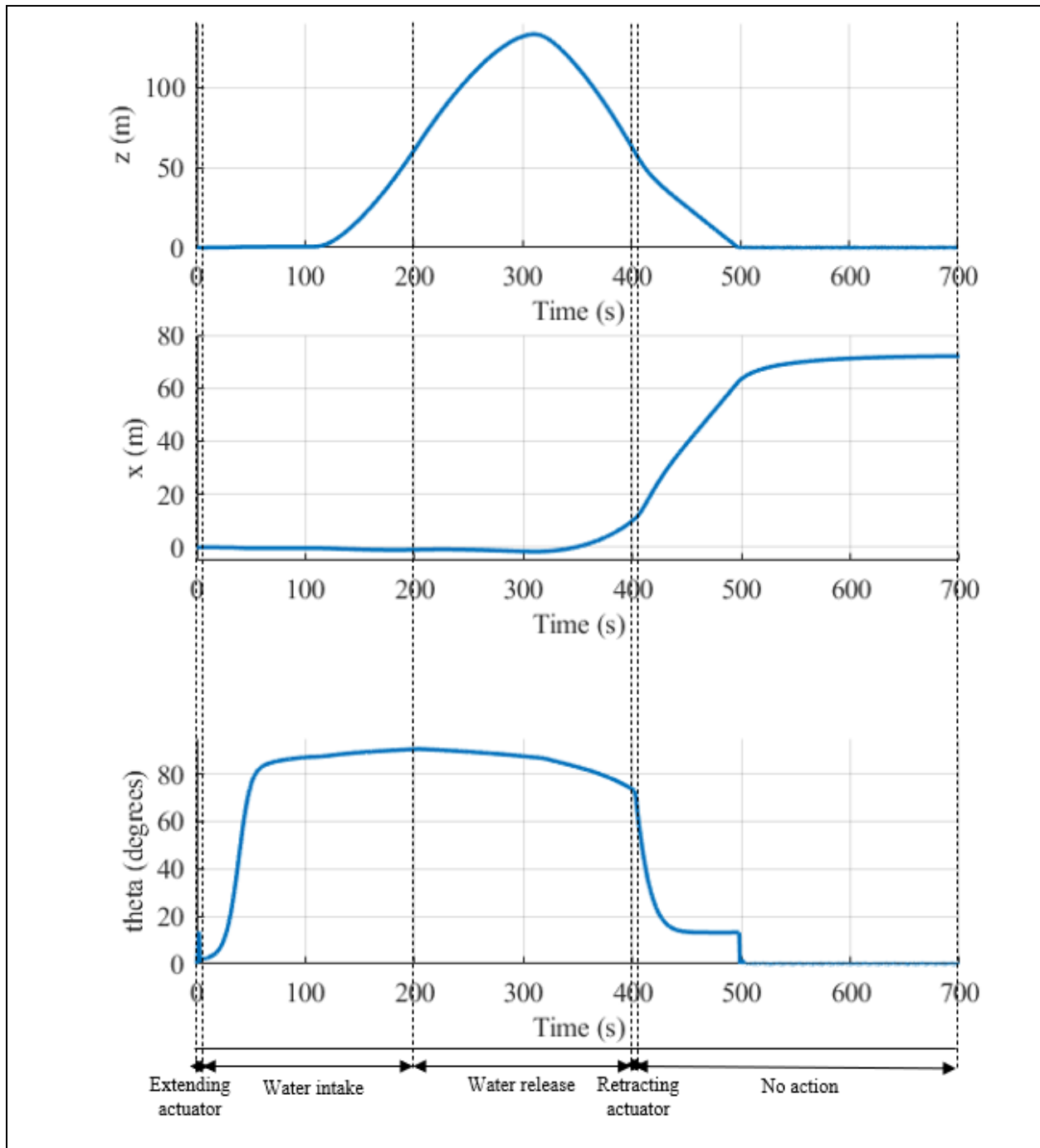


Fig 55 : System plots for sequence stated in (1)

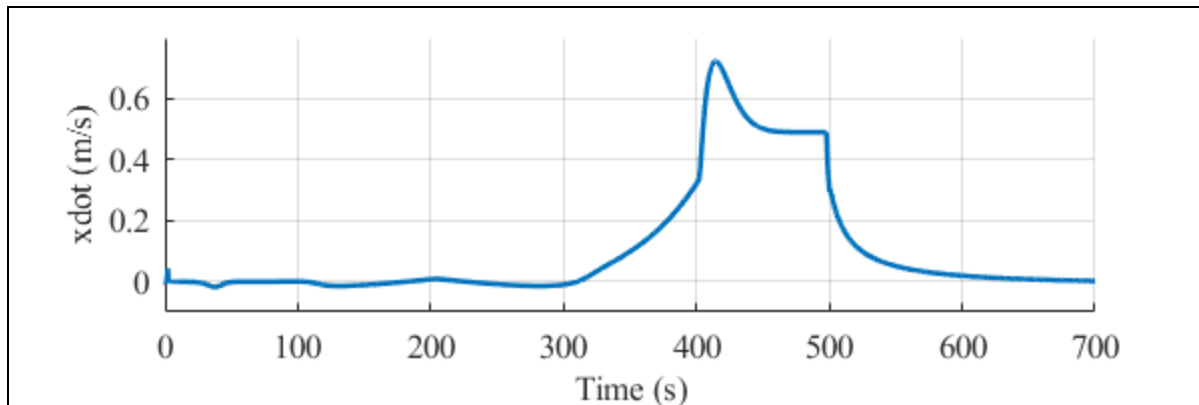


Fig 56 : Velocity in global X direction

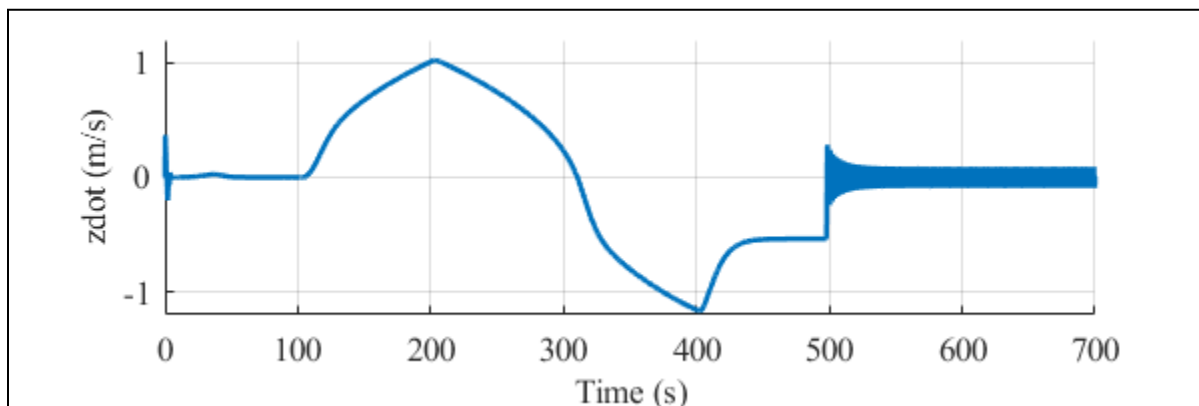


Fig 57 : Velocity in global Z direction

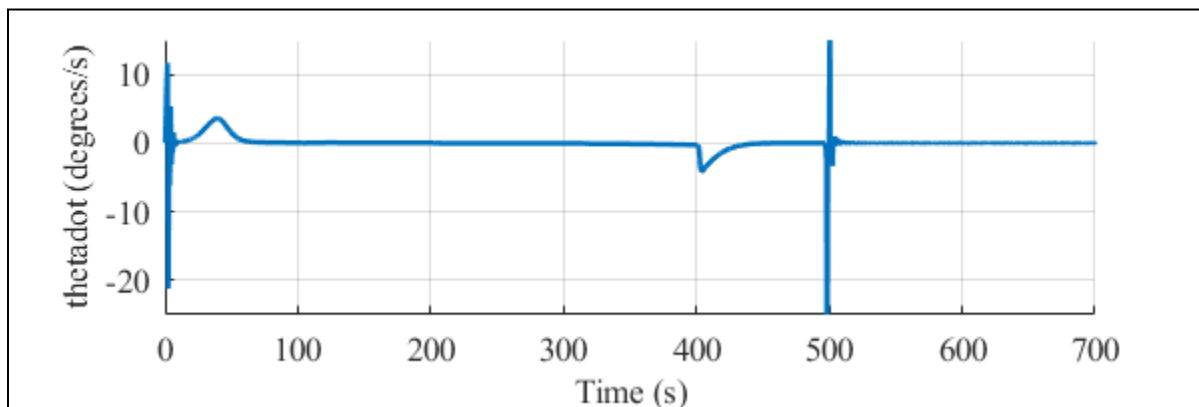


Fig 58: Angular velocity along global theta direction

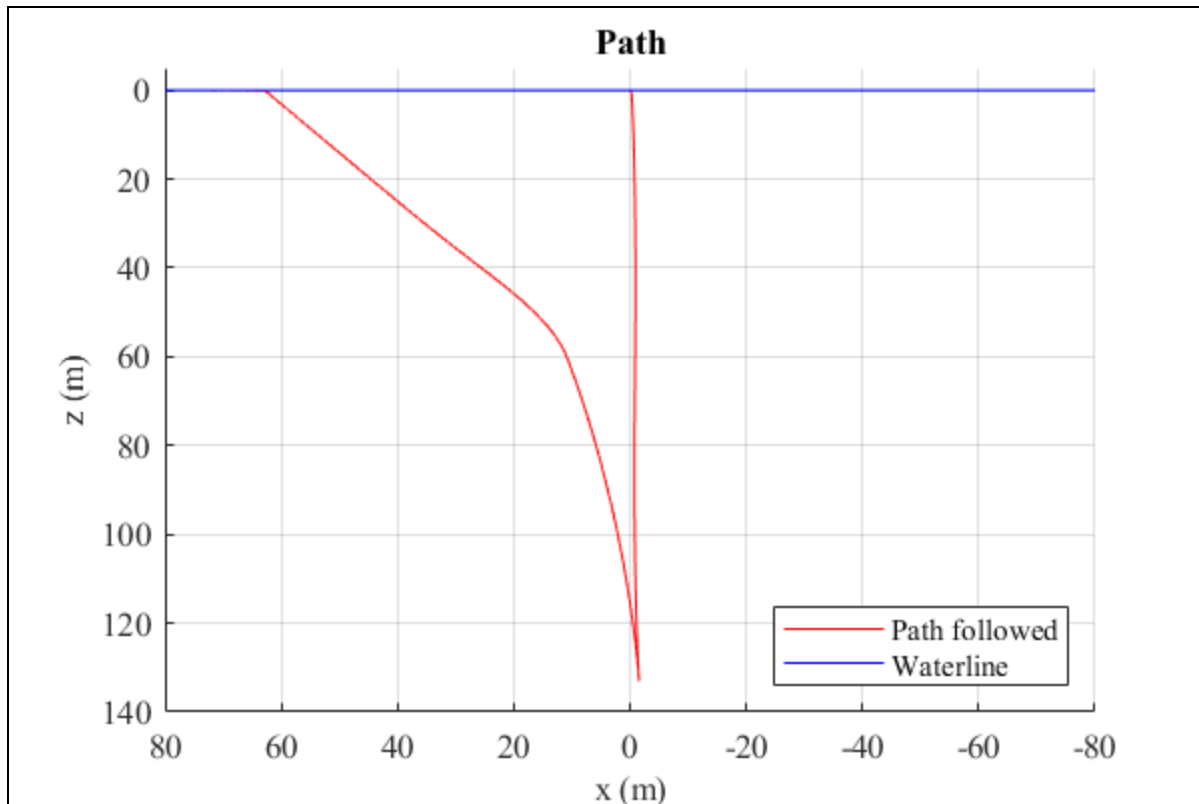


Fig 59 : Path followed by system for sequence stated in (1)

2. Initial state: System is positively buoyant and horizontal on surface. Sequences:
Extending actuator → Intake of water to make system negatively buoyant → Release of water to make system positively buoyant → Hold→ Retracting actuator

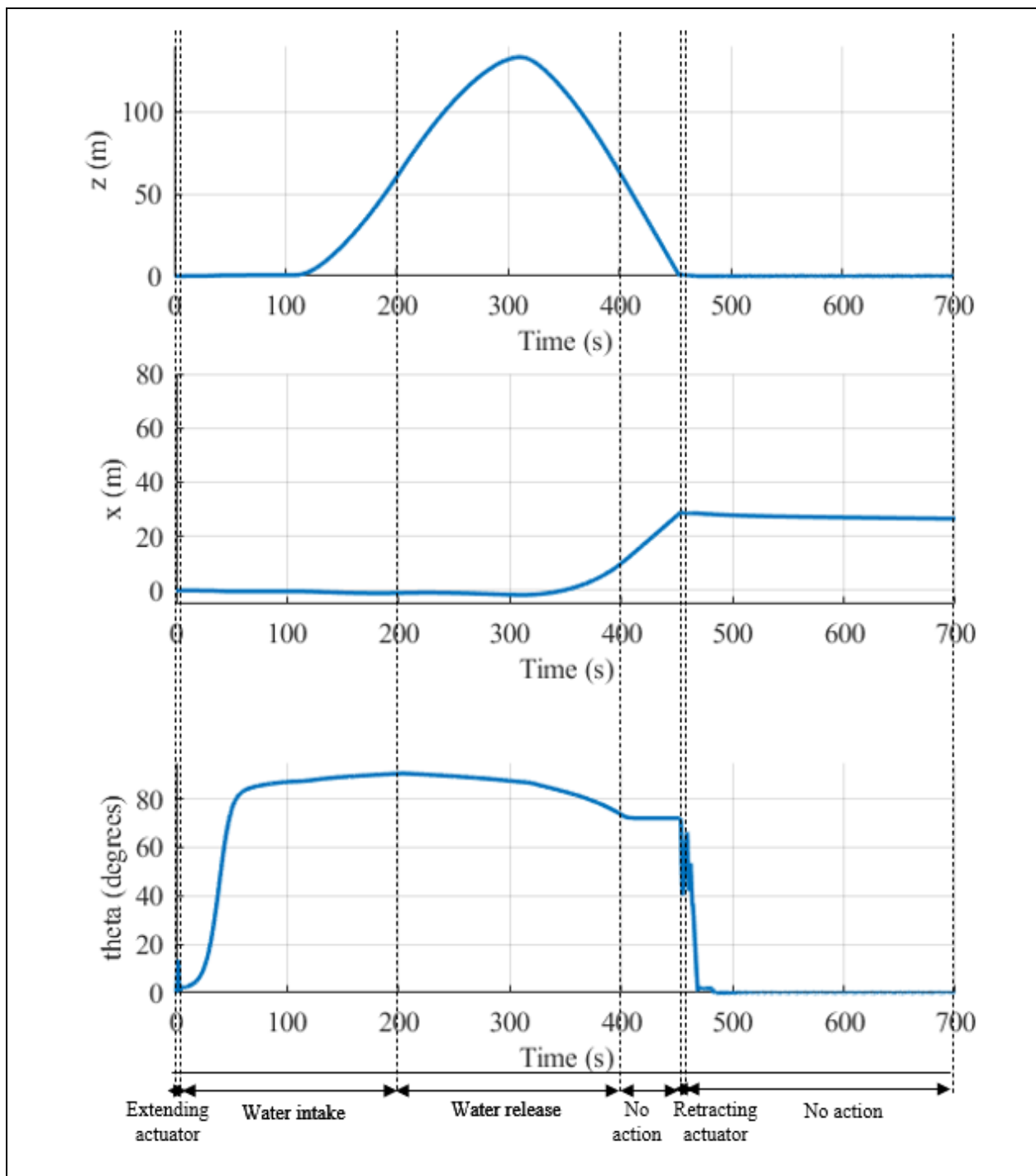


Figure 60 : System plots for sequence stated in (2)

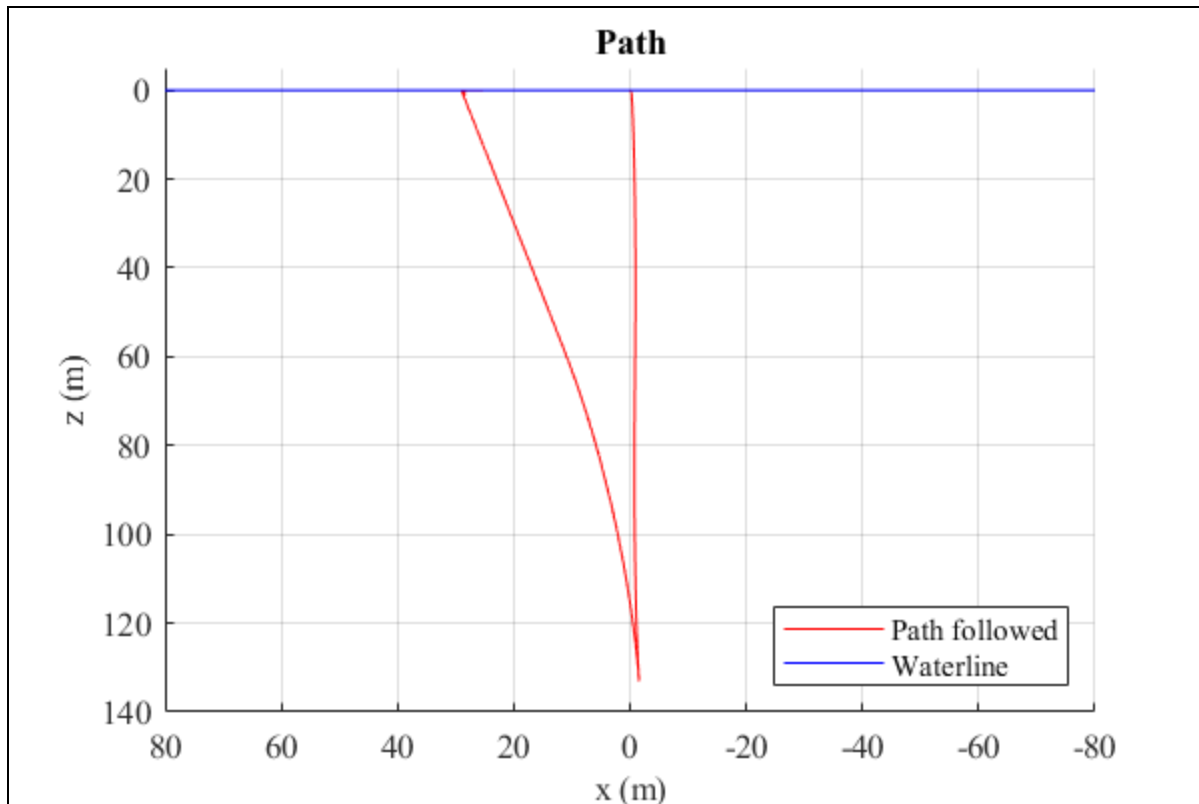


Fig 61 : Path followed by system for sequence stated in (2)

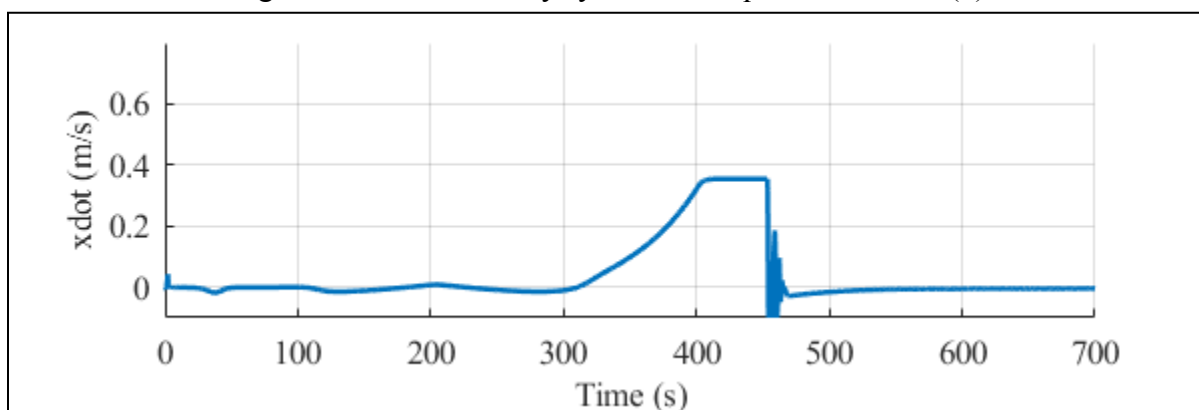


Fig 62: Velocity in global X direction

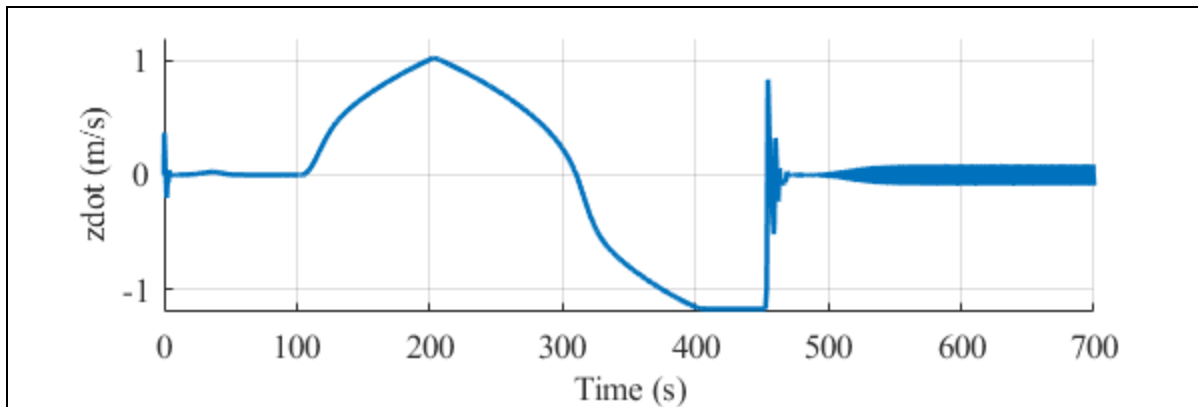


Figure 63: Velocity in global Z direction

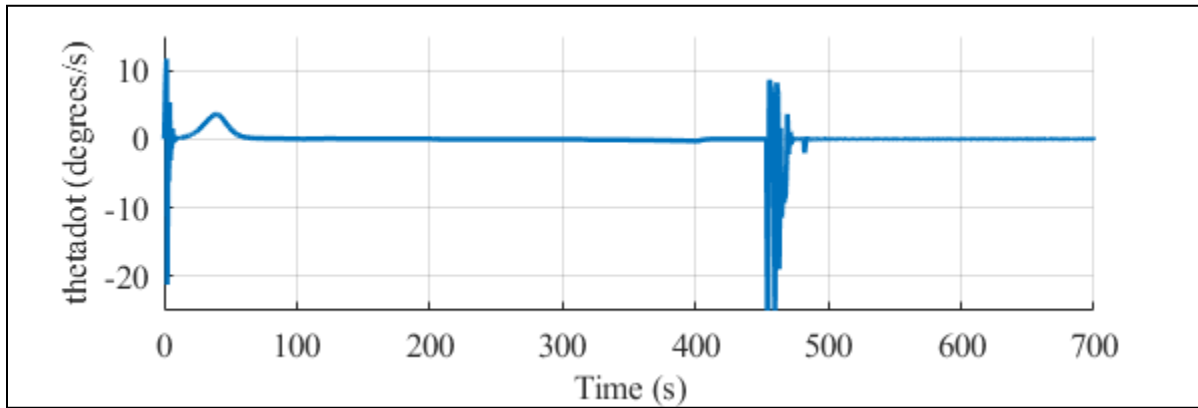


Figure 64: Angular velocity along global theta direction

Surface Navigation Plots:

0 degrees:

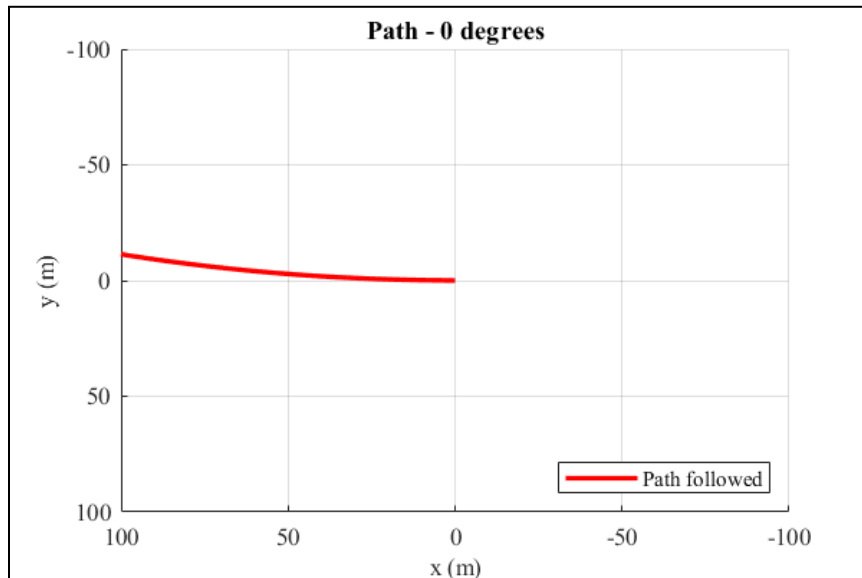


Figure 65: Observed path followed

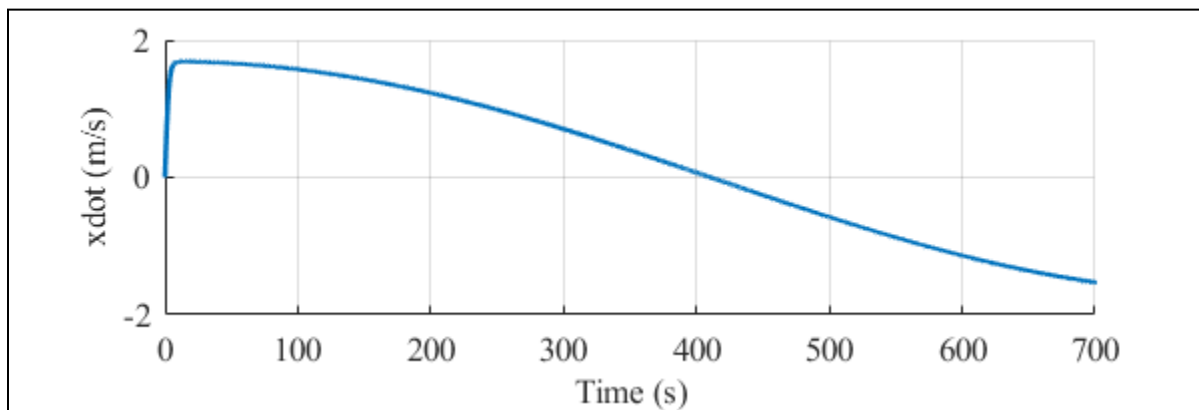


Figure 66: Velocity in global X direction

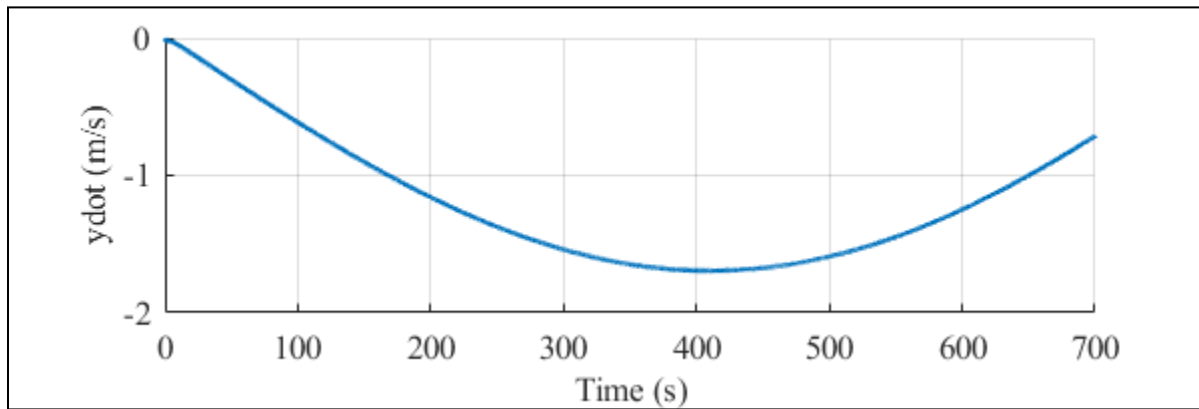


Figure 67 : Velocity in global Y direction

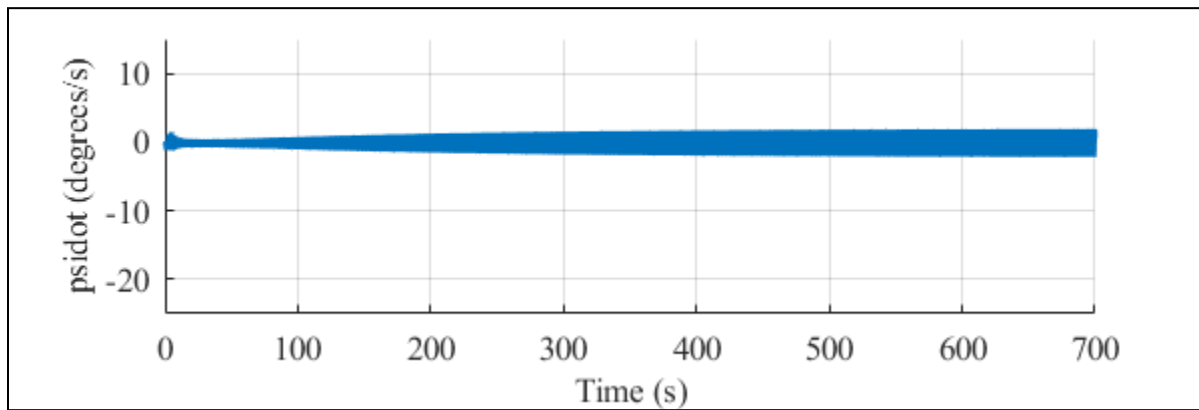


Figure 68 : Angular velocity along global psi direction

-5 degrees:

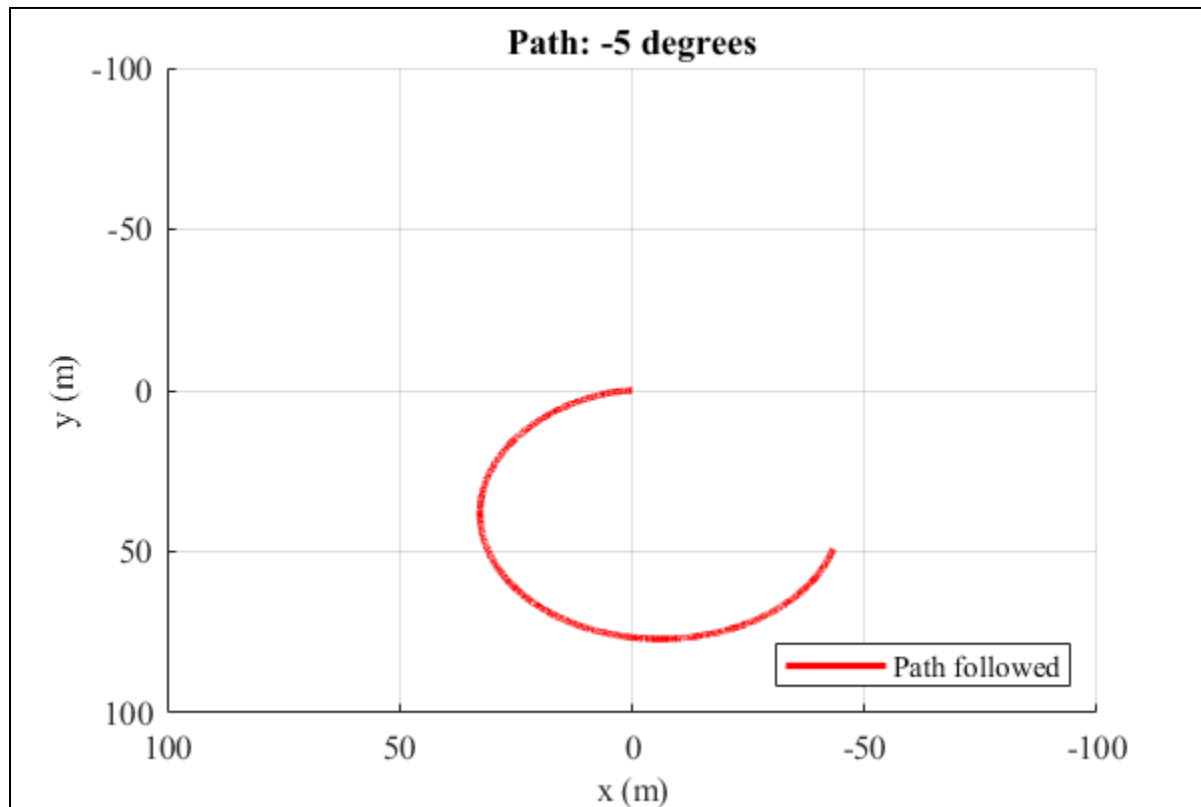


Figure 69: Observed path followed

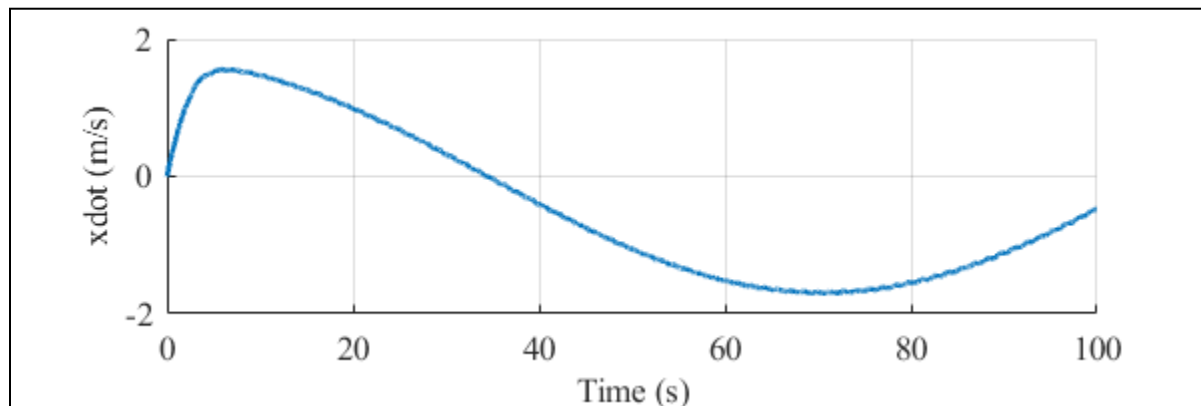


Figure 70: Velocity in global X direction

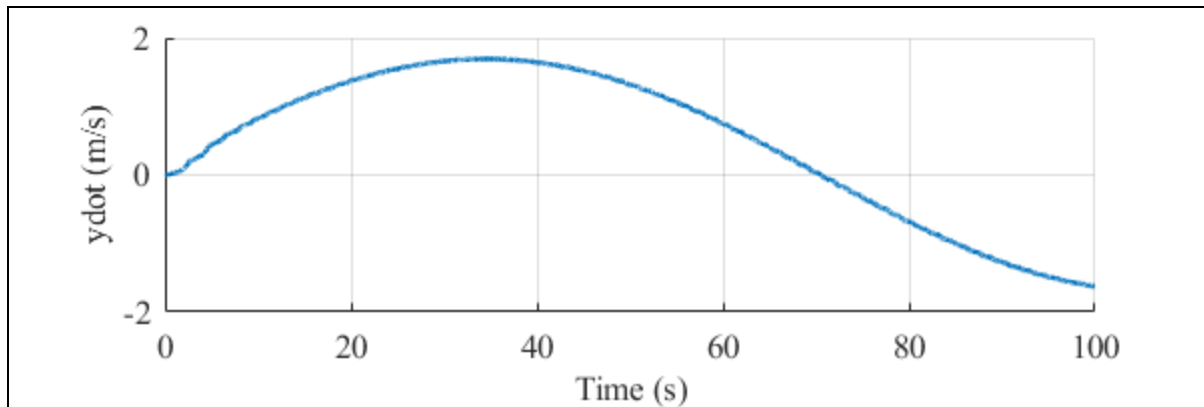


Figure 71: Velocity in global Y direction

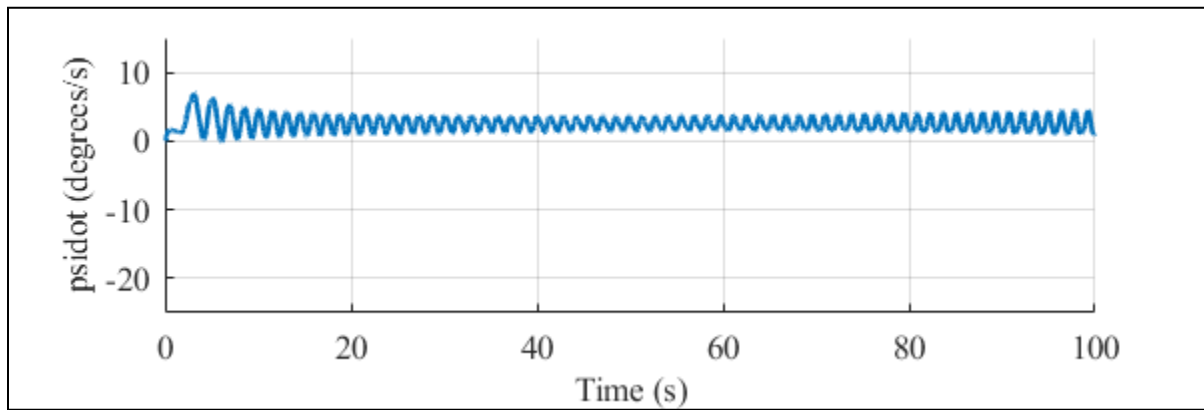


Figure 72: Angular velocity along global psi direction

-7.5 degrees:

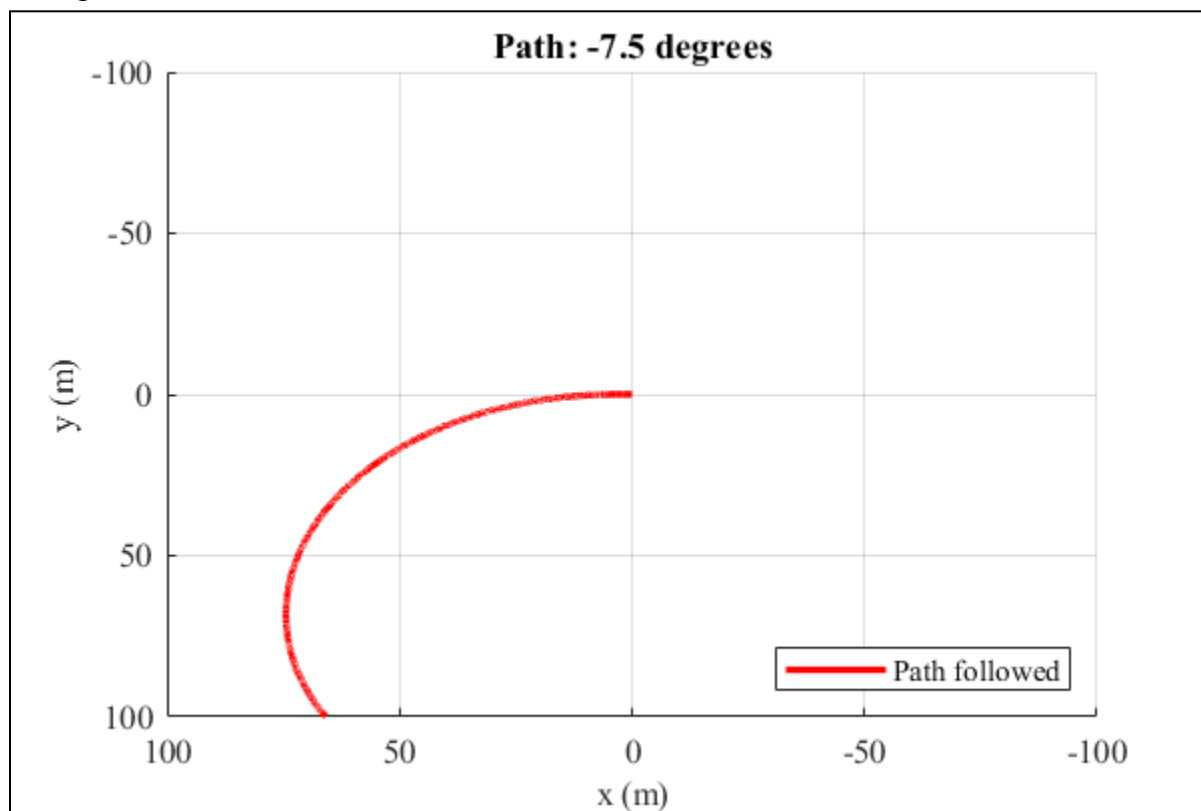


Figure 73: Observed path followed

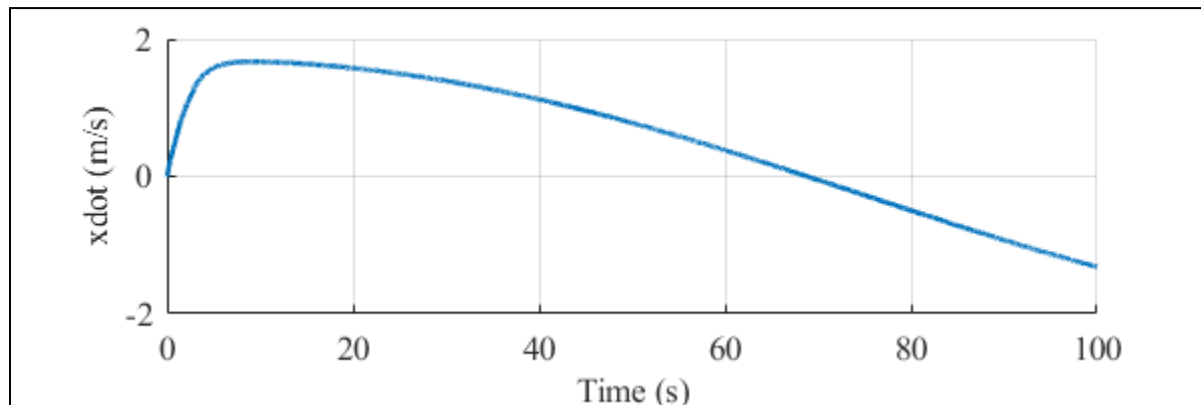


Figure 74: Velocity in global X direction

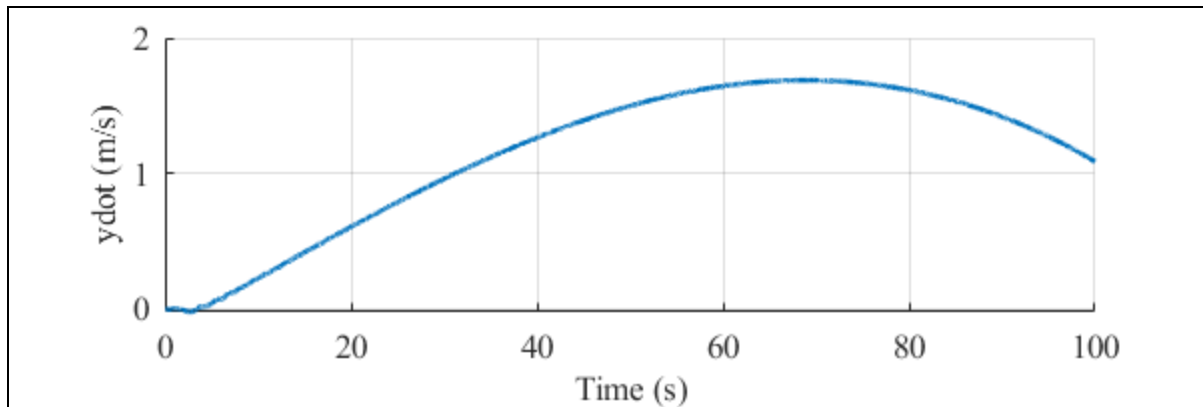


Figure 75: Velocity in global Y direction

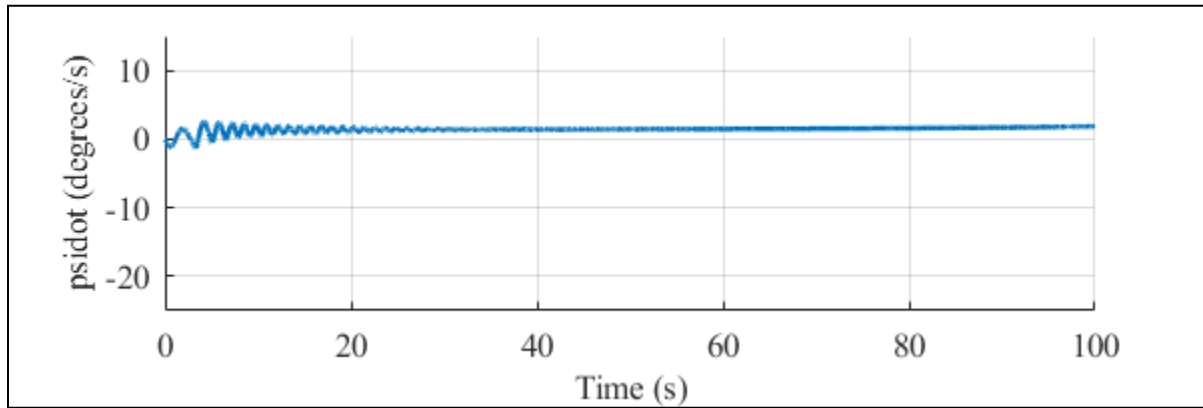


Figure 76: Angular velocity along psi direction

-10 degrees:

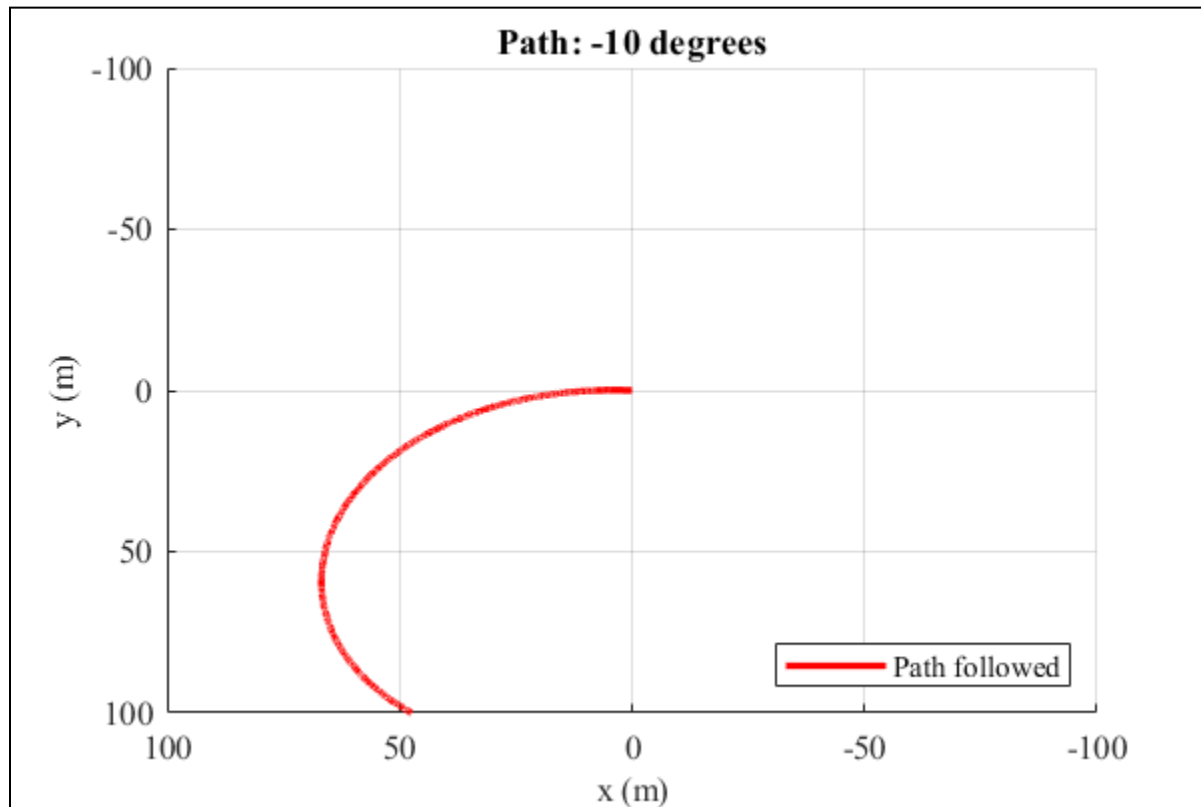


Figure 77: Observed path followed

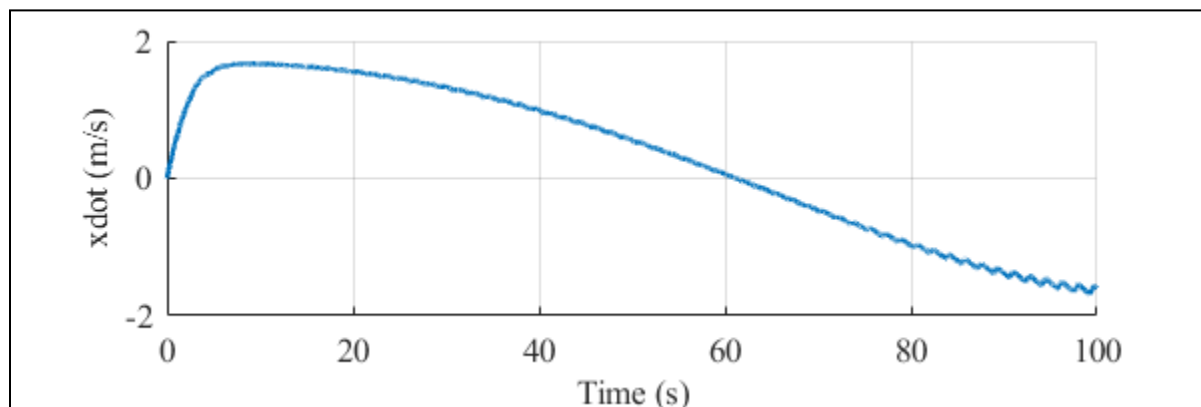


Figure 78: Velocity in global X direction

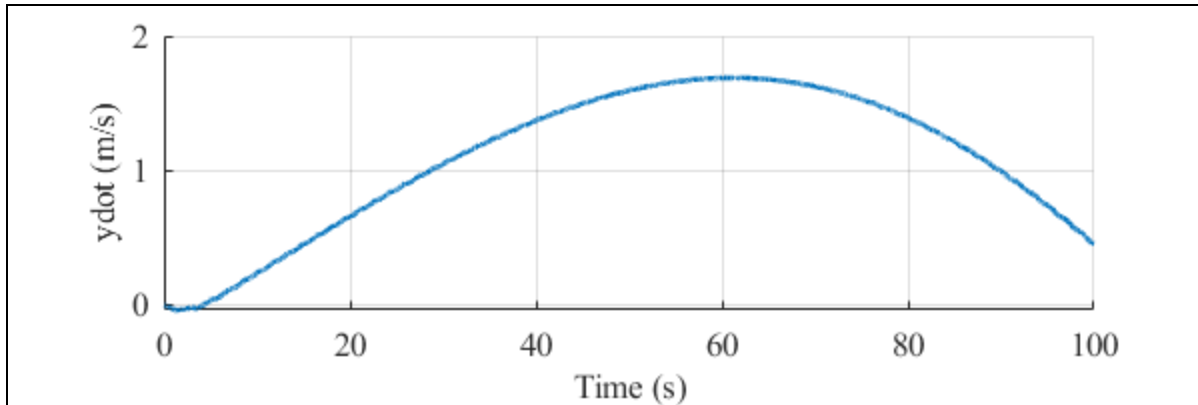


Figure 79: Velocity in global Y direction

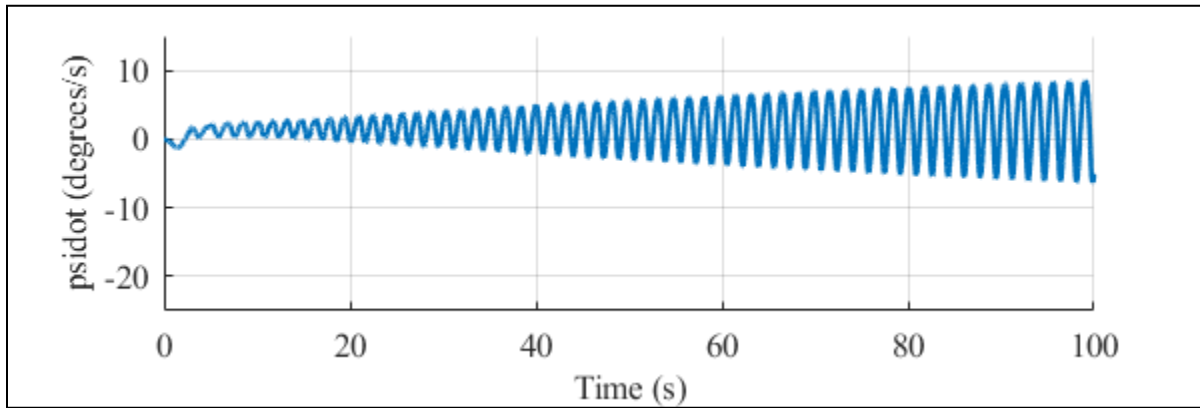


Figure 80 : Angular velocity along psi direction

Chapter 4.e: Results and Discussion

The following results were obtained and concluded as a result of the iterations:

1. The pitching motion must be decoupled from the change in mass. The pitching is therefore achieved by the movement of a battery pack inside the system with the help of an actuator.
2. For achieving perfect vertical pitch, the CoG must be closer to the X axis. This can be achieved by carefully rearranging the components of the system to maintain the CoG close to CoB.
3. On incorporating the damping taken in from CFD calculations, the results obtained follow a similar pattern but greater depths are achieved in this case thus indicating lesser damping forces than estimated.
4. Surface model also demonstrated similar results, but certain discrepancies were observed in the degree of turning. Validation is required to determine the errors.

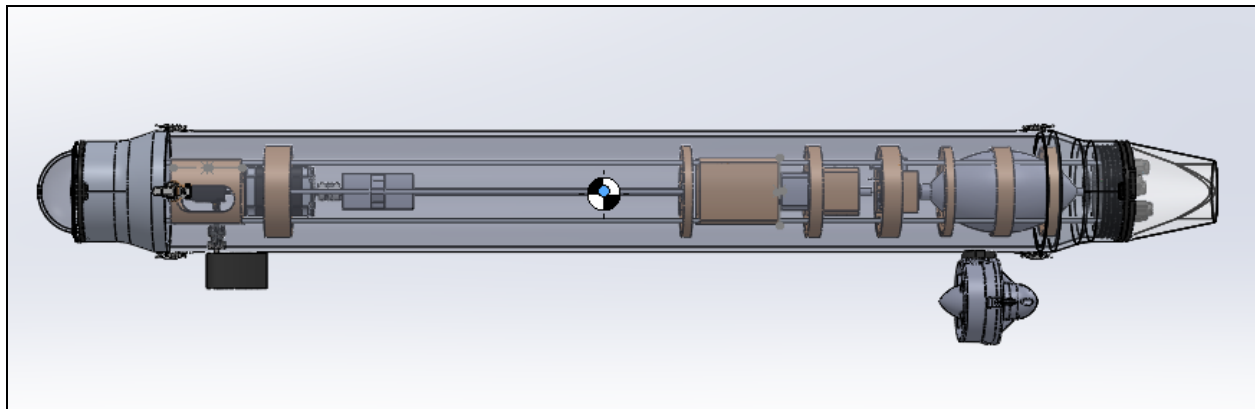


Fig 81: Initial position of Centre of Gravity and Origin of the System (Blue Dot)

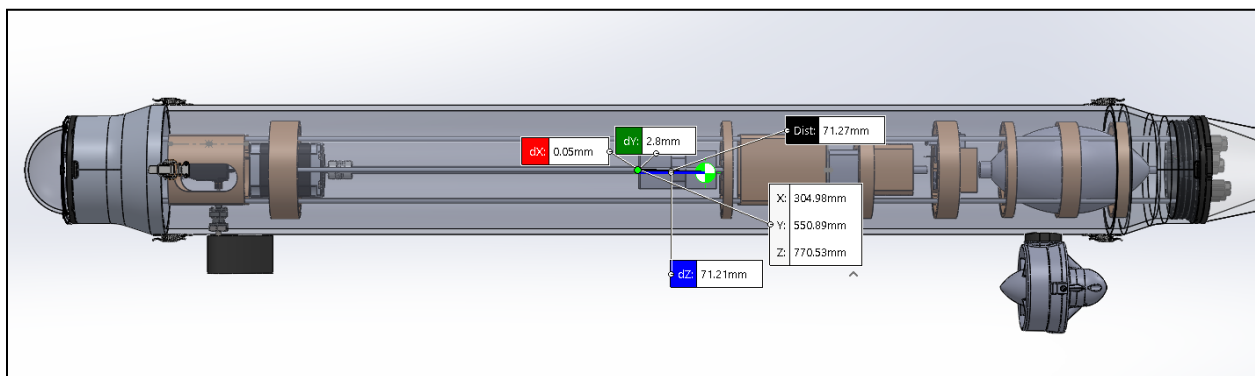


Fig 82: Final shift of Centre of Gravity due to movement of battery pack from the origin of the System

Shift along Z: 71.21 mm (7 cm shift backwards)

Chapter 5: Conclusion

The project work resulted in the completion of the entire design and development of the surface and underwater robot. We successfully designed both of the models for change of mass principle and also for change of volume principle in Solidworks. CFD simulations were performed using ANSYS Fluent to determine the respective drag and lift coefficients for respective rudder angles and the results obtained by incorporating these drag values into the mathematical model gave similar results, indicating correctness of the methodology employed in CFD calculations.

A concise and up-to-date mathematical model was developed, validated and tested several times throughout the project. The mathematical model provided valuable suggestions to the design process, determination of system parameters and a validation framework to test working of the system. The mathematical model thus developed is highly flexible and allows the user to test dynamics of the model for various sequences and types of operations. An important note is about the successful demonstration of surface transition effects that the model so accurately captured. The surface model incorporated from a theoretical basis also provided almost identical results as those obtained by incorporating CFD derived damping but certain discrepancies were observed which needs rechecking. To summarize, the mathematical model completely captures the behavior of the system while on surface, during transition and when underwater; thus fulfilling the objectives of this segment of the project.

The achieved outcomes lay the groundwork for the transition from conceptualization to practical implementation in the development of the surface and underwater robot.

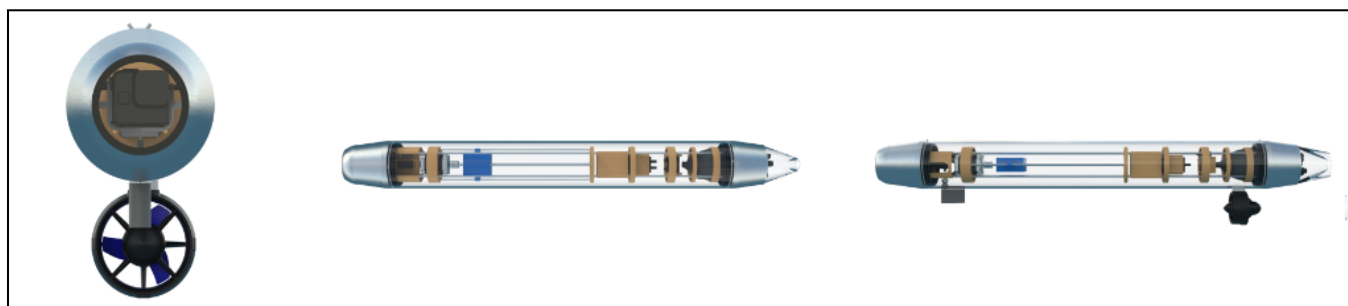


Fig 83: Front View, Top View and Side View for the Variable Mass Buoyancy System

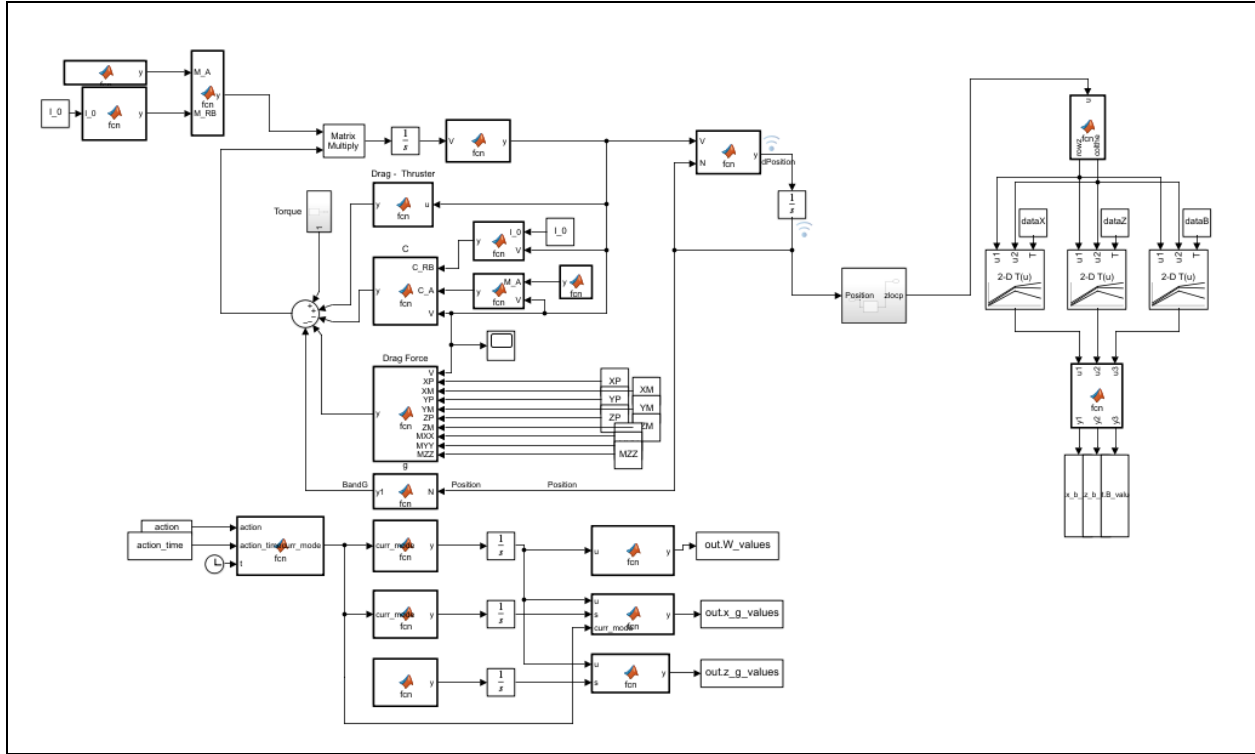


Fig 84: Mathematical model framework

Chapter 6: Future Work

The future work of the project will advance towards the fabrication of structures and the procurement of components needed for constructing the physical prototype. This phase bridges the transition from the conceptual design stage to the practical realization of the model, aligning the project with its ultimate goal of bringing the envisioned surface and underwater robot to life. Meanwhile the electronics parts also should be programmed side by side in order to make it work successfully.

Further steps also include designing a controller model which will help multiple bots to communicate with each other and to perform multiple tasks simultaneously. These controllers also in turn help the bot form respective shapes according to the user requirements and it performs the dive-in & dive-out perfectly. An overall path tracking controller should be devised if the model works on to detect the coordinate and to reach it with ease. This controller should also be robust enough to use the rudder, thruster and movable mass (battery movement) in the system to perform a 90 deg vertical dive in without any radial deviation.

Some more CFD simulations are required to capture the effect of angular velocity

components of flow on the forces and moments of the system. This will generally help us validate and help us finalize the rudder dimensions. Turning for various rudder angles needs to be revalidated or retried with proper feedback.

These processes will be carried on parallelly with the patent filing process.

Chapter 7: References

1. Mohan, Santhakumar & Asokan, T.. (2010). Investigations on the Hybrid Tracking Control of an Underactuated Autonomous Underwater Robot. *Advanced Robotics*. 24. 1529-1556. 10.1163/016918610X512587.
2. Thiyagarajan Ranganathan, Sundaravalli Aravazhi, Sambit Mishra, and Asokan Thondiyath, (2018). Design and Analysis of a Novel Underwater Glider - RoBuoy. 2089-2094. 10.1109/ICRA.2018.8462921.
3. Thiyagarajan Ranganathan, Vijendra Singh, Ranjith Nair, and Asokan Thondiyath (2017). Design of a controllable variable buoyancy module and its performance analysis as a cascaded system for selective underwater deployment. *Proceedings of the Institution of Mechanical Engineers, Part M: Journal of Engineering for the Maritime Environment*. 231. 147509021668881. 10.1177/1475090216688819.
4. Thor I. Fossen, *Handbook of marine craft hydrodynamics and motion control*, John Wiley & Sons.
5. Tristan Perez, *Ship Motion Control* (2005)
6. Yunus Cengel and John Cimbala, *Fluid Mechanics : Fundamentals and Applications* (2004), McGraw Hill.
7. Standard, RNG, and Realizable k- Models Theory - Fluent Manual (Module 12)